SYNTHESIS OF MULTI-WALLED CARBON NANOTUBES BY PLASMA ENHANCED MICROWAVE CVD USING COLLOIDAL FORM OF IRON OXIDE AS A CATALYST

By

DEVANATHAN RAGHAVAN

Bachelor of Engineering

Bharathiar University

Coimbatore, India

May, 2000

Submitted to the Faculty of the
Graduate College of the
Oklahoma State University
in partial fulfillment of
the requirements for
the Degree of
MASTER OF SCIENCE
May, 2005

SYNTHESIS OF MULTI-WALLED CARBON NANOTUBES BY PLASMA ENHANCED MICROWAVE CVD USING COLLOIDAL FORM OF IRON OXIDE AS A CATALYST

Thesis approved:

Dr. RANGA KOMANDURI

Thesis Advisor

Dr. SAMIT ROY

Dr. HONGBING LU

Dr. A. GORDON EMSLIE

Dean of the Graduate College

SUMMARY

Carbon nanotubes (CNTs) were discovered in 1991 by Sumio Iijima of NEC Corporation. They are rolled up sheets of graphene and have structure resembling that of an elongated fullerene molecule. Because of their potential in scientific and technological applications in various fields, they are investigated extensively in the past decade and the field is still active. Some of the applications of CNTs include advanced nanocomposites, conducting polymers, tips for scanning probe microscopy, flat panel displays, hydrogen storage, MEMS, NEMS, nanoelectronics, and nanocircuits. CNTs posses extraordinary mechanical, thermal, optical and electronic properties. They have Young's Modulus ranging from ~0.75-1TPa as compared to 200 GPa of steel. The exhibit thermal conductivity of ~2000 W/m/K, which is five times that of copper (390 W/m/K) and have an electrical resistivity of 10^{-4} Ω-cm.

Carbon nanotubes are synthesized using plasma enhanced microwave CVD. Though there are various techniques available, plasma enhanced microwave CVD was used in this investigation due to its simplicity, ease of scaling up, and better control of the process parameters. Colloidal form of iron oxide is used as a catalyst to grow carbon nanotubes. Experiments are designed to investigate and analyze methods to grow vertically aligned carbon nanotubes with fewer impurities. Since further purification of nanotubes will result in some loss of nanotubes, synthesis of nanotubes with fewer impurities would be preferable for use in various applications directly. The process

parameters and the experimental conditions are varied to investigate the growth of nanotubes. The process parameters investigated include catalyst concentration and method of application of catalyst, plasma pretreatment, variation of pretreatment time, growth time, chamber pressure, and flow rate of methane.

Scanning electron microscopy (SEM), scanning transmission electron microscopy (STEM), energy dispersive spectra (EDS), atomic force microscopy (AFM), and μ-Raman spectroscopy were used to characterize the nanotubes synthesized using the colloidal form of iron oxide as catalyst. The SEM micrographs showed the growth morphology and alignment as well as the impurities present in the nanotubes. The TEM micrographs showed the nanotubes to be multi-walled. Also, they enable in studying the tube diameter, internal structure morphology and surface defects, such as kinks in the tube. AFM is used to analyze the surface defects in the tubes along with diameter analysis. EDS showed the elemental composition of the deposited carbon nanotubes, the catalyst material and the substrate. μ-Raman spectroscopy showed the presence of D and G peaks which are characteristic of the multi-walled carbon nanotubes, thereby validating the TEM results, namely the tubes synthesized are multiwalled.

ACKNOWLEDGEMENT

"Mata Pita Guru Deivam"

The meaning of the adage above is "Mother, Father, Teacher and God is the order of people whom you should go and seek advise and guidance and even god comes only next to the teacher. The teacher by the way of his guidance earns a place above god as he creates, sustains knowledge and destroys the weed of ignorance."

I express my sincere and heartfelt thanks to my teacher and advisor, Dr. Ranga Komanduri, for his technical guidance, financial support, inspiration, motivation and being a great mentor. He gave me wisdom and knowledge in my area of study and that made it possible for me to quickly grow not only technically but also in all various aspects during the course of my M.S study. There are those initial times when there were a lot of hiccups and problems in the area of my study and he was patiently waiting and giving me more opportunities so that I could achieve what I have done now. I respect and salute him from the bottom of my heart.

I also would like to appreciate the encouragement, suggestions and technical guidance from my committee members: Dr. Samit Roy and Dr. Hongbing Lu. I also would like to thank Mrs. Phoebe Doss and Mr. Terry Colberg at the Oklahoma State University Electron Microscopy Laboratory for their help in taking the SEM and TEM pictures. I thank Dr. Elizabeth Catlos at the Geology Department for her help in taking

the EDS data. I also would like to thank Mrs. Sharon Green for her help with the TEM negatives during this study. I also thank the Edmon Low Library for providing an excellent opportunity to browse considerable number of online journals through their website which facilitated this study.

I wish to express my sincere gratitude to Mr. Madhan Ramakrishnan and Mr. Raju Nidadavolu for I have the best friends in them, and are excellent co-workers in the CVD lab and also for riding with me during the tough times and enjoying with me during the happy moments. They have been inspiring me and giving me a helping hand at times when my morale and confidence was low. I would forever remember working with them in the labs. This work was performed in collaboration with them and to meet the university requirements it is divided so that each of us can concentrate on a separate catalyst in the growth of CNTs. Also care was taken during the literature review to avoid overlapping and thereby the work complements each others work. I also would like to thank Mr. Sony Varghese for his help with AFM and PLD techniques. I would also like to extend my gratitude to all other members of our research group for their support and friendship.

I would like to thank the Department of Mechanical and Aerospace Engineering for providing me with the opportunity to pursue M.S at Oklahoma State University.

I do not have enough words of appreciation for my parents, my sister and my family members. If not for their constant support, inspiration and encouragement this goal could not have been realized. They have always wanted to see me come out with flying colors and I dedicate this work to them. Finally, I thank everyone again for being there for me and making this dream possible.

TABLE OF CONTENTS

LIST OF TABLES

LIST OF FIGURES

Figure No. Page

CHAPTER 1

INTRODUCTION

1.1 Introduction to Carbon Nanotubes

Carbon nanotubes are molecular scale carbon fibers with structures resembling that of fullerenes. They were first discovered accidentally by Iijima of NEC Corporation, Japan in 1991 [3]. Carbon nanotubes, abbreviated as CNTs have been investigated extensively in the past few years because of their potential in science and applications in many fields. Since their discovery, numerous scientists have postulated different theories, properties, and preparation techniques. Also the discovery of the nanotubes opened up a wide range of possibilities and options in many fields. Various methods are used to synthesize CNTs, such as arc-discharge, laser vaporization, pyrolysis, high-temperature heat treatment, ion-beam sputtering, chemical vapor deposition (CVD). CVD method is a promising candidate for synthesis of CNTs owing to its simplicity, low cost, low temperature growth, high yield, reasonable purity, and easy scale up.

Carbon nanotubes are stiffer than steel and are resistant to damages from physical forces. These intriguing structures exhibit numerous interesting properties and phenomenon. Carbon nanotubes have a Young's Modulus of ~1 - 1.28 TPa depending upon whether they are single-walled or multi-walled. They have thermal conductivity of ~2000 W/m/K and resistivity of 10^{-4} Ω-cm [70]. They also have a broad range of

electronic, thermal and structural properties which varies depending upon the kind of nanotube such as single walled or multiwalled, their diameter, their chirality and length.

Until two decades ago, just two types of all-carbon compounds were known for certain, the naturally occurring allotropes diamond and graphite. The breakthrough for studying other forms of carbon compounds came from experiments on clusters formed by laser vaporization of graphite. Kroto and Smalley are two scientists who were interested in synthesis of carbon clusters. Both of them along with some colleagues and students did experiments on vaporization of graphite. They were struck with a fascinating result. They observed C_{60} – Buckminsterfullerenes and said closed clusters containing 60 carbon atoms would have a structure of unique stability [1] and symmetry as shown in Figure 1.1. The buckmisterfullerenes are generally known as fullerenes or bucky balls.

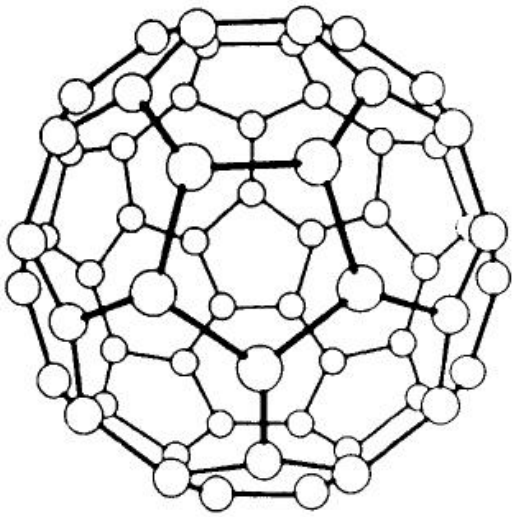

Figure 1.1: C_{60} – Buckminsterfullerene [5]

The experimentation by them involved vaporization of graphite into a high-density helium flow using a focused pulse laser. Also, clusters of up to 190 carbon atoms were formed and it was noted that for clusters of more than 40 atoms, the C_{60} was known

to be the dominant species. The diameter of the C_{60} molecule is ~7 Å, providing an inner cavity capable of holding a variety of atoms [1].

It took some time for further progress because the C_{60} produced by Kroto and Smalley were in small scale. Huffmann and Kratschmer [2] vaporized graphite using a simple carbon arc in helium atmosphere rather than a high-powered laser. The soot settled on the walls of the chamber were collected and dispersed it benzene and subsequently dried to form crystals of "fullerite" which contained 90% C_{60} and 10% C_{70}.

Iijima [3], an electron microscopist from Japan in 1991 discovered molecular carbon fibers consisting of tiny cylinders of graphite, closed at the each ends with caps consisting of six pentagonal rings. He also used the similar arc deposition apparatus such as the one used by Huffmann and Kratschmer but instead of concentrating on the carbon soot he concentrated on the deposit formed on the cathode. His experiments and analysis on those cathodes revealed novel cylindrical carbon structures which were named carbon nanotubes (CNTs). Also the carbon nanotubes observed by Iijima were multi-walled, such as tubes with 2 walls, 5 walls and 7 walls, but two years later he then observed single walled nanotubes [4].

1.2 Nomenclature of nanotubes and their split personality

Single walled nanotubes (SWNTs) can be imagined as rolled up sheet of graphene (an isolated graphitic crystal monolayer) with caps on both ends similar to half of a fullerene molecule. Based on the way the graphene sheets are rolled up, the chirality and the property of the nanotube varies.

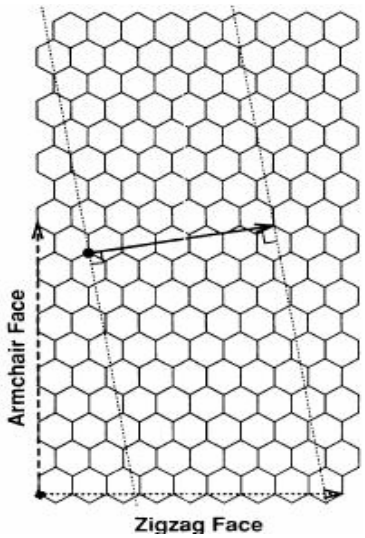

Figure 1.2 – Graphene sheet with chiral vectors [6]

The honeycomb lattice representing the single atomic layer of crystalline graphite (graphene sheet) is as shown in Figure 1.2. Single walled nanotubes are obtained by rolling up this graphene sheet to form a seamless cylinder along different chiral axes. The heavy dotted line in Figure 1.2 shows the armchair face axis, the dotted line the zigzag face axis and the solid line represents the chiral face axis [6]. When the sheet is rolled up with these axes, we get "armchair" nanotubes, "zigzag" nanotubes, and "chiral" nanotubes, respectively.

Technically speaking the tubes are named depending on the chiral angle θ between the chiral vector and the zigzag direction. The zigzag nanotube corresponds to chiral angle $\theta = 0°$ and armchair nanotube corresponds to $\theta = 30°$ and the chiral nanotube corresponds to $0° < \theta < 30°$ [7]. Figure 1.3 shows schematics of different models of nanotube nomenclature based on their chirality.

The SWNTs with different chiral vectors exhibit different properties, such as the variation in the mechanical strength, electrical conductivity, optical properties. In other words, it can be said that the SWNTs exhibit a split personality depending on the chiral

vector. A graphene sheet as such is semimetallic with zero band gap. The electrical properties of the nanotubes depend on the (m, n) indices and therefore on the diameter and chirality of the nanotube. Researchers have predicted that the (m, m) armchair tubes should be always metallic as the electronic lines always cross the corner points. For (m, n) nanotubes with $(m - n) \neq (3 \times \text{integer})$ the electronic lines misses the corner points and the tubes are semiconducting. For $(m - n) = (3 \times \text{integer})$, certain lines cross through the corner points and the tubes are semimetals but become small gap semiconductor due to curvature induced. Carbon nanotubes thus have the unique sensitivity of electronic properties on structural parameters and these concerns posses a challenge during synthesis of the tubes [7].

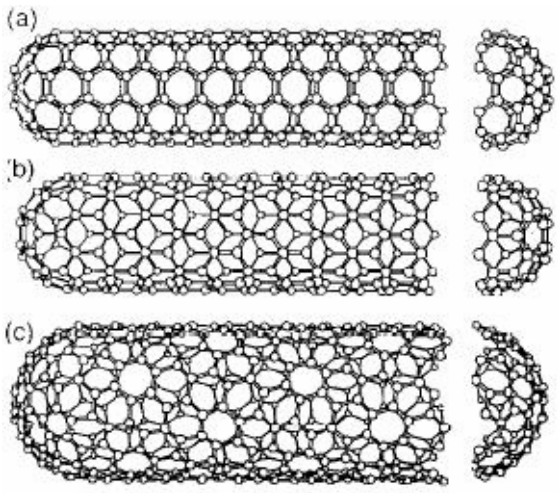

Figure 1.3 – Schematic models of SWNTs (a) armchair (b) Zigzag and (c) chiral [7]

Figure 1.4 shows a 2D graphene sheet with indices for vectors specifying different chiral nanotubes. Thus far carbon nanotubes have been used in building prototypes of functional devices for particular use and ensembles of nanotubes are used in the modern day composites with enhanced mechanical properties, field emitters for flat

panel display, tips for scanning probe microscopy, nanotweezers and chemical sensors. These real world applications of nanotubes require them in bulk quantities in kilograms to tons to become more simple and efficient. Considerable challenges are faced and some problems include having a better control of the chirality during growth, growing defect-free nanotubes to macroscopic lengths etc. Researchers are working and arriving at solutions to tackle these issues and overcome them [8].

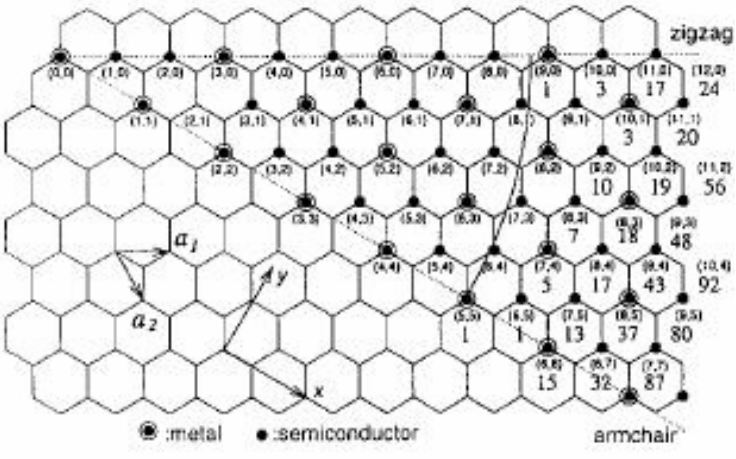

Figure 1.4 – 2D graphene sheet with the vectors specifying different chiral nanotube

1.3 Thesis Overview

This research involves the use of CVD techniques for the synthesis of CNTs using iron oxide in colloidal form as a catalyst. Though there are various CVD techniques available, Microwave Plasma Enhanced CVD (MPECVD) is used as it provides better yield, better alignment and better control over the process compared to other techniques. Also this technique requires much lower temperature compared to arc-discharge and laser ablation techniques which help the tubes to be used in microelectronics as tubes grown at lower temperature are more suited for microelectronics. There are a number of parameters which are common in various CVD techniques, such as the gas compositions

and the gas pressure. But there are other parameters which are technique specific, such as the gas activation modes which leads to different deposition rates and efficiency.

The size of the reactor, the geometry of the materials used, the source of plasma power, the design of the reactor and the process parameters determine the efficiency of CNT formation. CVD techniques can be used to form CNTs on various substrates of interest and the process is relatively inexpensive. Considerable research is directed in this area due to this reason. However still a number of problems exist in terms of alignment of the nanotubes formed, yield and problems relating to the separation of the tubes and purification so that individual tubes are used for a specific purpose.

The objectives of this research are to evaluate the effects of various process variables and to optimize the synthesis of CNTs on a silicon wafer substrate using a colloidal form of iron oxide as a catalyst. Also, microstructural characterization with scanning electron microscope (SEM), scanning transmission electron microscope (STEM) and atomic force microscope (AFM) was done for morphology analysis. Elemental characterization is done using Energy dispersive x-ray spectra (EDS). μ-Raman spectroscopy was used for in-depth characterization to determine the phase purity.

1.4 Thesis Outline

A brief description of the thesis outline and the description of each chapter in this thesis are given in the following: Chapter 1 gives a brief introduction to carbon nanotubes, how they were discovered accidentally and the unique structure of nanotubes, their nomenclature and split behavior and a brief overview of this thesis study.

Chapter 2 narrates in detail the different methods and processes used for the synthesis of carbon nanotubes giving an insight into those processes.

Chapter 3 presents the literature review on the history of carbon fibers, history of carbon nanotubes and a brief timeline of the nanotubes, exciting properties that the nanotubes posses, the applications where they are used. Also this chapter describes the catalyst that can be used for the nanotube growth, the growth mechanism of the nanotubes, the effect of the process gases and the effect of the process parameters.

Chapter 4 provides the problem statement describing the rationale and motivation behind the growth and synthesis of carbon nanotubes on substrates using colloidal form of iron oxide as a catalyst.

Chapter 5 deals with the description of the experimental setup and methodology. It also describes the catalyst deposition and the nanotube growth procedure.

Chapter 6 presents the characterization techniques used in this investigation.

Chapter 7 discusses in detail the growth and synthesis of carbon nanotubes, the variation in the growth process due to the variation in the process parameters and the process gases.

In Chapter 8, the results obtained due to the variation in the process parameters and the process gases are further discussed elaborately.

Chapter 9 finally draws conclusions based on this investigation and outlines the future work and its scope.

Appendix A narrates the specifications of the various instruments and apparatus used in this study.

CHAPTER 2

LITERATURE REVIEW ON CARBON NANOTUBE SYNTHESIS TECHNIQUES

The discovery of carbon nanotubes in 1991 marked the beginning of a new and prolific research area bringing together scientists from varied fields including carbon science, physics, chemistry, mechanical engineering, and materials science. These scientists have developed different techniques for the synthesis of carbon nanotubes and these are discussed elaborately in this chapter. Widely used techniques in the synthesis of carbon nanotubes are the arc discharge method, laser ablation technique, pyrolysis of hydrocarbon, and plasma assisted chemical vapor deposition (CVD).

2.1 Arc Discharge Process

Kratschmer – Huffman technique [2] for producing C_{60} was slightly modified by Iijima [3] for producing carbon nanotubes. In his method, the graphite electrodes are kept a short distance apart from each other during arcing rather than being kept in contact. Some of the carbon under these circumstances evaporate and re-condense in the cathode to form hard cylindrical deposits. In the central part of the deposits, Iijima found these deposits to carbon nanotubes and nanoparticles after characterization. This was a great breakthrough in the field of carbon sciences even though Iijima found out the yield of the

tubes to be very low. In order to overcome this low yield problem, Ebbesen and Ajayan [9] made significant modifications to Iijima's procedure and overcame that problem.

A schematic of the arc-evaporation apparatus is shown in Figure 2.1 [10]. Two graphite rods act as electrodes and the chamber is usually connected to both the vacuum pump and to the helium supply. Anode is usually a long rod with 6 mm in diameter and the cathode is a shorter rod of about 9 – 13 mm diameter. The more the cathode is water-cooled the better the quality of the tubes synthesized. A voltage stabilized DC power supply is used and the discharge voltage is usually ~20V and the discharge current ~50 - 100 A.

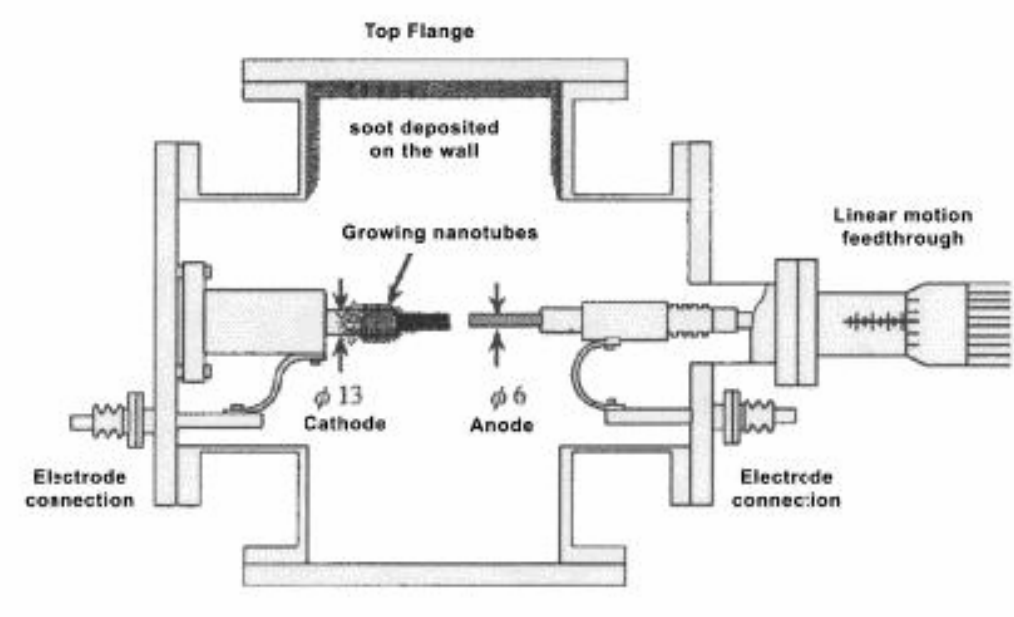

Figure 2.1 – Schematic of an Arc Discharge apparatus [10]

The anode is moved slowly towards to the cathode using the feedthrough mechanism until arcing occurs. A gap of 1 mm or less is maintained between the rods and the rods are usually consumed at a rate of a few mm per minute. The quality and yield of he tubes rely on a number of factors, crucial among which are the pressure of helium in

the chamber and the current. The yield is found to increase with pressure before attaining saturation and high current results in fewer nanotubes. Efficient cooling of the electrodes is found to result in good quality of tubes.

2.2 Condensation of Carbon vapor method

In 1992, Chernozatonskii *et al.* [11] proposed a method of nanotube production wherein an electron beam is used to evaporate graphite in high vacuum (on the order of 10^{-6} Torr). The condensed material is collected on a quartz substrate and the examination on the condensate revealed the presence of nanotubes. Ge and Sattler [12, 13] used a slightly different method for nanotube production wherein a carbon foil is heated resistively to produce a carbon vapor which was condensed onto a highly oriented pyrolytic graphite (HOPG) at a pressure of ~ 10^{-8} Torr.

2.3 Laser Ablation Method

Smalley and his team of researchers at the Rice University developed a method of laser ablation and vaporization for producing nanotubes in 1995 [14]. They used a neodymium-yttrium-aluminum-garnet (Nd-YAG) laser to vaporize a graphite target in a temperature controlled quartz tube. The carrier gas used is usually argon or helium. The quartz tube is heated to 1200°C, a much lower temperature than was previously necessary for making nanotubes.

The Nd-YAG laser is aimed at the graphite target thereby vaporizing it. When this carbon vapor comes into contact with the water cooled copper cathode they condense to form nanotubes. The nanotubes condensed in this form like a felt and can be scrapped off

for further investigation. One advantage of this method is that it is found to produce good quality single walled carbon nanotubes. The schematic of the laser ablation technique is shown in Figure 2.2.

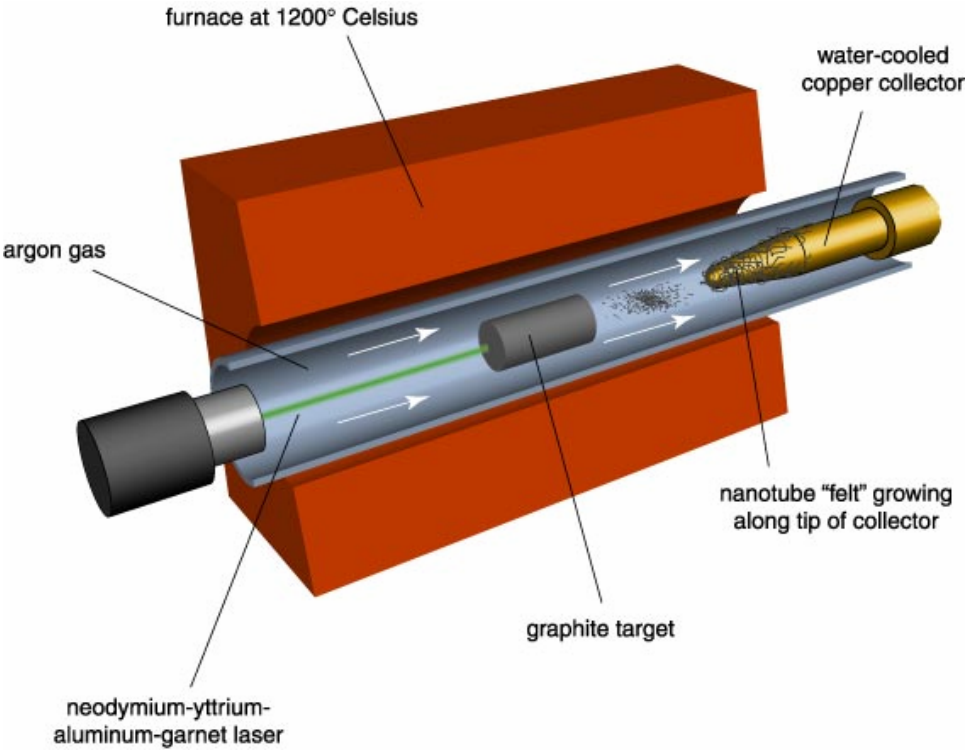

Figure 2.2 – Laser ablation method [14]

Scientists are trying to scale up this technique because of good quality of carbon nanotubes obtained. They have formulated two developments for the large scale synthesis of SWNTs – the ultra fast pulses from a free electron laser method and continuous wave laser-powder method.

2.3.1 Ultra Fast Pulses from Free Electron Laser (FEL) method

Eklund *et al.* [15] proposed a method for large scale synthesis of SWNTs using a laser. In order to obtain ultra fast pulses, the repetition rate has to be increased. The repetition rate of the laser is increased from 10 Hz to 75 MHz and in order to give the

beam higher energy than the Nd:YAG laser. The beam is focused using a lens beyond which the intensity of the laser is ~5 X 10^{11} W/cm^2 – about 1000 times that of the Nd:YAG laser. Schematic of the apparatus used is shown in Figure 2.3 where a metal loaded graphite target is used as target. The target is held in position by a spindle which rotates around its axis. A sonic shearing jet of preheated argon at 1000°C is directed in such a way as to carry away the vaporized carbon deposit on a cold collector. By using only ~20% power the yield was ~1.5 g/h and when the laser is operating at its full capacity this can increase to ~45 g/h which is really a significant yield rate compared to the regular laser ablation techniques.

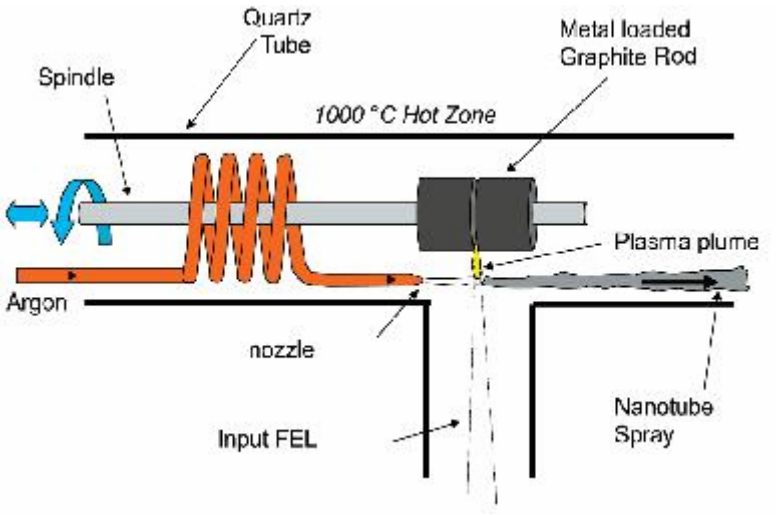

Figure 2.3 – Ultra fast pulses from free electron laser (FEL) method [15]

Another method was also proposed for the high production rate of carbon nanotubes based on the continuous wave CO_2 laser powder method.

2.3.2 Continuous Wave laser-powder method

A novel method for high production of carbon nanotubes involves laser ablation of graphitic and metal catalytic particles in the form of fine powder by a 2-kW

continuous wave CO_2 laser in argon or nitrogen atmosphere [16]. Thermal conductive losses are decreased significantly due to micrometer sized particles introduced in this system as compared to conventional laser ablation. This evaporates the powder material in a much efficient manner. A schematic of the experimental setup is shown in Figure 2.4.

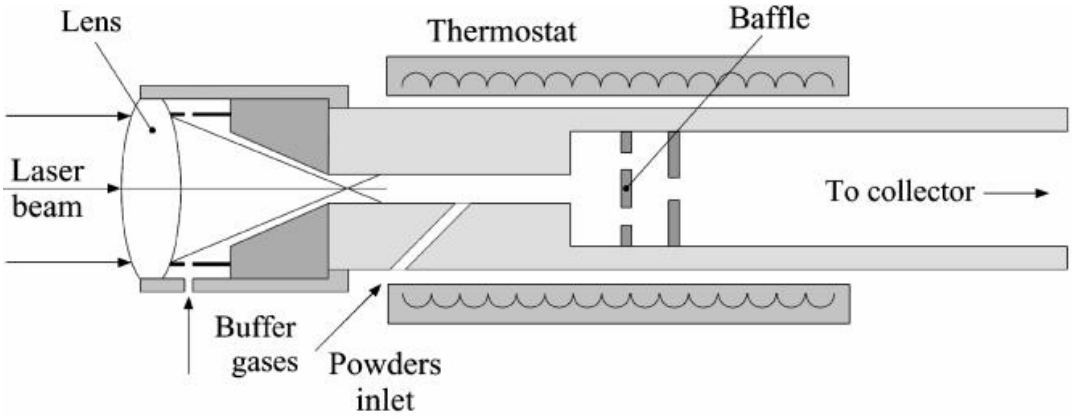

Figure 2.4 – Continuous wave laser-powder method [16]

The laser beam is focused by a NaCl lens into a narrow flow tube where the graphitic and metallic particles are dispersed in through a buffer gas which is usually argon or nitrogen. The laser effectively vaporizes the graphitic and metal particles and the soot deposits on the walls of the reactor. The yield rate was found to be ~5 g/h.

2.4 Pyrolysis of hydrocarbon

Endo and his team along with some workers from Sussex [17-19] showed that multiwalled nanotubes can be produced by pyrolysis of benzene in the presence of hydrogen. Benzene vapor and hydrogen are introduced into a ceramic reaction tube where a graphite rod in the centre acts as a substrate. The temperature is raised to 1000°C and held for an hour before cooling it to room temperature by flushing with argon. The

deposited material is scrapped off and subjected to 'graphitizing' heat treatment at 2500-3500 °C for ~10 minutes. TEM analysis on the material showed the presence of multiwalled carbon nanotubes.

Vander Wal and Ticich [20] used an ultrasonic nebulizer to create a fine aerosol of nanocatalyst particles and a dryer operating at 140°C to create metal particles from aerosol. The aerosol is made from ferrofluid or a metal nitrate solution. The dryer operates in an inert gas or CO environment. The gas flow is now combined with the reactive gases and let into the tube furnace for pyrolysis flame. The reactive gases are usually CO or C_2H_2 combined with H_2. On reaching a temperature of about 200°C the reduction of the aerosol into metal particles takes place first and then carbon nanotubes are formed. This synthesis requires much lower temperatures compared to previous methods. The pyrolytically formed nanotubes are collected using thermophoretic sampling where the aerosol from the flame is passed over a cold surface and the tubes are collected by the difference in the temperature gradient.

2.5 Electrolysis

Hsu *et al.* [21, 22] synthesized multiwalled carbon nanotubes by electrolysis of molten lithium chloride using a graphite cell. A graphite crucible acting as an anode and a graphite rod as cathode are immersed into the melt. A 30A current is passed for a minute and then allowed to cool. Water was added to dissolve the lithium chloride and left for 4 hours. Toluene was then added and agitated for several minutes. This results in the solid material passing into the toluene layer and separated by decanting. TEM

analysis showed the nanotubes to be imperfect multiwalled carbon nanotubes accompanied with some nanoparticles.

2.6 High Pressure Carbon Monoxide (HiPCO) disproportionation

Gas-phase catalytic process has been used for the production of SWNTs by thermal decomposition of the catalyst containing materials by the flow of carbon monoxide at pressures of about 1-10 atm and temperature of 800-1200°C. The process parameters are varied and controlled to get desired yield and diameter. This process is capable of producing carbon nanotubes in bulk and diameters ranging from 0.7 nm to a few nanometers.

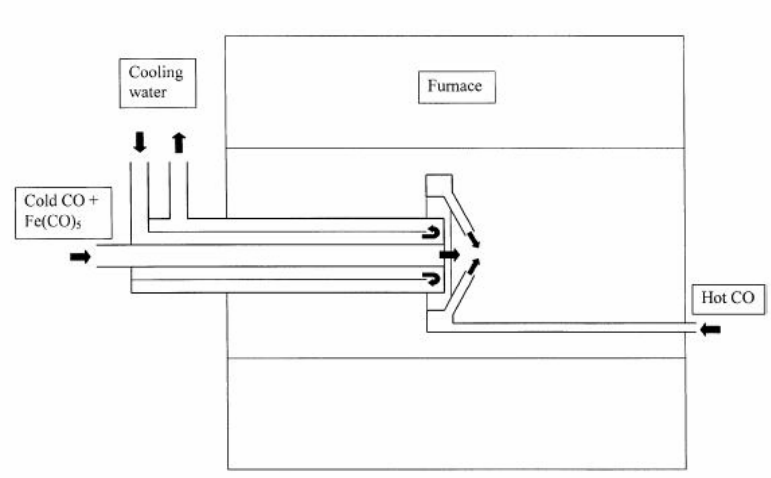

Figure 2.5 – Schematic of High Pressure Carbon Monoxide method (HiPCO) [23]

Smalley *et al.* [23] at the Rice University produced SWNTs by HiPCO process. The experimental setup for the production of SWNTs is shown in Figure 2.5. Iron pentacarbonyl ($Fe(Co)_5$) is used as the catalyst containing precursor and carbon monoxide (CO) is used as carbon feedstock gas. Iron pentacarbonyl is thermally decomposed in the gas phase to produce clusters of iron which in turn act as nuclei for

the growth of CNTs. The Boudouard reaction states that CO disproportionation results in solid carbon and this occurs and settles on the surface of the catalyst particles.

$$CO + CO \rightarrow C\,(s) + CO_2 \quad \text{(Boudouard Reaction)}$$

Similar type of apparatus and catalytic particle was developed by Tibbetts *et al.* [24] of General Motors Corporation in production of CNTs wherein methane was used as the carbon feedstock. Tibbetts has been working in the field of carbon science for quite some time and is a pioneer in this field. Even before the discovery of carbon nanotubes by Iijima, Tibbetts has made significant contribution where he identified them as carbon filaments rather than carbon nanotubes.

2.7 CoMoCat Process

Resasco *et al.* [25] at The University of Oklahoma developed a process known as CoMoCAT process (cobalt molybdenum catalytic process) for the synthesis of SWNTs. SWNTs are grown by dissociation of CO into C and CO_2 at a total pressure ranging from 1 to 10 atm and temperature ranging from 700 - 950°C. They found a synergetic effect between the catalysts Co and Mo is necessary for the effective production of SWNTs. Co and Mo catalysts are dispersed on a silica support and if separated, the catalysts are either inactive (Mo) or unselective (Co). This unique Co-Mo catalyst inhibits the sintering of Co particles and also inhibits the formation of other undesirable forms of carbon. Cobalt is progressively reduced to its metallic form and molybdenum is converted into Mo_2C. The carbon from the decomposition of the CO gas diffuses onto the metal particles. Once the given configuration and carbon surface concentration are reached they develop into SWNTs. The schematic of the reactor used in CoMoCAT process is shown in Figure 2.6.

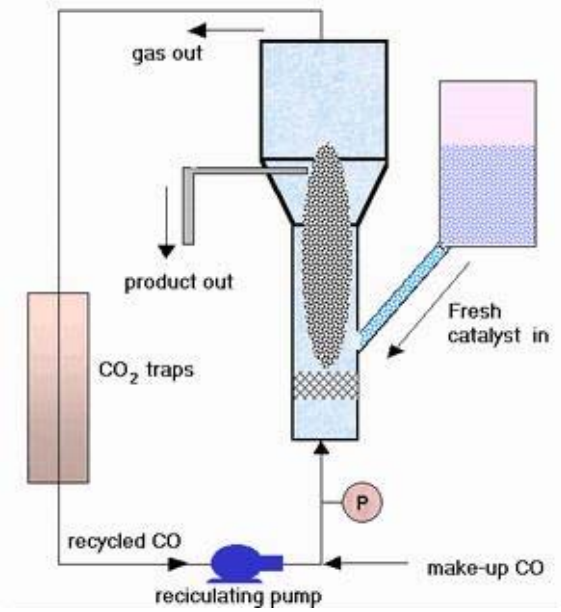

Figure 2.6 – CoMoCAT process [25]

The advantage of this process is that it can be scaled up and it operates under less severe conditions compared to other processes. It also helps to have a better control in the structural characteristics of the nanotubes. Because of its simplicity, it is reported that this process can synthesize SWNTs at much lower costs.

2.8 Chemical Vapor Deposition (CVD)

Chemical vapor deposition (CVD) process requires a catalyst material to be heated to a high temperature in a tube furnace and a hydrocarbon gas is allowed to flow through the tube reactor for a stipulated period of time. The schematic of the set up is shown in Figure 2.7. On cooling the reactor and its contents to room temperature, the materials grown over the catalyst are collected [26]. The transition metals are generally used as effective catalyst particles. Important parameters for the growth of nanotubes are hydrocarbon gas and its flow rates, catalysts, and the growth temperatures. The reason for

choosing these metals as catalyst for CVD growth of nanotubes lies in the phase diagram for the metals and carbon.

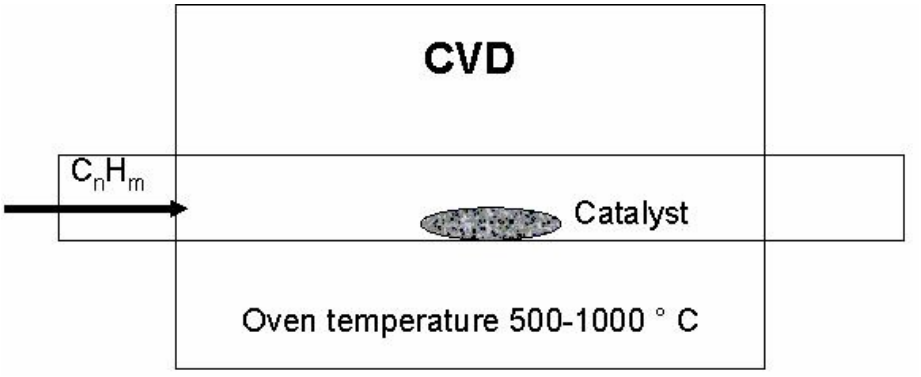

Figure 2.7 – Schematic of chemical vapor deposition (CVD) for CNT synthesis [26]

A major drawback for the growth of nanotubes by the CVD techniques is the MWNTs grown are prone to high defects compared to SWNTs produced by laser ablation or arc discharge. This may be accounted to the temperature difference in the methods. The CVD technique generally requires a much lower temperature for CNT synthesis compared to arc discharge or laser ablation. Also, CVD techniques produce SWNTs which are defect-free.

There are different methods of chemical vapor deposition techniques employed in the synthesis of CNTs. Thermal CVD, hot filament CVD, plasma enhanced CVD, microwave assisted CVD are some of the different CVD techniques used in the synthesis of CNTs.

2.8.1 Thermal CVD

Thermal CVD produces both SWNTs and MWNTs. Single-wall nanotubes were synthesized by using thermal CVD process (Figure 2.8). The optimized catalysts consist of Fe/Mo bimetallic species supported on a novel silica-alumina multicomponent

material. Typically, 0.1 g of the catalyst was placed into a quartz boat and kept in the center of a 1 in diameter quartz tube mounted in an electric tube furnace. Argon gas was flown over the catalyst as it was heated from room temperature to 900 °C. The reaction begins as argon is replaced by CH_4 (flow rate 6000 sccm) for the desired reaction time (2-45 min). The flow is then switched to argon and the furnace is cooled to room temperature. When producing large quantities of SWNTs typically 5g of catalyst was used and the CVD reaction time was 30 min. The nanotubes consist of individual and bundled SWNTs that are free of defects and amorphous carbon coating [27].

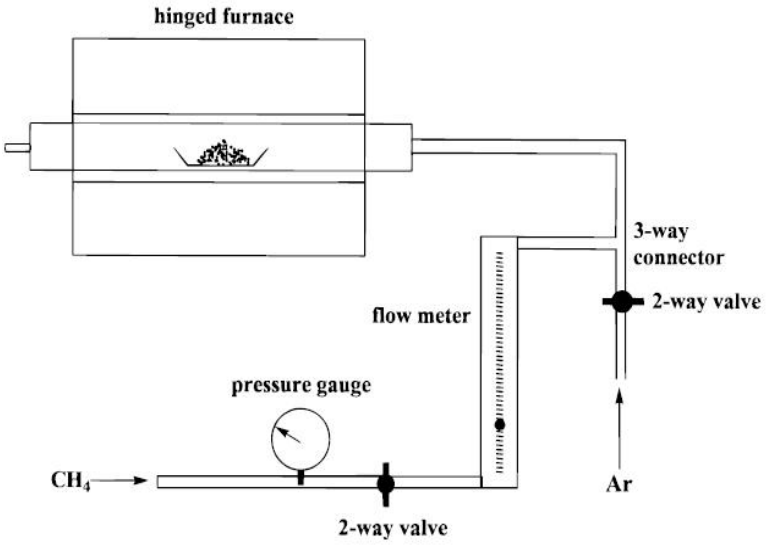

Figure 2.8 – Schematic of a thermal CVD [27]

Andrews *et al.* [28] used the experimental setup shown in Figure 2.9 for the synthesis of high purity aligned MWNTs through catalytic decomposition of ferrocene - xylene mixture.

A two-stage tubular quartz reactor wherein approximately 6.5 mol% of ferrocene is dissolved in xylene is used as a feedstock and fed continuously into the reactor using a syringe pump. Ferrocene (sublimation temperature ~140°C) is chosen as the catalyst as it is shown to be a good precursor for producing Fe catalyst particles which can seed

nanotube growth. Xylene is chosen as the carbon source gas as it boils (boiling point ~140°C) below the decomposition temperature of ferrocene (~190°C). Prior to its entry into the furnace the liquid feed is preheated to ~175°C in a capillary tube. At this temperature, the liquid exiting the capillary is immediately volatilized and swept into the reaction zone of the furnace by argon flow with 10% hydrogen.

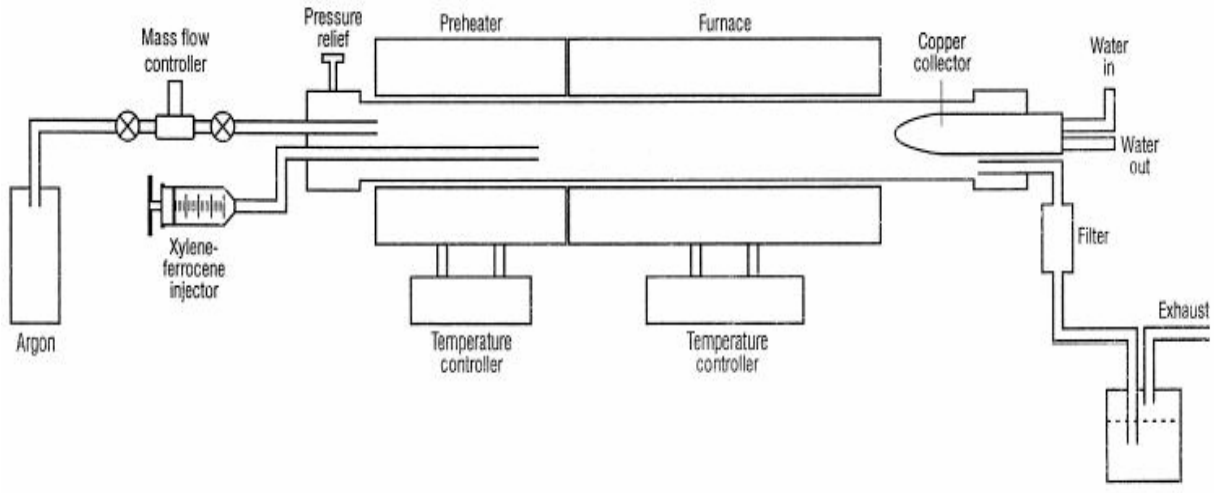

Figure 2.9 Thermal CVD apparatus [28]

Various parameters, including the furnace temperature (650–1050°C), ferrocene to xylene ratio and feed rate, total reaction time, and argon gas flow rate were adjusted to determine the growth conditions for high purity aligned MWNTs. After the reaction, the preheater and the furnace were allowed to cool to room temperature in flowing argon. The carbon deposits formed on the furnace tube and the substrates when subjected to SEM and TEM characterization revealed the presence of MWNTs.

2.8.2 Hot-Filament CVD (HFCVD)

Okazaki *et al.* [29] describe a method for the synthesis of SWNTs and MWNTs using hot filament CVD (HFCVD). Pure alcohol vapors (ethanol, methanol and 2-

propanol) were used as the carbon gas source. The schematic of the hot filament CVD apparatus is shown in Figure 2.10.

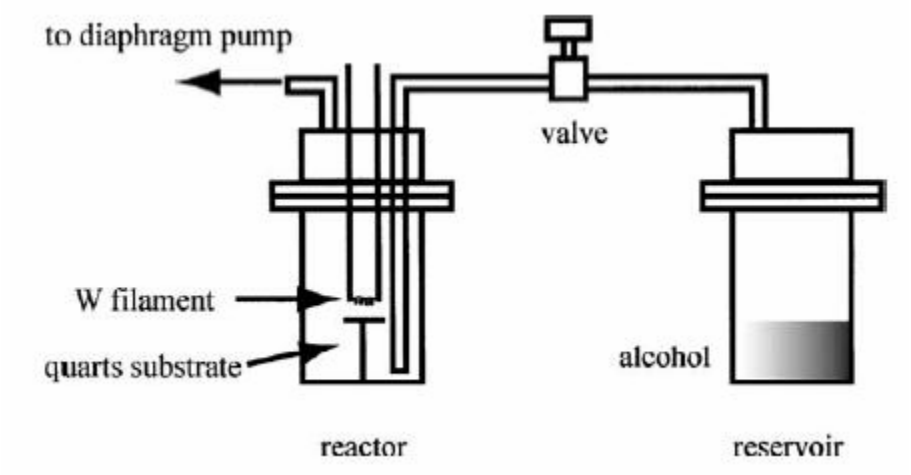

Figure 2.10 – Hot filament CVD apparatus [29]

The alcohol reservoir and the reactor both are made of glass and in the reactor the tungsten filament is set approximately ~3 mm from the quartz substrate. The catalyst precursors used are iron acetate and cobalt acetate and are supported using zeolite support materials. They are sonicated for 30 min and dried at 80°C for one day. The resultant powder is taken in the quartz substrate and loaded in the reactor. The alcohol vapors from the reservoir are decomposed by the high temperature tungsten filament heated from 1200°C– 1800°C. A black soot is deposited in the substrate even after a short reaction time of 30 sec. SEM and TEM images confirms the presence of SWNTs and MWNTs.

Chaisitsak *et al.* [30] also used HF-CVD employing a carbon filament for the synthesis of single-walled nanotubes using C_2H_2 and H_2 as reactive gases. Sol-gel method is used for preparing the catalyst iron-cobalt supported on silica. This sample is loaded onto a quartz reactor. The reactor consists of a quartz reaction tube, a carbon filament, a substrate holder, a DC power supply and a rotary pump. The loaded sample in the reactor is calcined in H_2 environment for 5 min, 450 Pa, and 600°C. Then, C_2H_2 was introduced

into the reactor and the total flow rate, growth pressure and growth time were 100 sccm, 250-750 Pa, and 20 min, respectively. Raman scattering, X-ray diffraction and SEM techniques were used to characterize the SWNTs synthesized by this process. The apparatus used in the process is shown in Figure 2.11.

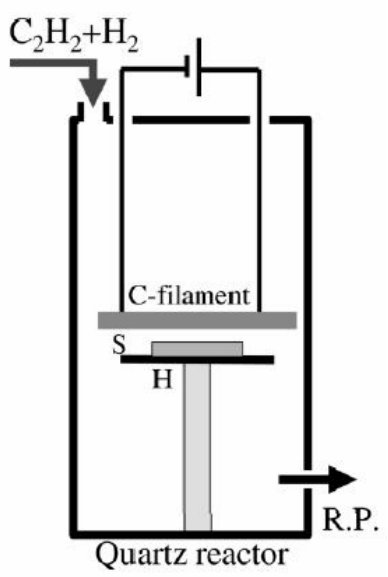

Figure 2.11 – Schematic of Hot filament CVD [30]

2.8.3 Plasma Enhance CVD (PECVD)

Meyyappan *et al.* [31] used a RF-plasma enhanced CVD technique for the synthesis of MWNTs on silicon substrates coated with a multilayered Al/Fe catalyst. The reactor is inductively coupled and high density plasma is formed from methane and hydrogen mixture. Schematic of the reactor used in the experimental setup is shown in the Figure 2.12. The reactor has two electrodes – the upper and the lower electrodes. The upper electrode has six turns of copper-coil inductively coupled to the plasma by a pyrex window. The lower electrode is heated by a resistive coil heater and both the electrode and the coil are heated by rf generators.

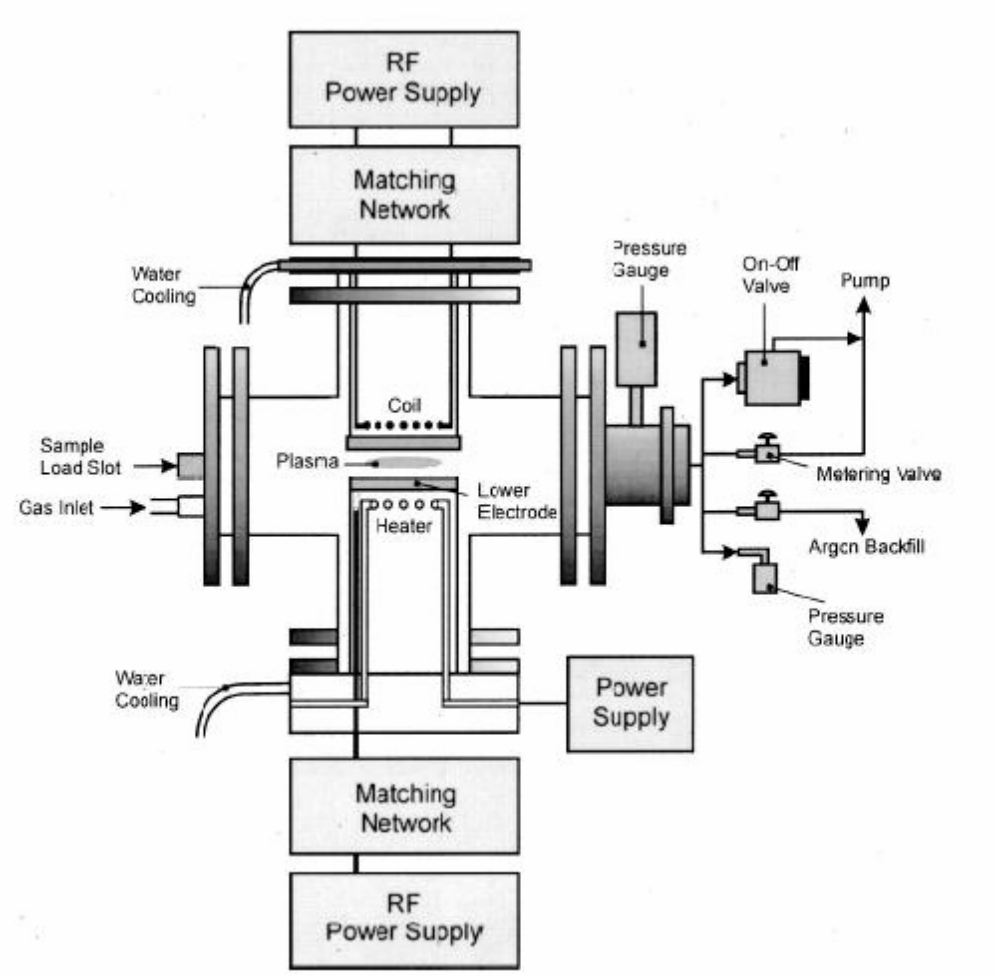

Figure 2.12 – Schematic of Plasma Enhanced CVD [31]

Thin layer of Al followed by Fe is coated as catalyst by ion beam sputtering onto silicon substrate. The substrate was heated to desired temperature by a substrate heater. Argon is flushed during loading and unloading the sample. The reactive gases methane and hydrogen at high temperature forms plasma and the process time is 10 mins. The substrate temperature is slowly lowered to under 300°C before exposure to air. They studied the effect of temperature and power in optimizing the synthesis of MWNTs. HRTEM, Raman spectra and SEM were used to characterize the tubes produced by this process.

A low frequency RF-PECVD is used to synthesize CNTs on silicon substrates covered with diamond-like carbon film and iron catalyst film by Yu *et al.* [32]. E-beam evaporation is used to deposit iron catalyst film on already diamond-like carbon coated silicon wafers. Spinose like CNTs are grown on this substrate by using $C_2H_2 - H_2$ as reactive gases in a low frequency rf power generator. The good contact of carbon nanotube with DLC film was acquired by the accumulation of the graphite sheets and the reaction between the iron particles and DLC film. The CNTs were characterized using Raman spectra and scanning electron microscopy.

Apart from RF-PECVD, plasma enhanced HFCVD is also used to grow nanotubes. One such technique was employed by Ren *et al.* [33] using acetylene as a source gas to grow highly oriented carbon nanotubes. Also, Microwave plasma enhanced CVD (MPECVD) is used to produce nanotubes. The use of MPECVD for the synthesis of CNTs is discussed in the next section.

2.8.4 Microwave Plasma Enhanced CVD (MPECVD)

Qin *et al.* [34] used plasma enhanced microwave CVD to produce carbon nanotubes. Hydrogen and methane were used as the source gases and iron particles reduced from ferric nitrate were used as the catalyst particles. Figure 2.13 is a schematic diagram of the MPECVD experimental setup used.

Alumina substrates were first coated with ferric nitrate [$Fe(NO_3)_3.6H_20$] solution. This substrate was placed into the apparatus and on treatment with the plasma the ferric nitrate was reduced to iron catalytic particles for seeding the growth of nanotubes. A

mixture of methane and hydrogen is introduced into the chamber for the growth of carbon nanotubes at a pressure of 15 torr and a microwave power of 600 W. The growth took place when the substrate was heated to a temperature of about 850°C-900°C. The nanotubes produces by this process was characterized using scanning electron microscopy.

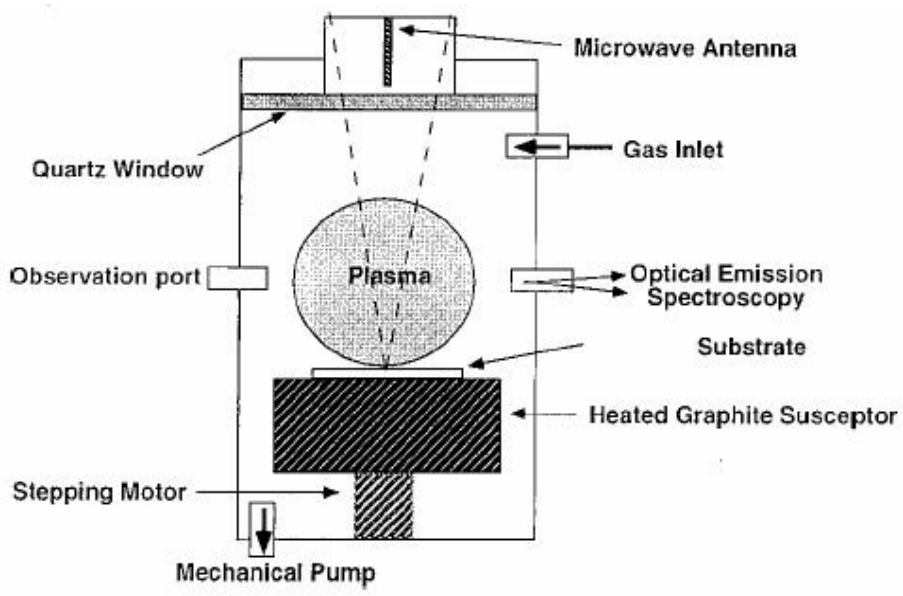

Figure 2.13 –Plasma Enhanced Microwave CVD [34]

A similar technique was used by Choi *et al.* [35]. They used rf-ion sputtering for coating a thin layer of Ni film onto the silicon substrates and then the samples. Plasma was used to reduce the nickel film into nanoparticles. They also reported that density and length of nanotubes depend on the temperature of growth. They also reported that curly tubes were formed at low temperature and self-aligned tubes were formed at high temperature. Methane and hydrogen were the reactive gases used and growth temperature was varied from 520°C-700°C. The characterization techniques employed were SEM, HRTEM, Raman spectroscopy, AFM and X-ray diffraction.

2.8.5 Electron Cyclotron Resonance CVD (ECRCVD)

Sung *et al.* [36] used an ECRCVD apparatus for the synthesis of nanotubes because the ECRCVD provides a higher plasma density at lower temperatures compared to other CVD processes such as rf, hot filament or microwave assisted CVD systems. Chen *et al.* [37] also used an ECRCVD method to grow carbon nanotubes on silicon wafers sputter coated with a Co catalyst. The process temperature was ~600°C and the power was 800 W. They also used a mixture of methane and hydrogen as the source gas. Apart from just synthesizing the tubes they emphasized that because of the defects in the nanotubes they are hard to implement for any application. They also reported the two step process of removing the metal particles by treating the CNTs for an hour in nitric acid and hydrochloric acid. The resulting nanotubes were found to be free of metal impurities. Wang *et al.* [38] also used an ECR-CVD reactor for CNT synthesis. A schematic of the reactor used by them is shown in Figure 2.14.

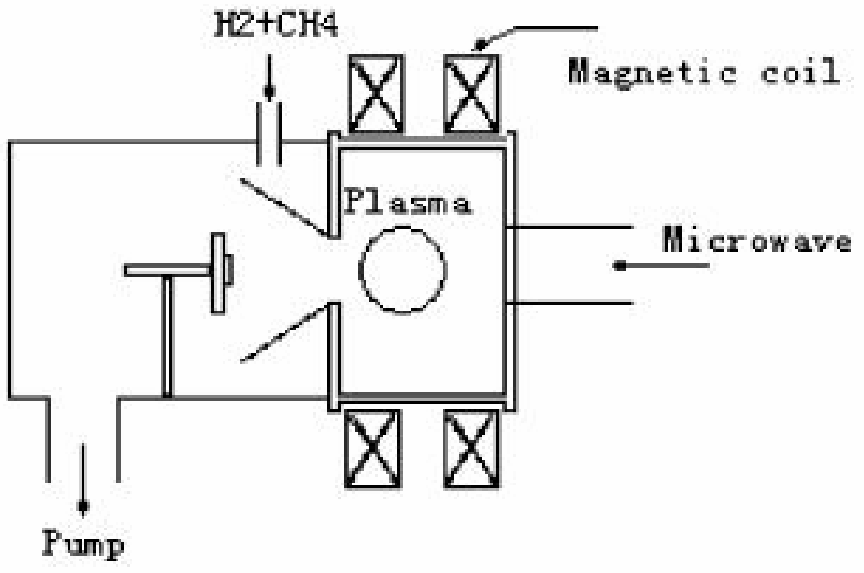

Figure 2.14 – Schematic of Electron Cyclotron Resonance CVD

2.8.6 Alcohol Catalytic Chemical Vapor Deposition

Zeolite supported iron or cobalt catalytic particles are used by Miyauchi *et al.* [39] for diffusion of the evaporated vapors from alcohol, methanol and ethanol thereby forming SWNTs. Alcohol catalytic CVD (ACCVD) was used for the large scale production of SWNTs at low cost and also at relatively low temperature of ~550°C. Schematic of the experimental setup is shown in Figure 2.15. The catalyst placed in a quartz boat is kept into a quartz tube and both into the electric furnace. The quartz tube was evacuated with a rotary pump. Alcohol vapors from the reservoir was let into the reactor at a pressure of 10 torr and after the reaction the apparatus was turned off and cooled down to room temperature to obtain the SWNTs.

The hydroxyl radical from the decomposition of alcohol facilitates in the removal of carbon atoms with dangling bonds thereby resulting in the production of SWNTs with high purity. This process is reported to be capable of scaling up for large scale synthesis of SWNTs with high purity at relatively low temperatures. Since this is a low temperature process, it can also be used for direct growth of SWNTs on semiconductor devices.

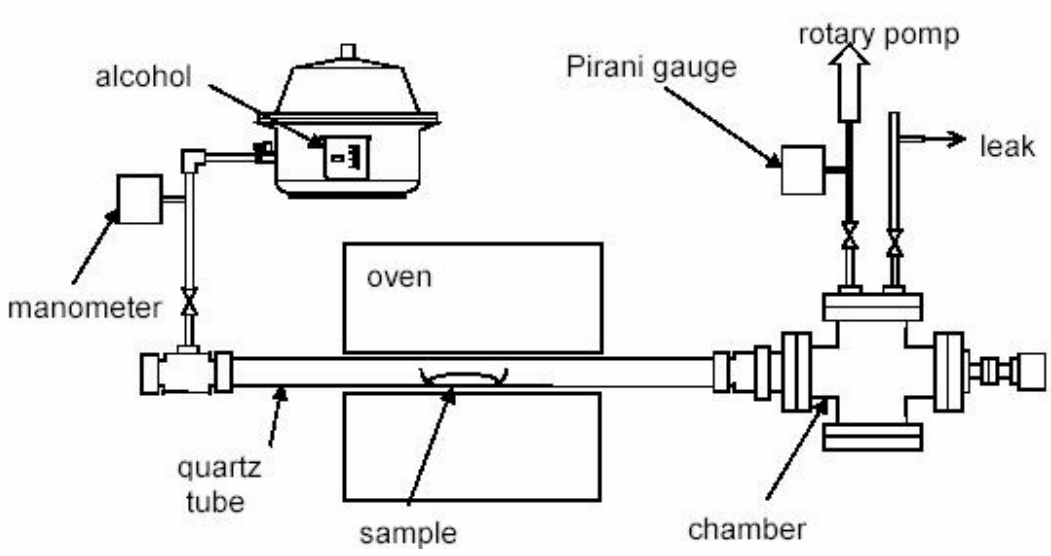

Figure 2.15 – Schematic of an Alcohol Catalytic CVD Reactor

2.9 Other Methods

2.9.1 Carbon Ion Bombardment

Carbon ion bombardment is also another method that is used for the synthesis of carbon nanotubes and carbon whiskers [40]. Carbon whiskers are high crystalline graphitic material whose diameters ranges from ~ 0.1 – 1 μm and several mm in length. Vaporization of carbon takes place in high vacuum by means of ion or electron irradiation and the deposit is collected in a cold surface. The deposit contains carbon nanotubes and whiskers along with other materials.

2.9.2 Use of solar energy to synthesize SWNTs

In this method solar energy is focused onto an experimental crucible and a temperature of 3000 K can be achieved on a sunny day [41]. Ni and Y catalysts mixture is used in an argon atmosphere at a pressure of ~ 450 mbar and CNTs are grown.

Very little is known about the process parameters and efficiency of the last two techniques. Optimization should be done in order to increase the nanotube yield and decrease the carbon nanoparticle impurities and amorphous carbon produced.

This chapter thus gives an overview of various synthesis methods for growing carbon nanotubes. The next chapter will deal in detail with the literature review of carbon nanotubes.

CHAPTER 3

LITERATURE REVIEW ON CARBON NANOTUBES

3.1 History of Carbon Fibers

Carbon fibers are macroscopic analog of carbon nanotubes and their history is stimulated by the need for material with unique properties. Thomas Alva Edison prepared the first carbon fiber for use as a filament in his early models of electric light bulb [42]. Coiled carbon filaments are produced through pyrolysis which can be heated so that it can be used in the light bulb. Sturdy tungsten filaments replaced carbon filaments in the light bulbs and subsequent research on carbon filaments proceeded more slowly. Schutzenberger [43], Pelabon [44] and others [45, 46] worked in this field and focused on vapor grown carbon filaments (VGCF), where carbon filaments are grown from thermal decomposition of hydrocarbons.

The need for lightweight composite materials for the aircraft industry led to carbon fibers research in the 1950's and 1960's. This led to the preparation of carbon fibers based on polymer precursors, such as rayon and polyacrylonitrile (PAN). Also, this led to the growth of carbon whiskers [45] and the theoretical studies showing the remarkable mechanical properties of whisker structures evolved. In 1962, Ubbelohde and his co-workers [46] discovered highly oriented pyrolytic graphite (HOPG) when they were working on the synthesis of carbonaceous materials with properties approaching

single crystal graphite. Efforts to reduce the defects and structural deformities and the desire to synthesize carbon filaments under more controlled environment let to the synthesis of carbon filament by catalytic chemical vapor deposition (CVD). This formed the basis for an understanding of the mechanism and thermodynamics behind the vapor phase grown carbon fibers. The highly perfect form of carbon fibers was first prepared by Bacon [45].

The technique used to produce graphitic whiskers involves a DC carbon arc which is similar to arc-discharge method of nanotube synthesis. However, there are a number of structural and size differences between graphitic whiskers and carbon nanotubes. The whiskers have a diameter of ~5μm and a length of ~3 cm whereas the nanotubes have a diameter of a few nanometers and length of a few micrometers. Similarly, the whiskers have scroll-like structures whereas the nanotubes have a honey-comb like structure. Occasionally, very small diameter filaments are observed but no detailed studies were carried out. A bright field TEM shows the image of thin vapor grown tubules Figure 3.1. Catalytic production of fine tubules has been known for years now, but these have a much less perfect structure than the fullerene related tubes. VGCF's did not have fullerene-like caps but usually a metal particle attached at an end.

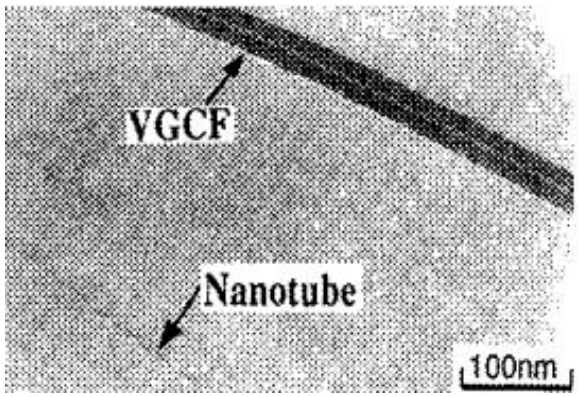

Figure 3.1 – Thin Vapor Grown Carbon Fiber (VGCF) and a nanotube [26]

These small and thin tubules of carbon interested many researchers and it finally led to the discovery of fullerenes by Kroto and Smalley [1]. About 20 years before the discovery of fullerenes, a British chemist Jones, under a pen-name Daedalus predicted the presence of spherical carbon molecules. Also in 1986, he predicted about the existence of rolled up sheets of graphite [47]. A workshop on carbon-carbon composites was conducted in 1990 where leading scientists put forth their research on carbon fibers, filaments and fullerenes. Smalley [48] detailed his research on fullerene, Huffman [49] presented his efficient synthesis method for fullerene production and Dresselhaus [50] discussed research on carbon fibers. This led Smalley to speculate the existence of carbon nanotubes comparable to C_{60} dimensions. Fowler [51] described theoretical studies of small cylindrical fullerene molecules. Two groups, one at Naval Research Laboratory, Washington DC [52] and another at MIT submitted papers on fullerene tubes electronic properties. The real breakthrough on nanotubes came in 1991 with Iijima's report on observation of carbon nanotubes using a transmission electron microscope [3]. This bridged the gap between predictions of nanotubes and the theoretical framework of carbon nanotubes. After this discovery of nanotubes extensive research and study has been done and reported progressively.

3.2 History of Carbon Nanotubes

The carbon nanotube discovery by Iijima in 1991 was a significant step in the field carbon science and it acted as a stimulus for the many more nanotube related findings later. Since the discovery of the nanotubes, the findings related to nanotubes and

research in this field has grown exponentially. This section lists few important incidents in nanotubes research after the nanotube has been discovered.

Though Iijima discovered nanotubes, the amount of nanotube yield was rather small. The electronic structure of the nanotubules was described by Saito *et al.* in 1992 [53]. In July 1992 Ebbessen and Ajayan, described a method for making nanotubes in gram quantities [9]. They found that increasing the pressure of helium in the arc-evaporation chamber increased the yield of nanotubes formed in the cathodic soot.

In 1993 Iijima [4] as well as Bethune *et al.* [54] synthesized single walled carbon nanotubes. Smalley *et al.* [14, 15] used a different technique for nanotube synthesis using laser ablation. Li *et al.* [56] used a technique where they embedded nano-iron particles into mesoporous silica to catalyze the decomposition of acetylene at ~700°C [56]. Also in 1996, Ebbesen *et al.* [57] discussed about the electrical conductivity of individual nanotubes and their young's modulus [58]. Dillon *et al.* [59] proposed a method in 1997 for hydrogen storage in SWNT's and Terrones *et al.* [60] proposed a method for controlled production of aligned nanotubes. Also in 1997 Smalley *et al.* [61] described the quantum conductance of the nanotubes. Ren *et al.* [62] described a method for growing well aligned nanotubes on glass using CVD as shown in Figure 3.2. Smith *et al.* [63] described the synthesis of fullerene balls encapsulated in the nanotubes. Dresselhaus *et al.* [64] described a method for hydrogen storage in nanotubes at room temperature.

Carbon nanotubes became the center of attraction for researchers from various fields, once they became familiar with their unique properties and structure. The unusually high thermal conductivity of the nanotubes was measured by Berber *et al.* [65]. Vigolo *et al.* [66] reported growth of macroscopic sized and ribbon-like nanotubes.

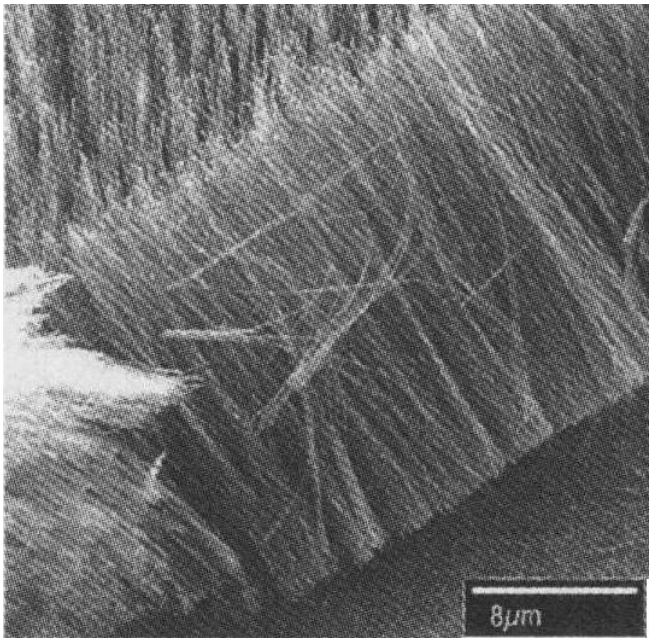

Figure 3.2. Aligned growth of nanotubes on glass [62]

Apart from the unusual mechanical and thermal properties of the nanotubes, the superconducting properties of the nanotubes interested many researchers [67] in the microelectronics industry and researchers started working on implementing the nanotubes into logic circuits [68].

The carbon science has evolved a great deal since the discovery of the first carbon filament for use in light bulb. Having said about the way it has evolved it can be said that what has been explored until now in the nanotube research is only a bit of information and what more to come will be interesting to watch out for. The fascinating properties of the nanotubes are discussed in the ensuing section.

3.3 Properties of Carbon Nanotubes

Carbon nanotubes are rolled up sheets of graphene. The electronic properties of the tubes arise from the manner in which or the direction in which the tubes are rolled up. They exhibit split personality meaning they exhibit two different properties. Some of the nanotubes exhibit metallic characteristics namely high electrical conductivity while others behave like semiconductors with large band gaps. They also have very good mechanical properties. Hence, they can be used to strengthen the composites. Also since they are completely made up of carbon and hollow, they have low specific weight which makes them a better candidate for incorporation into composites used for aerospace industry which requires lesser weight but greater strength [69].

3.3.1 Elastic Properties of Carbon Nanotubes

The C=C bond in graphite is the strongest bond in nature. In a graphitic sheet every carbon atom is bonded to three other atoms which make graphite strong along the basal planes. At the same time, the interlayers of graphite are connected by weak van der Waals forces so that layers of graphite can be easily separated out. Single wall nanotubes do not have interlayer interactions but in the case of multiwalled nanotubes weak interlayer interactions between the layers of the nanotubes exist. Carbon nanotubes are considered the ultimate high-strength fiber from the fact that they are strong directionally along their axis. Also, the single wall nanotubes are highly flexible in the direction normal to the nanotube surface. From theoretical predictions the nanotubes are stiffer and stronger than steel. When nanotubes are subjected to axial-compression they bend without any damage to the structure as such. They bend at a large angle, ripple, and

buckle. But all these deformations are elastic and they revert back to their normal position once the load is removed [70].

When a graphene sheet is rolled up to form a single walled nanotube the total energy of the nanotube is increased by the strain energy associated with the curvature of the nanotube. The strain energy increases with decreasing diameter. This means that the nanotube with small diameter is less stable compared to the one with larger diameter [47]. Various researchers have come up with different set of values for the moduli and strengths of the nanotubes. This discrepancy could be attributed to the way the thickness and the diameters are interpreted in calculating the properties. If the nanotubes are considered as solid cylindrical fiber they will have a lower modulus, whereas nanotubes when considered as hollow have higher modulus. Also, the lower the wall thickness of the nanotubes the greater the modulus [70].

The measure of stiffness of a material is its Young's modulus. Ebbessen and Treacy [58] measured the Young's modulus of multiwalled nanotubes. They fixed the bottom of the nanotubes and they measured the vibrational amplitude at the free end using a transmission electron microscope (TEM) which was found to be 1 TPa and about five times that of steel. Schonenberger *et al.* [69] from their scanning force microscopy examinations reported the modulus for both single walled and multi-walled nanotubes should approach 1.25 TPa.

Salvetat *et al.* [71] used an atomic force microscope to calculate the bending stiffness of the nanotubes. They placed nanotubes into well a polished alumina with nanopores of about 200 nm. When the nanotubes spanned over the pores, the AFM tip would bend the tubes and the deflections are measured. The deflections are inversely

proportional to the Young's modulus and can be varied with applied force. Figure 3.3 shows the experimental set up where in a single walled nanotube is adhered on to a porous alumina substrate and the schematic shows the application of load by the AFM tip on the nanotubes for direct measurement of the induced deflection. The results of the experimentation showed that SWNTs have an elastic modulus of ~1 TPa and shear moduli of ~1 GPa. Also, experimentation of multi-walled nanotubes from arc discharge yielded an elastic modulus of ~1 TPa whereas the one from catalytic decomposition of hydrocarbons gave a value of modulus on the order of one or two magnitude lower. This indicates that the arc discharge method yield tubes with fewer defects compared to other catalytic decomposition methods as also observed from TEM images.

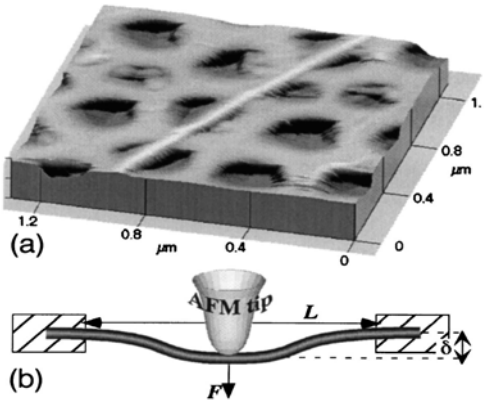

Figure 3.3 – Bending stiffness calculations on nanotubes by AFM [71]

Table 3.1 shows a comparison of the Young's modulus, tensile strength and the density of the nanotubes with some other materials [72].

Table 3.1 – Comparison of physical properties of materials [72]

Material	Young's Modulus (GPa)	Tensile Strength (GPa)	Density (g/cm^3)
SWNT	1054	150	1.36
MWNT	1280	150	2.6

Steel	208	0.4	7.8
Epoxy	3.5	0.005	1.25
Wood	16	0.008	0.6

Yu *et al.* [73] analyzed sliding between nested shells of multiwalled nanotubes using a loading stage in a SEM. A stick-slip motion and a smooth pull out motion were observed for different tubes. The shear strength between the shells and the surface energy of the multiwalled tubes were calculated. In Figure 3.4(a) the microscopic tips have not stretched the tube fully and we see a slack in the nanotube and in Figure 3.4(b) we see two remains of the broken nanotube. The part of the upper tube has curled up and the lower part remains up straight. They found that the shear strength varied between 0.1 and 0.3 MPa which is similar to graphite. Cumings and Zettl [74] in a similar experiment pulled and pushed the inner part of a multiwalled nanotube in and out repeatedly and found no wear for over 20 cycles.

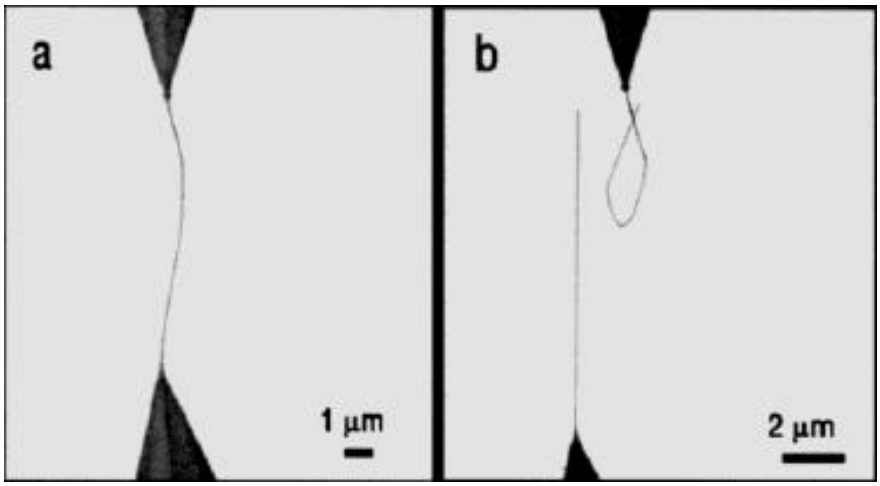

Figure 3.4 – Shear experimentation on MWNT [73]

Yu *et al.* [75] also conducted experiments to determine the elastic properties of single walled nanotubes. They used a sample of the so-called bucky paper and isolated a single walled nanotube with the tip of an atomic force microscope. They found that the

single walled nanotubes are entangled and could not be stretched across two tips as shown in Figure 3.5. Figure 3.5(a) and 3.5(c) shows the SWNT before and after the break, respectively. The magnified images of the tip before and after the break are shown by Figure 3.5(b) and 3.5(d). After testing with 15 individual nanotubes they found the mean elastic modulus to be ~1 TPa which is in accord with the theoretical predictions and the works from other researchers. Forro *et al.* [69] found the modulus of MWNTs did not depend on the diameter of the nanotube but rather the amount of disorder and defects in the MWNTs. However, they showed that the modulus of SWNTs depend on their diameter.

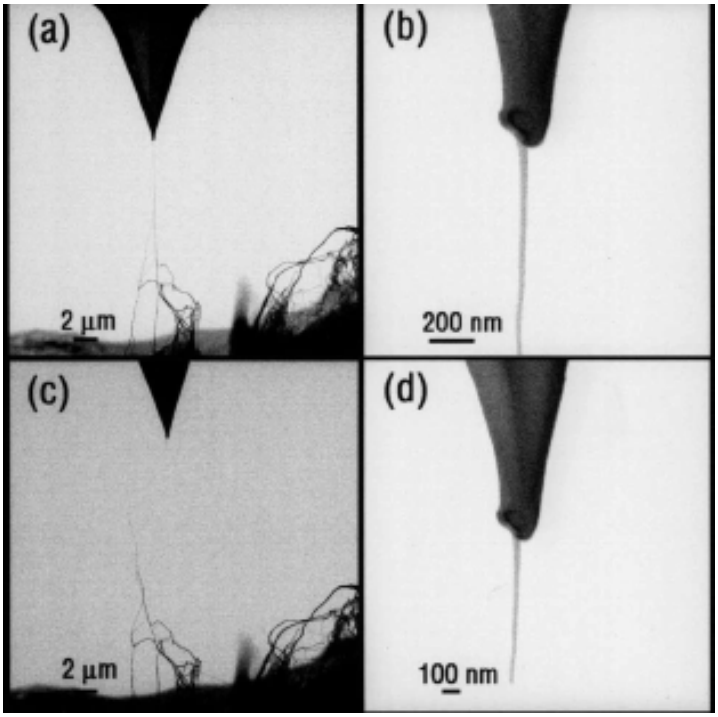

Figure 3.5 – Elastic modulus measurement on SWNTs [75]

Being the ultimate high-strength fiber, the carbon nanotubes are the privileged candidates for use in reinforcement application. Before using them, care should be taken on the following problems. First, the properties of individual tubes should be optimized.

Then, the tubes should be efficiently distributed and bonded in the matrix of the material to be reinforced. Finally the load must be distributed evenly within the nanotube itself to ensure that the outermost layer do not shear off [69].

3.3.2 Electronic and Electrical properties

Carbon nanotubes are giant molecular wires wherein the electrons can move freely as in metals in contrast to conducting polymers where electrons are localized. Polymers are originally insulators and they act as conductors when heavily doped. A sheet of graphite (graphene) is a “semimetal” and a “zero gap” semiconductor. When graphene sheet is rolled up to form a tube, a stationary electron wave can develop only when the circumference of the tube is a multiple of the electron wavelength which makes them a true metal or a semiconductor. Because of their unique properties they can be used for a wide range of electronic applications ranging from quantum wires to field effect transistors [69].

Carbon nanotubes can be metallic or semiconducting depending on their diameter and chirality. Metallic tubes can act as nanowires and the one dimensional nature of these wires gives rise to phenomenon, such as proximity-induced superconductivity. Semiconducting nanotubes, on the other hand, can act as transistors in the nanoworld. Armchair nanotubes behave like a ballistic conductor because elastic scattering is suppressed by the symmetry of the conducting electrons and because of the local potential of defects is small. Electron-phonon interactions seem to be the main scattering mechanism [76].

A nanotube acts as a ballistic conductor meaning there is only negligible resistance. They have a tolerance for very high current density and a constant resistivity which is independent of its length. This means Ohm's law does not hold good for this case. A superconductor (which has no electrical resistance) is the only better conductor. Frank *et al.* [77] states that nanotubes conduct current ballistically and do not dissipate heat. They also state that nanotubes are several orders of magnitude greater in size and stability than other typical room temperature quantum conductors. They found the electrical conductance to be about two times that of quantum conductance, $G_o = 2(e^2/h)$ where e is the electron charge and h is the Planck constant. Conductance of arc-produced MWNTs was found as $G_o = (12.9 \text{ kilo ohms})^{-1}$.

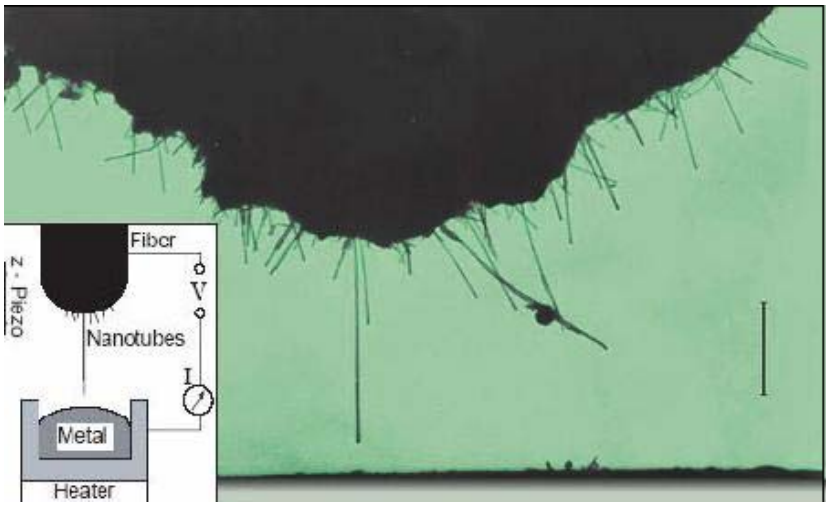

Figure 3.6 – Conductance tests [77]

Frank *et al.* [77] measured the conductance of the nanotube by replacing the tip of a STM by a nanotube and then dipping the nanotube into a liquid metal (mercury) to have electrical contact at the tip of the tubes. Since the nanotubes stick out from the fiber as shown in Figure 3.6 the resistance of the individual nanotube is measured by dipping the nanotube to different depths. The inset in Figure 3.6 is a schematic of the experimental

setup. Figure 3.7 shows a plot of the variation of the conductance with depth. This was a different method for making electrical contact and measuring conductance. However the coefficient of quantum conductance was found to have surprising integers and non-integers such as 0.5 G_o.

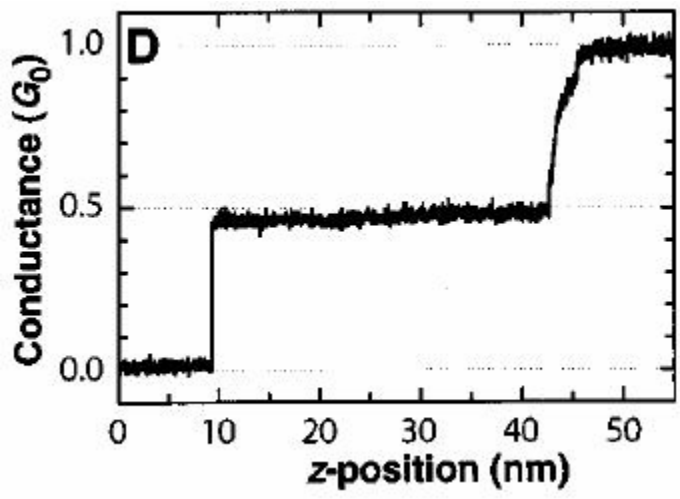

Figure 3.7 – Variation of Conductance with Depth [77]

In 1999, Sanvito *et al.* [78] found the reason for these surprising values of coefficient of quantum conductance. They used a scattering technique to calculate the ballistic conductance of the MWNTs and found the interwall interactions block some of the quantum conductance channels. This provides an explanation for the discrepancy found in Frank *et al.* [77] calculations.

The transport properties of carbon nanotubes reveal that they are ballistic conductors over 100 nm to μm length. A ballistic limit can be observed in experiments by having highly transparent contacts. The resistance of the nanotubes depends linearly on the applied voltage along the length of the tube.

3.3.3 Thermal Properties

Carbon nanotubes are stable at high temperatures and also against strong acids. High temperatures and acids are often used to purify the nanotubes from carbonaceous impurities in the deposits. Also sometimes gas phase purification is done in an Argon environment as they are stable in that environment as well. The thermal conductivity of the carbon nanotubes changes with respect to temperature, current applied, and vacancy concentration.

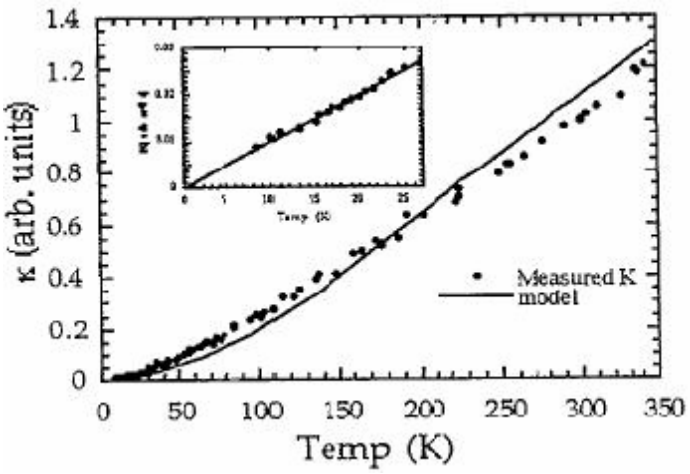

Figure 3.8 – Variation of Thermal conductivity with Temperature [79]

Hone *et al.* [79] measured thermal conductivity (*k*) of bulk samples of single walled nanotubes and found that the *k* values were linear with respect to temperature from 7 to 25 °K, slope increases between 25 and 40 °K and later rises monotonically with temperature above room temperature. The thermal conductivity is large and dominated by phonons at all temperatures. Figure 3.8 shows the variation of thermal conductivity with temperature of SWNTs and the inset in Figure 3.8 shows the low temperature behavior of the thermal conductivity. At low temperatures *k* is strictly linear with T and this phenomenon is associated with one dimensional phonon thermal conductivity. They found that the longitudinal thermal conductivity of a single rope of SWNT ranges from

1800 – 6000 W/m/K at room temperature. They modeled the phonon thermal conductivity of a single tube using Equation 3.1. In Equation 3.1, C is the heat capacity, v_z is the sound velocity at a given phonon state and τ is the relaxation time.

$$K_{zz} = \Sigma\, C\, v_z^2\, \tau \quad \text{---------- (Equation 3.1)}$$

Che *et al.* [80] calculated the thermal conductivity of nanotubes by increasing the current applied to the nanotubes. They found that the value of *k* to approach 2980 W/m/K as the current increases. They used molecular dynamics (MD) simulations to evaluate the convergence behavior. Figure 3.9 shows the convergence of thermal conductivity approaching 29.8 W/cm/K which is very high compared to conventional materials.

Berber *et al.* [65] in the year 2000 determined thermal conductivity of the nanotubes and its dependence on temperature and the results confirmed the earlier results by Hone *et al.* Berber *et al.* found that thermal conductivity is ~6600 W/m/K at room temperature.

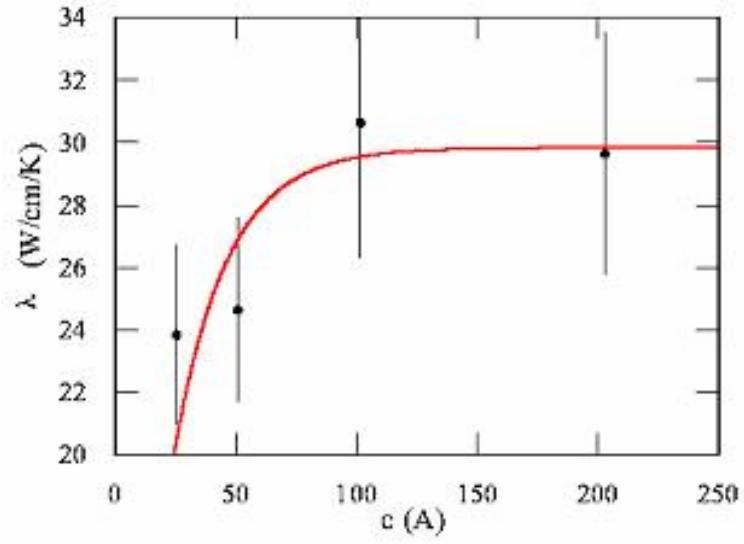

Figure 3.9 – Convergence of thermal conductivity [80]

However they also showed that thermal conductivity Vs temperature plot is less linear than that reported by Hone *et al.* as shown (See Figure 3.10 A). They have

unusually high thermal conductivity of ~ 37000 W/m/K at 100K and then drops drastically to 3000 W/m/K at 400K. The Figure 3.10 B shows a comparison of thermal conductivity of carbon nanotube (solid line) with a graphitic monolayer (dashed dotted line) and a basal plane of graphite (dotted line).

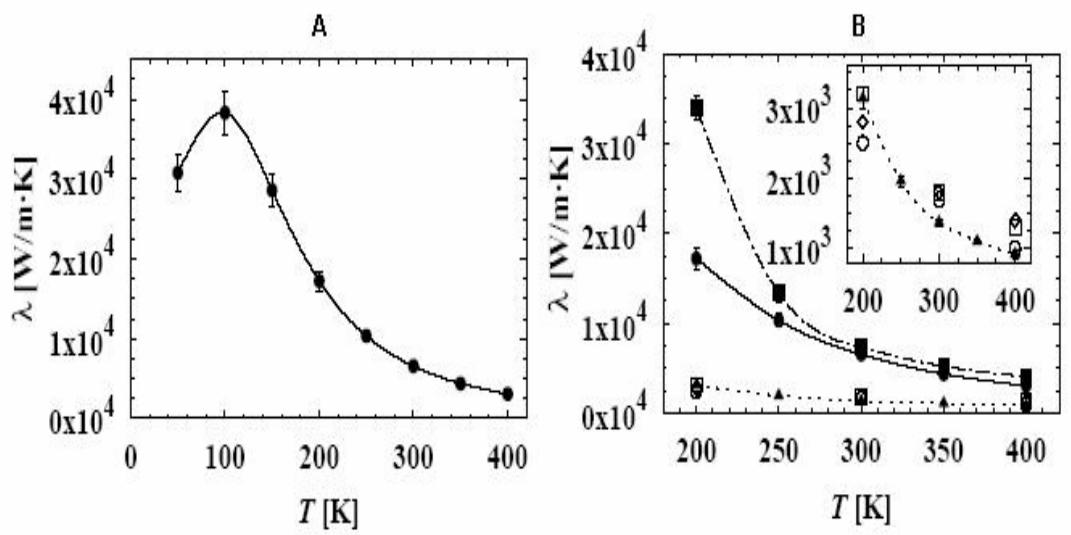

Figure 3.10 –Thermal Conductivity and its dependence with Temperature [65]

These results show that nanotubes have excellent thermal properties and the thermal conductivity is atleast ~5 times that of copper (400 W/m/K).

3.3.4 Magnetic Properties

The magnetic properties and susceptibility of the nanotubes to a magnetic field depends on the alignment of the tubes to the field i.e. parallel, perpendicular or randomly oriented. Ramirez *et al.* [81] studied unpurified nanotubes over temperature from absolute zero to room temperatures. The results show that nanotubes behave differently compared to other carbon materials as shown in Figure 3.11. They have a large diamagnetic susceptibility which increases with decreasing temperature and it is larger than graphite. Since the tubes were randomly oriented with the field it is not

evident the high susceptibility is due to parallel or perpendicular orientation. They speculated that the large susceptibility of the nanotubes is due to the ring currents flowing around the tube circumference.

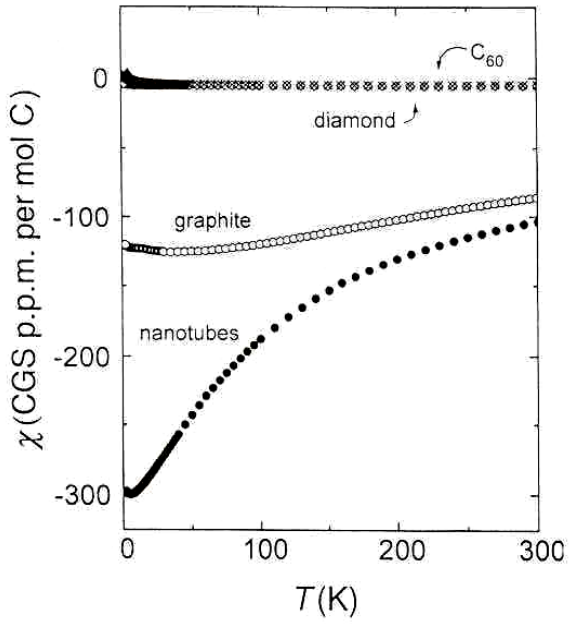

Figure 3.11 – Magnetic susceptibilities of carbon allotropes Vs temperature [81]

Wang *et al.* [82] measured the magnetic properties of aligned nanotubes from the deposits obtained from arc-evaporation and obtained results similar to Ramirez *et al.* but indicated the presence of some anisotropy. This was the first evidence of anisotropy in magnetic properties of nanotubes but we also should note that the degree of alignment is not high.

Chauvet *et al.* [83] carried out magnetic measurements on samples of nanotubes with higher degree of alignment wherein the tubes are aligned perpendicular to the film. The tubes were aligned parallel and perpendicular to the field and susceptibilities were measured from 4 to 300 °K. They show that nanotubes are diamagnetic with a pronounced anisotropy of susceptibility. The magnetic susceptibility of tubes aligned

perpendicular to the field was found to be much lesser that the tubes aligned parallel to the field as shown in Figure 3.12.

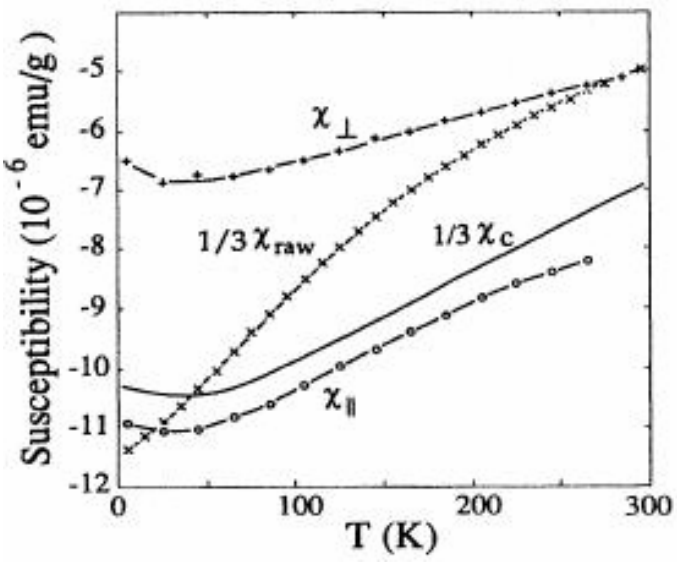

Figure 3.12 – Magnetic Susceptibility Vs Temperature for nanotube samples [83]

3.3.5 Optical Properties

Carbon nanotubes have excellent optical properties for field emission applications. Field emission is the property by which emission of electrons from the surface of a condensed phase into another phase occurs usually in vacuum, under the action of a high electrostatic field (10^8 V/cm). The CNTs have excellent optical properties which make them attractive candidates for field emission devices. They have a large aspect ratio (>1000), atomically sharp tips, and small diameters, high temperature and chemical stability, and high electrical and thermal conductivity [84].

A stronger electric field develops at the free ends of the nanotubes even for moderate voltages because of its sharpness. The field emission properties were first found by de Heer *et al.* [85]. For making the multiwalled nanotubes as source for field emission,

the tubes were mounted onto a gold tip. They were kept in place by the van der Waals forces and no adhesive was used.

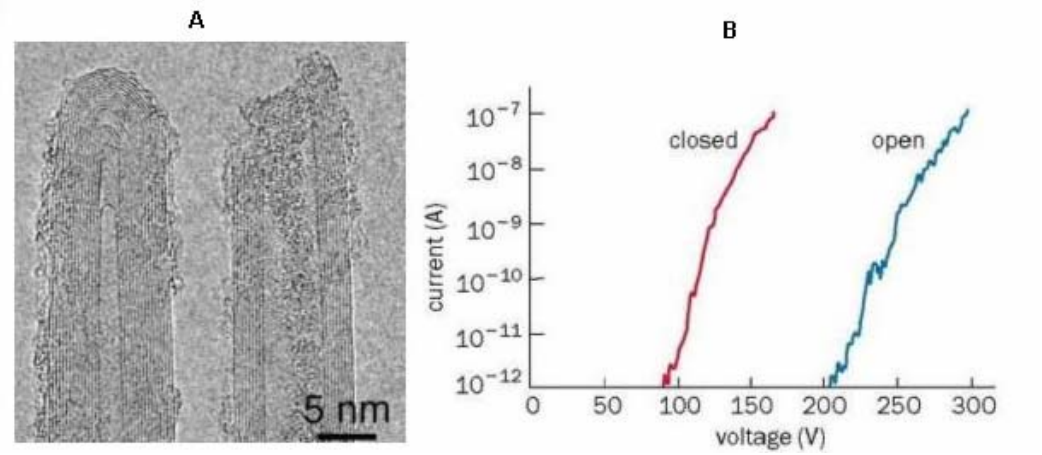

Figure 3.13 – Field emission of closed and open MWNTs

Bonard *et al.* [86] compared the field emission characteristics of closed and open tip MWNTs. Both of them emitted currents as high as 0.1 mA which is a high current density keeping in mind the smaller size of the tubes. They also observed significant differences between the two types of nanotubes. The results showed that nanotubes should be multiwalled, closed and well ordered tips for good performance as well as long emitter lifetime. The large amplification factor arising from the small radius of curvature is responsible for the good field emission characteristics. Closed nanotubes can produce significant emission currents at much lower applied voltages than open nanotubes. Figure 3.13(A) shows TEM images of closed and open MWNTs used for field emission experiments. A comparison of emitted current between them is seen in Figure 3.13(B). Electron microscopy and flat panel displays are some applications where field emission effect by nanotubes would be of great use.

3.4 Applications of Carbon Nanotubes

Carbon nanotubes began to revolutionize various fields which have taken the carbon science to a whole new planet. Many potential applications for nanotubes have been proposed. Some of the applications include conductive and high-strength composites, energy storage and energy conversion devices, hydrogen storage media, field emission displays and radiation sources, probes for scanning probes, nanosized semiconductor devices, nanocircuits and interconnects [87]. The cost of nanotubes, lack of availability of desirable quantities and limitations in processing and assembly methods are some barriers in the use of nanotubes for a specific application. Some of the important applications are described in this chapter.

3.4.1 Nanotubes as tips for scanning probe microscopy

The outstanding mechanical properties and unique geometry of carbon nanotubes have led to the suggestions that nanotubes would make ideal candidates as tips for scanning probe microscopes (SPMs). Certainly nanotubes would seem to have advantages over the tips currently used for atomic force microscopy (AFM), which typically consists of microfabricated pyramids of silicon or silicon nitride. These tips can be relatively blunt on the scale of the features which are being imaged, and are thus often unable to probe narrow crevices of the specimen surface. The elongated shape and the small diameter of CNTs should enable them to probe into the narrowest of fissures. There is also the possibility of functionalizing the nanotubes in order to carry out 'chemical force microscopy'. There are potential problems with using nanotubes for atomic resolution imaging due to the relatively large thermal vibrations observed at room temperature [5].

Smalley and co-workers [88] were the first to demonstrate the use of nanotubes as SPM tips. They described a method of attaching bundles of MWNTs to the tips of commercial silicon pyramids, and then drawing out a single tube from the bundle to act as the imaging probe. The nanotube tips were then used to obtain tapping-mode AFM images of a patterned film on silicon wafer. It was found that the tips could reach to the bottom of the deep trenches in the film, and produce much more realistic images than those obtained using pyramidal tips. Because the nanotube tips were electrically conducting, they could be used for scanning tunneling microscopy (STM) as well as AFM. Smalley *et al.* [88] obtained atomic resolution images of TaS_2 surfaces using the tips in the STM mode.

Leiber *et al.* [89] investigated the possibility of using CNT tips for imaging and analyzing biological systems. They used similar method as that of Smalley *et al.* and obtained tapping-mode AFM imaging of amyloid fibrils. The images were found to show more details than conventional tips and the nanotube tips were found to be both robust and relatively resistant to contamination. A SEM image of MWNT tip attached to the conventional single crystal silicon cantilever tip as used by Leiber *et al.* is shown in Figure 3.14. The MWNT extends to about 1.8 μm from the pyramidal silicon tip. The high aspect ratio of the nanotubes helps in good imaging capabilities in deep crevices and steep features.

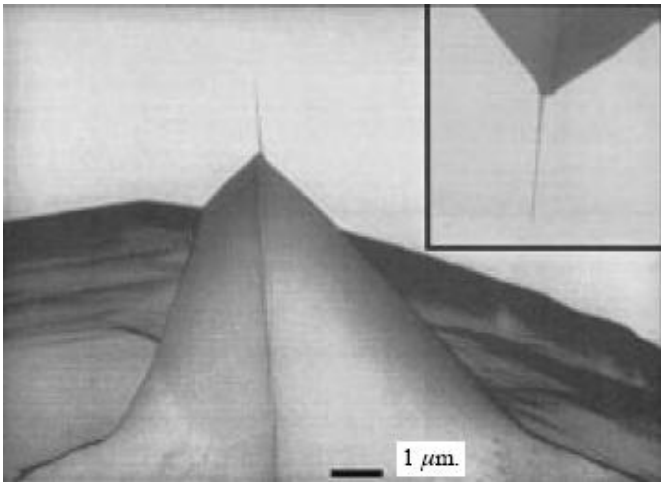

Figure 3.14 – An attached MWNT used as AFM tip on top of silicon pyramid [89]

Leiber *et al.* [89] also prepared functionalized tips to sense specific interactions with functional groups on substrates. The tubes were initially oxidized resulting in the formation of carboxyl surface groups. These tubes were then used to carry out chemically sensitive imaging of surfaces patterned with different molecules. Tubes terminated with amine groups were used in a similar way [90].

Nanotubes also have potential for nanolithography. Dai *et al.* [91] have used nanotube AFM tips to draw patterns and words on silicon oxide wafers. Nanotubes can write nanostructures at a speed of up to 0.5 mm/s. Nanotubes were found to have greatly improved wear properties compared to conventional tips. Experimental and theoretical work has shown that the nanotubes are impervious to high compressive and lateral forces and they could become the important elements in future miniaturization.

Figure 3.15 shows images of nanolithography pattern and images written by nanotube tips on silicon oxide samples. Also from the experimentation they found that nanotubes has survived extensive writing without wearing by depositing particle like debris. It is possible now to fabricate 10 nm scale structures over hundreds of squares

micrometers without wearing the tip at the atomic level. The nanotubes obtained from chemical synthesis are found to be the workhorses for nanofabrication.

Figure 3.15 – Nanolithography pattern by nanotubes on silicon oxide [91]

The critical problem that a conventional silicon tip faces is brittleness. As the tips wears out quickly, degradation of the image is unavoidable resulting in replacement of probes frequently. The extraordinary strength and the ability to retain structural integrity during operation make them a better choice for AFM tips [92]. Figure 3.16 shows the TEM image of a CNT probe grown by thermal CVD at the AFM tip.

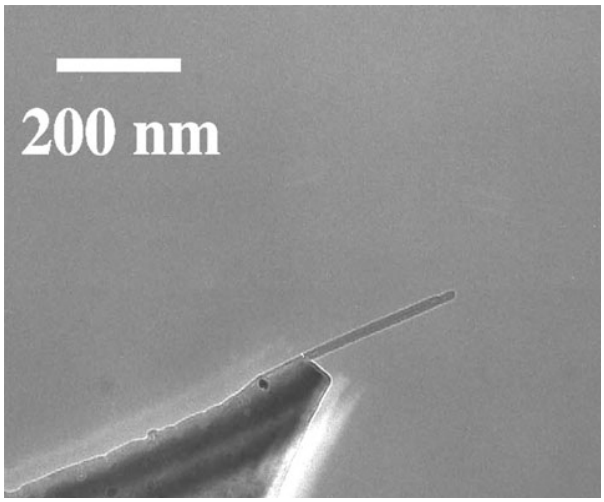

Figure 3.16 – TEM image of CNT used as an AFM tip [92]

3.4.2 Carbon nanotube composites

The high aspect ratio also means that excellent conductivity of the nanotubes makes them good candidate for use in conducting composites. Depending on the polymer matrix, conductivities of ~0.01 to 0.1 S/cm can be achieved for 5% loading. The low loading levels and nanofibers morphology of the MWNT allow electronic conductivity to be achieved while avoiding or minimizing degradation. Conducting composites are used in conductive plastic automotive parts, such as mirror housing that are electrostatically painted in the assembly line. This avoids separate painting and the associated color mismatch [87].

Composites of MWNTs in epoxy resin achieving percolation at loadings of 0.01% and even 0.004% is shown in Figure 3.17 which are extremely low loading. Better surface finish is exhibited by nanotube composites compared to carbon black or carbon fiber composites. Composites with conductivity of 1 S/cm could be used as shielding of electromagnetic interference. Conducting composites are also used as transparent conductor if they are thin enough and they are highly flexible and compatible with polymer substrates.

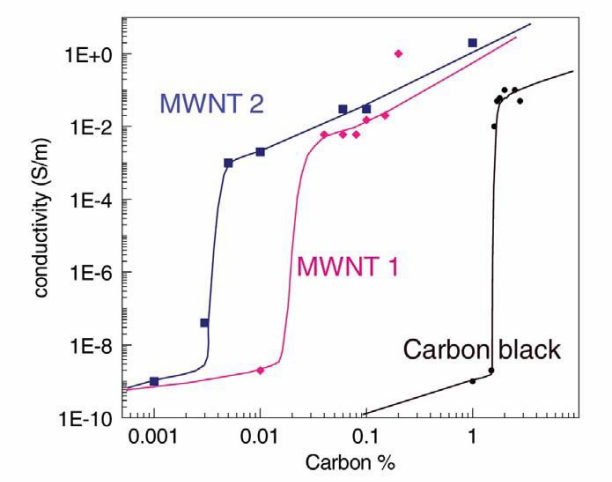

Figure 3.17 – Conductivity Vs carbon content for 3 different systems [93]

Incorporation of carbon nanotubes into a polymer matrix and proper bonding between them are also studied. Still considerable research is going on in this field as there are a few methods for properly dispersing the nanotubes and the results from the experiments are yielding low values contrary to expectations [93]. However, Biercuk *et al.* [94] observed that the monotonic increase of resistance to indentation by ~3.5 times. The matrix into which the nanotubes are incorporated can be plastic, epoxy, metal or carbon. The incorporation not only adds to the strength and elasticity of the material but also increases the toughness and its ability to cracking. Firstly, the fibers are shaped into a 'preform' and then the liquid matrix is added under pressure. Fibers are not added directly into the matrix as it may have a thickening effect. The addition of nanotube to composites and polymers enhances the tensile strength, elastic modulus and decreases the resistivity of the material. Figure 3.18 explains this through a bar graph [95].

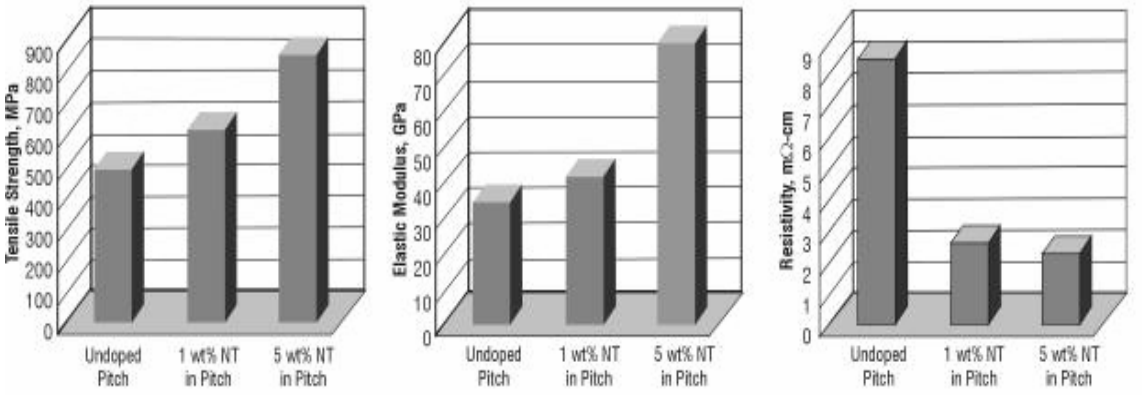

Figure 3.18 – Variation of properties due to nanotube addition [95]

There are some problems and difficulties in incorporating the nanotubes into the polymer matrix. Surface tension, pressure, cost of the process, orientation of the nanotubes in the matrix, bonding between the tubes and the matrix and finally bonding within layers of MWNTs are some issues which need to be taken care of. Leaving back

the hiccups, this area still has some promising aspects which can help in the arrival of advanced composites.

3.4.3 Flat Panel Displays

A lot of focus is now on SWNTs and MWNTs as field emission electron sources especially for used in flat panel displays, lamps, gas discharge tubes providing surge protection, x-ray and microwave generators. The local fields cause electrons to tunnel from the nanotube tip into the vacuum. Electric fields direct the field-emitted electrons towards the anode, where a phosphor produces light for flat panel display applications. Schematic of a triode type field emission display (FED) is shown in Figure 3.19 [93].

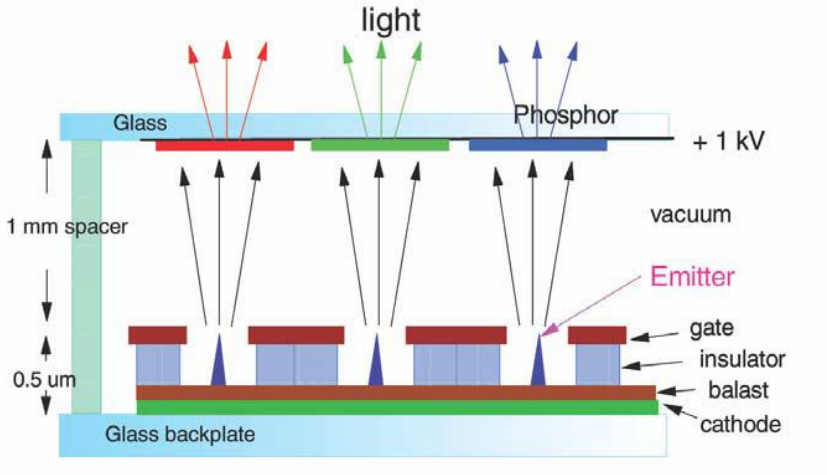

Figure 3.19 – Schematic of a triode-type FED [93]

Nanotubes based FED provides stable emission, longer lifetime and low emission threshold potentials. Current densities as high as 4 A/cm^2 have been obtained as compared to 10 mA/cm^2 needed for flat panel emission displays and the >0.5 A/cm2 required for microwave power amplifier tubes.

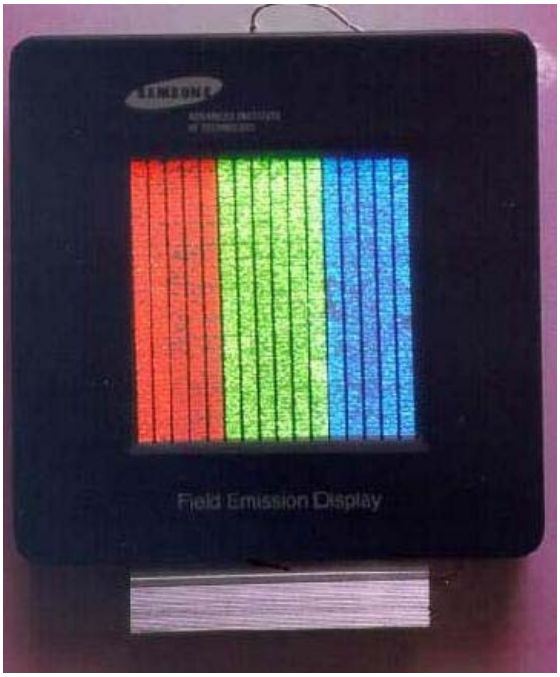

Figure 3.20 – Samsung 4.5” full color nanotube flat panel display

The advantage of nanotubes based FED over the liquid crystal display (LCD) are low power consumption, high brightness, a wide viewing angle, a fast response rate and wide operating temperature range [87]. Samsung developed prototypes of flat panel displays and one such prototype is shown in Figure 3.20. Despite many developments it is unclear whether these flat panels would be commercially available considering the relatively low cost liquid crystal displays and emerging organic and polymeric light emitting diode displays.

3.4.4 Nanocircuits and Nanoelectronics

Besides the above mentioned applications, nanotubes have also invaded electronics industry. Field-effect transistors (FET) use single semiconducting nanotube between two metal electrodes as a channel through which electrons flow [96]. Voltage is applied to a nearby third electrode to switch on or off, the current flowing in this channel.

These devices perform remarkably better than the regular silicon devices at room temperature. Figure 3.21 shows a field effect transistor (FET). Nanotubes with variety of band gaps and conductivities are available increasing the possibilities for nanodevices.

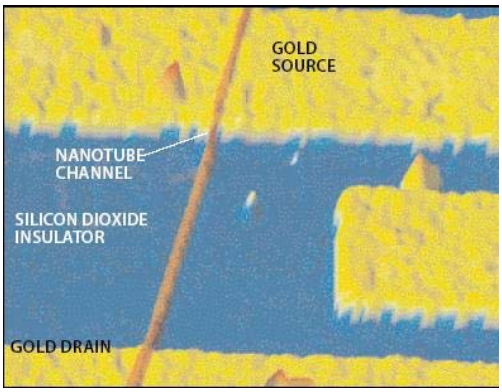

Figure 3.21 – Field Effect Transistor [96]

Graham *et al.* [97] proposed a vertical nanotube transistor which is shown in Figure 3.22. Nanotubes are used to produce a vertical CNT transistor by including a ring-gate between top and bottom contacts and growing SWCNTs. A significant problem for electronic applications of the nanotubes is their chirality. The cohesive energy depends weakly on diameter and very weakly on the chirality which is a huge advantage for the electronics industry [93].

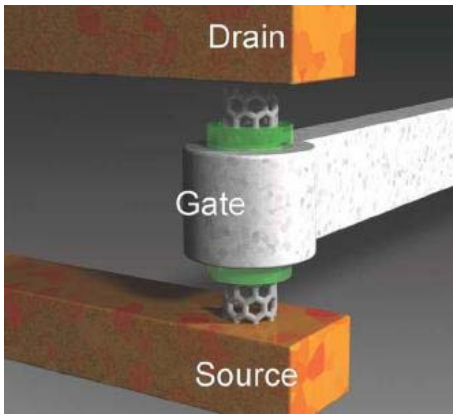

Figure 3.22 – Vertical CNT transistor [97]

A number of ongoing research in the use of nanotubes for hydrogen storage, electrochemical devices, bioengineering is going at full pace and pretty soon we will be seeing lot of options and doors open because of nanotubes invasion in that industry.

3.5 Choice of catalyst used in CNT growth

Choice of a catalyst is very important for the growth of carbon nanotubes using catalytic methods. The catalysts that are used for the growth of CNTs are the 'transition metals'. Transition metals are the 38 metals in the group 3 through group 12 in the periodic table. They are ductile and malleable, conduct electricity and heat, lustrous and except for copper the other are white in color. The valance electrons of these elements are present in more than one shell. The three key elements in the transition metals family are iron, cobalt and nickel as these are the only elements known to produce a magnetic field. In other words, these three are the ferromagnetic transition metals.

The transition metals either in their purest form or as compounds or as precursors in gaseous states act as catalysts for the growth of nanotubes. The ferromagnetic transition metals are popular among the transition metals for the growth of nanotubes. The growth of the nanotube not only depends on the substrate where it is grown but also the crystal structure and morphology of the catalyst material that is used for growth.

Carbon has finite solubility in transition metals at higher temperatures and metal-carbon solutions are formed which is clear from their phase diagrams. This is the reason behind choosing these transition metals as catalyst for the growth of carbon nanotubes [8, 98]. Figure 3.23 shows iron-carbon phase diagram.

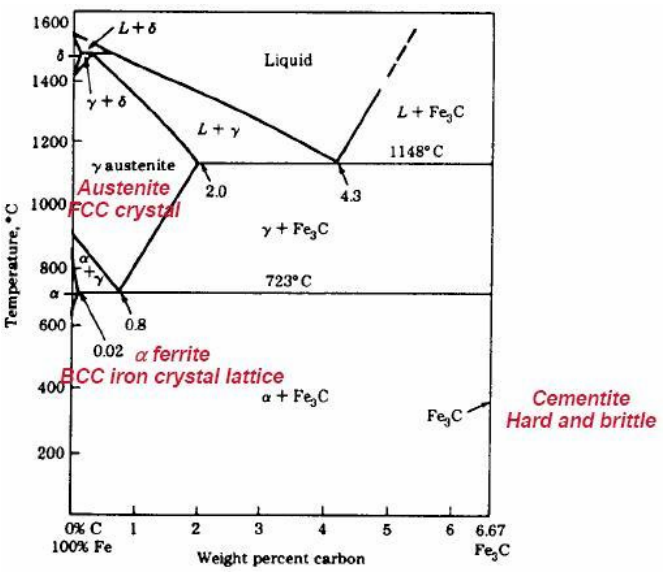

Figure 3.23 – Iron-carbon phase diagram

The importance of the nanotube synthesis lies not only in the use of these transition metals as their catalyst but also on the thickness or the concentration of the catalyst being used. Also, care should be taken during the growth process making sure that the catalyst surface is not passivated. The more active the catalyst surface is the more the yield of nanotubes. The size of the catalyst particles determines the diameter of the nanotubes grown. Ren *et al.* [99] say that the choice of the catalyst determines the tube diameter, the growth rate, yield, morphology and microstructure. Shin *et al.* [100] studied on the growth control, tube diameter, length of the tube and the microstructure depending on the morphology of the catalyst film. These catalyst particles help in the diffusion of carbon and the nanotubes grow based on some growth mechanisms.

3.6 Growth mechanisms for the nanotube synthesis

Carbon being finitely soluble in the transition metals at high temperatures follows a procedure for getting diffused on the catalyst and becoming a nanotube. There are two

types of growth mechanism based on the interaction of the catalyst particle with the substrate: tip growth mechanism [101, 102] and base growth mechanism [103, 104]. Extensive literature review on the growth mechanism of carbon nanotubes is done by Ramakrishnan [148] in his study. Baker [105] best describes the growth mechanism of carbon to form carbon filaments which holds good for carbon nanotubes also. The hydrocarbon gas first decomposes into hydrogen and carbon and this carbon diffuses on top of the catalyst particle. The diffusion takes place from the hotter leading surface of the catalyst to the cooler rear surface. This diffusion is driven by the exothermic reaction at the front faces and the endothermic reaction at the rear faces. The excess carbon deposited on the outer surface is transported to the periphery of the particle to form the graphitic skin of the tube. The growth rate slows down due to the decrease in the temperature gradient and the carbon decomposition rate. When the leading outer catalyst face is encapsulated by carbon, the growth ceases due to passivation of the catalyst. The growth rate is also determined by the measure of activation energies for the growth of the tubule and also the rate of diffusion of carbon through the catalyst nanoparticles. The nanotube grown is mostly in the form of a bamboo structure [106].

3.7 Effect of process gases

The reactive gases normally used are CH_4, H_2 and NH_3 or N_2. A number of variables goes into the chemical reaction and depends on the process kinetics taking place between the reactive source gases. The flow rates of these gases and their effects play a major role in the nanotube formation. Excess decomposition of hydrocarbon at high temperature and the polymeric encapsulation of the catalyst at low temperature results in

the metal catalyst being passivated. On the other hand, excess hydrogen prevents the passivation resulting in the CNT growth [107].

3.7.1 Effect of hydrocarbon gas

A hydrocarbon gas or a hydrocarbon precursor is used as a carbon source in the growth of carbon nanotubes. The hydrocarbon gas is decomposed into C_2 and CH radicals which act as carbon source for CNT formation. The process gases and their flow rates play a major role in the formation of the nanotubes. As the intensity of the dimeric C_2 radical increases the growth of the carbon nanotubes also increases. This condition is true only as long as the catalyst surface is active. But when the carbon particles encapsulate the catalyst and passivation of catalyst takes place the growth ceases. When a nitrogen containing gas is also used there is both CH and CN radicals which also acts as sources of carbon for nanotube formation. But CH and CN radicals also are found to have an etching effect. The atomic hydrogen however was found to be the main etching species [108].

3.7.2 Role of Hydrogen

The plasma decomposes the hydrogen gas into atomic hydrogen when subjected to high temperatures and pressure. The amount of atomic hydrogen produced depends on some of the process parameters, such as chamber pressure, and process temperature. Jung *et al.* [107] described the effect of hydrogen in the CVD process in synthesis of carbon nanotubes which are as follows:

- To change the decomposition kinetics of the hydrocarbon used.

- When the hydrogen concentration is high the rate of decomposition of the hydrocarbon is suppressed.
- Lower decomposition of the hydrocarbon suppresses the rate of passivation of the catalyst layer.
- Indirectly influences to keep the catalyst surface active.

In most cases the catalyst particles are in the form of a thin continuous film which is either coated through lithographic technique or pulsed laser deposition or just applied as paint on the substrate. This thin film should be broken down into nanosized catalyst particles which inturn act as seeds for nanotube growth. Nanotubes are not formed if the catalyst film is not broken down into small particles. Kuttel *et al.* [109] states that the atomic hydrogen in the plasma not only breaks the catalyst films, but when the plasma ball engulfs the sample, the atomic hydrogen also etches the growing nanotube film. They also state that the presence of atomic hydrogen is an advantage in the nanotube growth process as in the case of diamond growth. They observed only nanotubes and onion-like structures suggesting that the atomic hydrogen is rather acting as a purifying agent which helps in the removal of impurities and amorphous carbon.

Qin *et al.* [110] also state that the atomic hydrogen in the plasma breaks the catalyst thin film into nanoparticles and also it enhances in the diffusion of carbon into the catalyst particles.

3.7.3 Role of Nitrogen

Similar to the hydrogen plasma the nitrogen plasma also has its advantages. Lin *et al.* [111] describes the advantageous role of nitrogen in CNT formation as following:

- The nitrogen plasma has more bombardment energy than the hydrogen plasma.
- Helps to keep the front surfaces of the catalyst particle clean.
- Prolongs the catalyst surface passivation thereby enhancing the carbon bulk diffusion.
- Under CH_4/H_2 plasma, the carbon concentration was a rapidly decreasing function of depth whereas under CH_4/N_2 it was a slowly decreasing function of depth
- Favorable for the formation of bamboo like CNTs.

Enhanced growth is closely related to the N_2 incorporation in the CNT wall and cap during growth. The enhancement in growth is also due to decrease in the activation energy required for nucleation due to the presence of nitrogen [112]. The effect of nitrogen on the growth rate and the diameter was studied by Lee *et al.* [113]. The growth rate of the nanotubes increases with increase in nitrogen content whereas, the diameter decreased except when nitrogen was not introduced. It is possible to grow nanotubes with a limited presence of amorphous carbon on the surface by using suitable methane to nitrogen ratio. Formation of metallic aligned tubes was seen with increasing nitrogen fraction in the plasma atmosphere [114]. The nitrogen plasma was found to increase diameter, straightness in CNTs, formation of bamboo-like CNT, deterioration in field emission properties and Raman peak shift toward lower frequency side [115].

3.7.4 Role of Ammonia

Mung *et al.* [107] also described about the role of ammonia in the synthesis environment which are described as follows:

- If the nitride surface enhances the separation of deposited carbon from the catalyst surface, the passivation of the catalyst would be suppressed.
- Suppresses the surface or bulk diffusion flux of carbon from the edge of the catalyst particles.
- The higher concentration of the atomic H_2 in NH_3 environment suppresses the decomposition of the hydrocarbon which prevents passivation of the catalyst.

The effect of NH_3 gas in the viewpoint of catalyst passivation was investigated by Jung *et al.* [116]. They observed significant catalyst passivation in H_2 environment at a hydrocarbon concentration of 2.4 vol% whereas aligned nanotubes are observed even at 16 vol% of NH_3 environment. Activated nitrogen atoms are generated by the decomposition of NH_3 apart from the generation of atomic hydrogen. In other words, NH_3 can be said as a good source for atomic hydrogen as well as activated nitrogen. These activated nitrogen atoms enhance the formation of graphitic layers and improve the separation kinetics of the graphitic layer from the catalyst.

These source gases and the reaction kinetics between these gases help in the decomposition of the gases, diffusion of carbon in the catalyst particles and further precipitation as nanotubes. The plasma treatment of the substrate first reduces the thin film of the catalyst into nanosized particles and helping in the deposition of the carbon over them.

3.8 Effect of process parameters

To better understand and to formulate a good design of experiments a thorough analysis and study of the process parameters involved should be done. The variations in

the pressure, temperature [117], growth time, pretreatment time, plasma intensity, flow rates of the gases used, composition of the reactant gases [118], their process kinetics, and the effect of microwave power should be studied in order to optimize the growth of nanotubes. This will help in increasing the efficiency of the growth process and help us have better control over the experiments.

3.8.1 Effect of pressure

The yield of the nanotubes is defined by the weight ratio of the carbon nanotubes versus that of the catalyst. In order to evaluate the effect of the pressure on the growth and yield of nanotubes in CVD, Ren *et al.* [119] conducted experiments and discussed the results of CNTs growth influenced by the variation in pressure. They conducted experiments from 0.6 torr to 760 torr. They found that nanotubes yield increases significantly with gas pressure and reaches 600% for 600 torr and decreases then after. Figure 3.24 shows SEM images of nanotubes grown at various pressures.

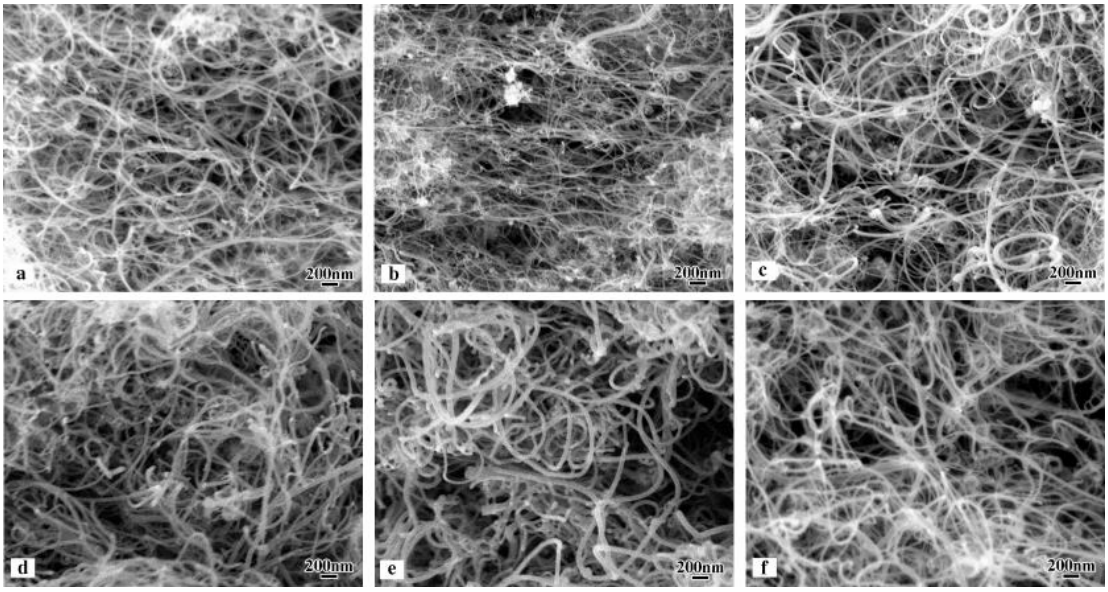

Figure 3.24 – SEM images of CNTs grown at different pressures (a) 0.6 torr (b) 50 torr (c) 200 torr (d) 400 torr (e) 600 torr (f) 760 torr [119]

They also observed there is a great difference in the morphology of the tubes grown at various pressures. They noticed that the tubes produced at lower pressures were completely hollow. As the pressure increases the wall thickness was found to increase and after one stage bamboo structure tubes were observed. The density of the compartments also increased as the pressure increases.

Figure 3.25 depicts the TEM images of tubes grown at various pressures (a) 0.6 torr, (b) 200 torr, (c) 400 torr and (d) 760 torr. The variations in the morphology of the tubes can be clearly seen from Figure 3.25. The results suggest that there is a strong dependency on the yield and structure of the tubes on gas pressure.

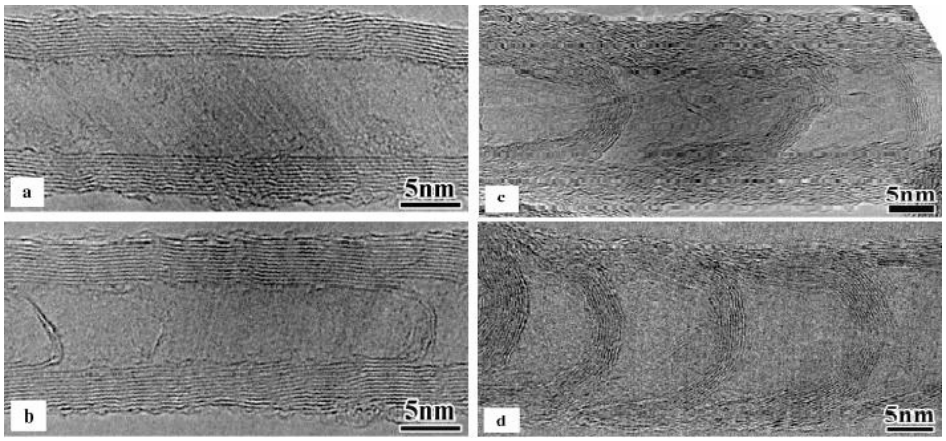

Figure 3.25 – Effect of pressure on CNT morphology [119]

A similar kind of phenomenon was observed by Wang *et al.* [120] where they found that the length of nanotubes is influenced on the growth pressure. They observed that the average length of tubes grown at 15 torr is longer than the tubes at 30 torr. Also they found that the growth is rarely seen at 5 torr. Though they did not calculate the yield, the results suggest that the growth rate varies depending on pressure used. This point is substantiated by Lin *et al.* [115] where they found that higher pressure increases the

growth rate, reduces the tube diameter and improves the field emission properties and the tube quality.

The effect of pressure on the yield of the tubes was not only conducted on CVD experiments but also on arc discharge and laser ablation. Ebbessen and Ajayan [130, 9] varied the pressure of helium in arc- discharge chamber (50 torr, 100 torr and 500 torr) and found that the yield increases as pressure is increased from 50 torr to 500 torr and the yield was found to decrease afterwards. Munoz *et al.* [121] conducted similar experiments on yield based on variation in pressure in laser ablation.

This section thus states that the variation in pressure affects the growth rate, yield, morphology, tube diameter and the properties of nanotubes and significant care has to be taken on designing the experiments in order to get optimum results.

3.8.2 Effect of temperature

Similar to pressure, the growth temperature also has some beneficial properties and its own shortcomings. The increase in temperature is also found to have an increase in the growth rate as in the case of pressure. Lee *et al.* [122] found that the growth rate increases by four times as temperature is increased from 750°C to 950°C. Also the average tube diameter was found to increase from 30 nm to 130 nm while the density decreased by a factor of two. The morphology of the tubes obtained at various temperatures are also different. It was found that the tubes at 950°C were found to have better crystalline structure than the tubes grown at 750°C.

The increase in the growth rate could be accounted from the fact that the increase in temperature helps in the enhanced carbon diffusion and reaction rates of carbon.

Similarly the increase in the diameter can be accounted from the fact that at higher temperature bigger nanoparticles are created than at lower temperature. The smaller nanoparticles tend to agglomerate and become bigger nanoparticles and thereby ending up as bigger seeds for the tubes. The variation in the growth rate due to the variation in temperature can be seen from Figure 3.26 and the length of tubes grown increases with temperature. Figure 3.27 shows the improvement in crystallinity of the tubes for temperatures 750°C, 850°C and 950°C.

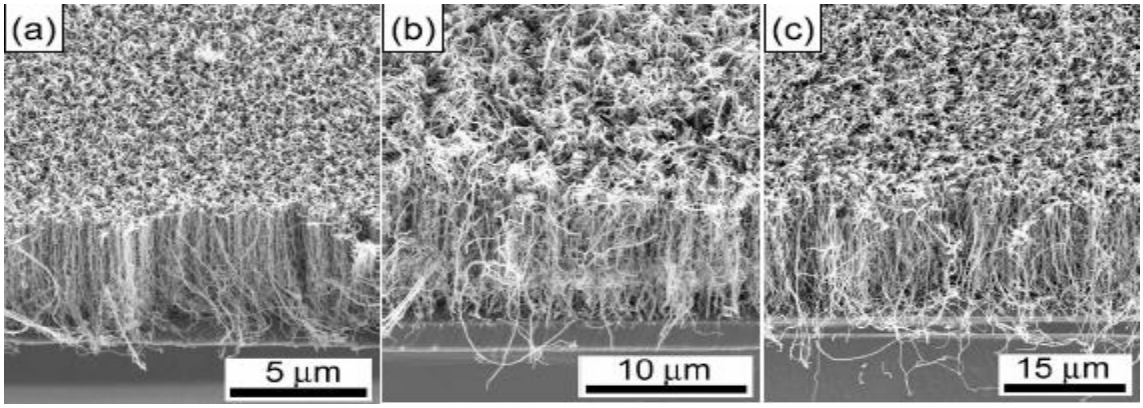

Figure 3.26 – Effect of temperature on CNT growth rate (a) 750°C (b) 850°C (c) 950°C [122]

In case of arc discharge, Iijima *et al.* [123] found that the yield of SWNTs is maximum in the temperature range of 400°C to 600°C. The yield is >70 wt% at 600°C and the yield is about ~30-40 wt% at room temperature.

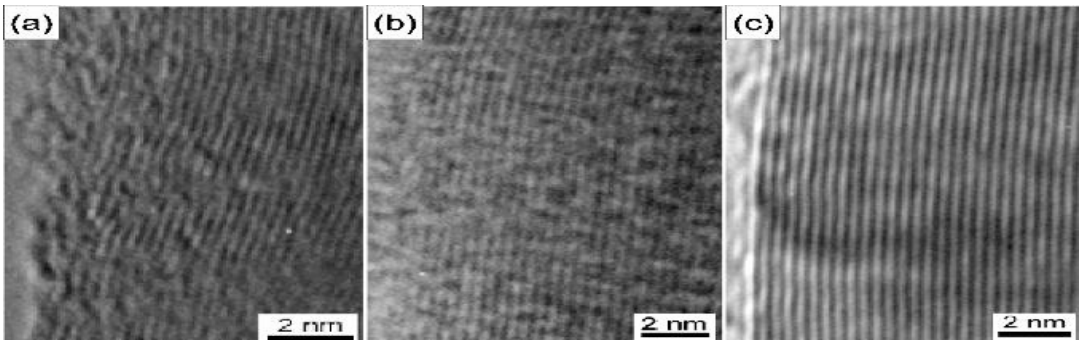

Figure 3.27 – Effect of temperature on crystallinity of the tubes [122]

The results of temperature varied experiments suggest that not only pressure is a determining factor for the growth rate and yield but also temperature. Also the results state that the tube diameter also depends on the temperature.

3.8.3 Effect of pretreatment time

Plasma pretreatment is the process that helps in breaking down the thin continuous catalyst film on the substrate into nanosized catalyst particles. Variation in the pretreatment time varies the catalyst particle size obtained. The catalyst particle size inturn controls the diameter of the nanotubes grown.

Lee *et al.* [124] conducted experiments on the plasma pretreatment time and found the variation in the catalyst particle size. They found that as the pretreatment time was increased the catalyst particle size decreased. The pretreatment time was varied accordingly to get the required tube diameter. Figure 3.28 shows the variation in the catalyst particle size for various pretreatment times (a) 60 s, (b) 90 s and (c) 120 s.

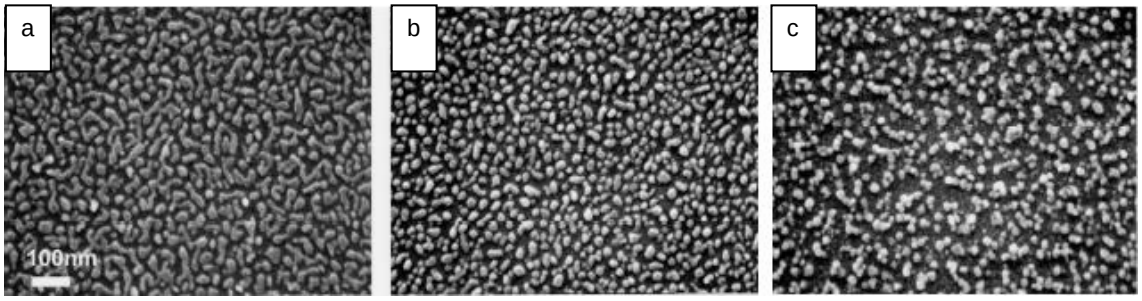

Figure 3.28 – Effect of pretreatment time (a) 60 s, (b) 90 s and (c) 120 s [124]

The distribution of the diameter of the carbon nanotubes is closely related to the catalyst particles size distribution. The variation of the tube diameter and the catalyst particle size with respect to the pretreatment time is shown in Figure 3.29. Yen *et al.*

[125] also observed similar phenomenon where they found that the catalyst particle size getting reduced in H_2 plasma compared to H_2 annealing.

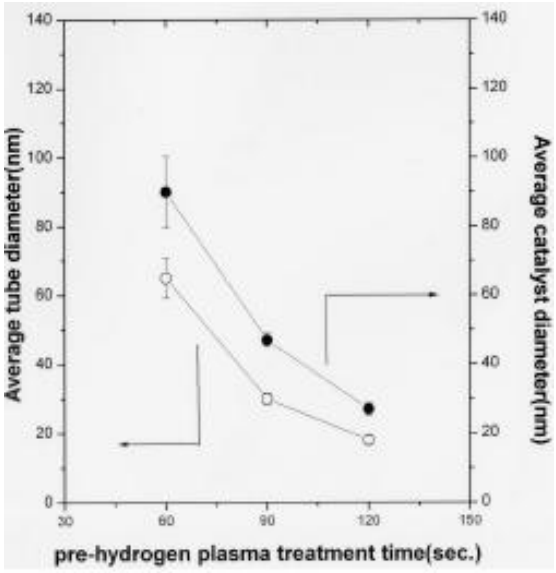

Figure 3.29 – Variation of tube diameter and catalyst diameter with pretreatment

The plasma pretreatment decreases the size of the catalyst particle only until a threshold value. If the sample is pretreated for a longer amount of time the catalyst particle start to partially melt and form a melt pattern and tend to agglomerate with each other and due to agglomeration the catalysts are no longer helpful in synthesis of nanotubes [126]. Figure 3.30 shows the melt pattern wherein a sample is pretreated for a prolonged time of 5 mins.

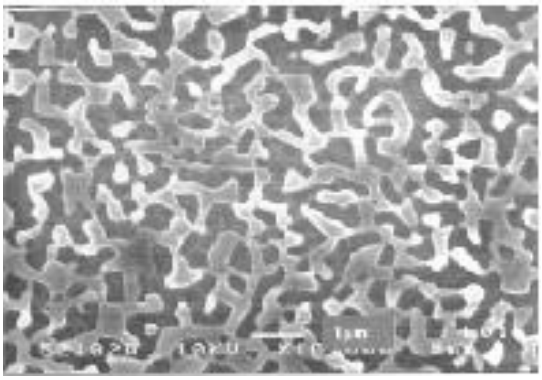

Figure 3.30 – Melted catalyst pattern due to prolonged pretreatment time [126]

These results suggest that pretreatment time plays a major role in determining the size of the catalyst particle which inturn decides the tube diameter. Also care should be taken during pretreatment, not to pretreat the sample for a prolonged time which results in melt pattern and resulting in no tube growth.

3.8.4 Effect of growth time

The growth time or deposition time also plays a vital role in optimizing the growth of the nanotubes. Yan *et al.* [127] found that during CVD the growth rate of SWNTs was found to be large during the ignition for few minutes and the growth rate starts to decrease and then attains a saturation point beyond which there is no significant nanotube growth. Also, they found that the quality of tubes in the initial few minutes was low due to lots of defects, whereas longer growth time forms higher quality tubes. It was found that the yield of carbon deposits is higher but was found that it is inevitable to avoid other forms of carbon like amorphous carbon and suggested that there is always a compromise between the yield and the quality of nanotubes produced.

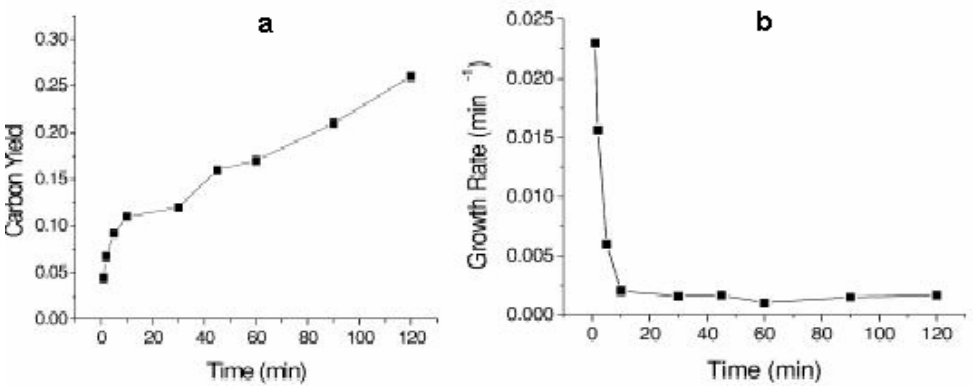

Figure 3.31 – Carbon Yield and growth rate dependence on time [127]

Figure 3.31(a) shows the dependence of carbon yield with time and Figure 3.31(b) shows the variation of growth rate with time. It suggests that the carbon yield increases

significantly until 30 mins of growth time. The yield is about 12% for 30 mins and 23% for 120 min. Figure 3.31 B shows that the carbon nanotube growth is high during the initial few minutes and then drops down and attains saturation. Figure 3.32 shows TEM image of SWNTs grown at 2 min (left) and 30 min (right).

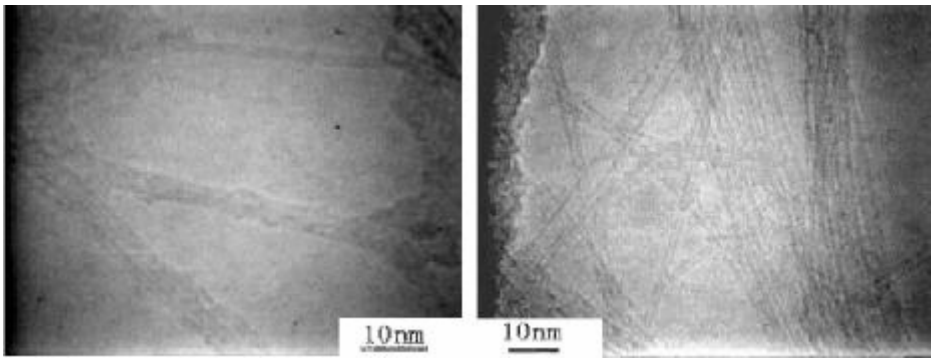

Figure 3.32 – TEM image of SWNTs growth for 2min (left) and 30min (right) [127]

These results indicate that the growth time has significant effect on the yield of nanotube, quality of the nanotube produced and the carbon yield.

3.8.5 Effect of power

The microwave power or the laser power is found to have its effect on the nanotube growth and its properties. The increase in power is found to have an increase in diameter. This is in correlation with the increase in temperature. As the power increases, the temperature also increases and the desired effect is similar to that of increased temperature. Section 3.8.2 states that increase in temperature increases the catalyst size and thereby resulting in increased diameter of the tubes. Huang *et al.* [128] found that increase in the microwave power in a CVD system increases the temperature of the substrate and also changes the morphology of tubes obtained. The emission property of the nanotube film also changes with microwave power.

Figure 3.33 shows the SEM micrographs of the nanotubes grown at 1000 W, 900 W and at 800 W. Figure 3.33 suggests that at 1000 W, there is no clear tube appearance and at 800 W there is lot of carbonaceous particles. 900 W was found to have clear tubes with less carbonaceous materials. These tubes were analyzed for emission properties and the 900 W tubes were found to have the best emission properties. Also the Raman peak was found to be sharp only for the 900 W grown tubes. Similar observations were made by Zhang *et al.* [129] in a laser ablation experiment where they increased the laser power. The increase in the laser power was found to increase the average diameter of single walled nanotubes produced.

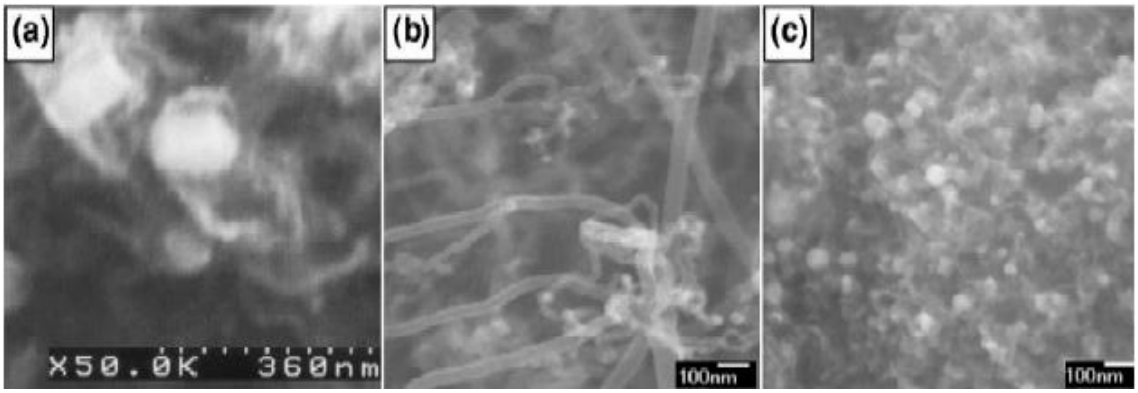

Figure 3.33 – SEM image of CNTs grown at (a) 1000W (b) 900W (c) 800W [128]

These observations suggest us that the power can be tuned up or down depending on the diameter of the tubes required and also can be varied depending on the required emission properties of the tubes.

These variations in the process parameters help us understand and analyze the processing conditions in a better manner and help us develop a better design of experiments so that the conditions are optimized based on requirements. Together with the understanding of the process gases, their reaction kinetics and their effects, this study helps to narrow down the process conditions and obtain optimized results.

CHAPTER 4

PROBLEM STATEMENT

Carbon nanotubes require a transition metal catalyst or its precursors for their growth in MPECVD. Each catalyst has its own unique properties and grain structure and this really affects a great deal on the nanotubes grown on them. In other words, choice of a catalyst or its precursor itself is an important parameter. This study focuses on growth and synthesis of carbon nanotubes using iron oxide in colloidal form as a catalyst. The catalyst is a stable colloidal suspension of sub-domain magnetic iron oxide particles in a liquid carrier. The average particle size is about 100Å (10 nm) and to prevent agglomeration of the particles they are coated with a stabilizing dispersive agent (surfactant). The liquid carrier fluid is either water or mineral oil. Growth of carbon nanotubes using this catalyst in microwave plasma enhanced CVD is an unexplored field. This study focuses on optimizing the growth of carbon nanotubes using colloidal form of iron oxide as a catalyst by varying the process parameters.

Silicon wafer being a semiconductor and since carbon nanotubes are largely used in the semiconductor industry and in field emission devices, silicon wafer is used as a substrate in this study. Though the process gases play an important role in the synthesis of CNTs, an equal and important role is performed by the substrate preparation method

and the catalyst coating on the substrate for activation of the synthesis. The method of catalyst coating also plays an important role which is varied to get the optimized growth.

This study concentrates on the growth of carbon nanotubes and involves the analysis of the growth by varying the following process parameters.

- Method of application of the catalyst coating
- Concentration of the catalyst being coated
- Varying the pretreatment time
- Varying the growth time
- Varying the chamber pressure
- Varying the flow rates of the process gases

Better control of the process requires proper evaluation of the above mentioned process parameter. The process of obtaining nanotubes by varying these process parameters are analyzed and studied in order to better understand and optimize the process and have a better control in getting the tubes what we want. This research aims at the following:

- Using colloidal form of iron oxide as a catalyst for the growth of carbon nanotubes.
- A detailed investigation of the process parameters and their effect in the synthesis of the carbon nanotubes using microwave plasma enhanced CVD.
- Relating the process parameters to get optimum yield and good quality of CNTs.
- Optimizing the process parameters so as to obtain vertically aligned nanotubes with fewer impurities so that they can be used for given application without the need for further purification.

- Characterization of surface morphology of the CNTs using SEM, TEM and AFM.
- Elemental analysis of the deposited coating using energy dispersive X-ray spectra (EDS).
- Characterization of CNTs using μ-Raman spectroscopy to determine the phase purity.

CHAPTER 5

EXPERIMENTAL SETUP AND METHODOLOGY

5.1 Description of the Microwave Plasma Enhanced CVD (MPECVD) reactor

The MPECVD reactor uses an ASTeX Plasma Deposition Equipment (PDE) as a tool for the deposition and growth of carbon nanotubes on a given substrate. The ASTeX PDE consists of an AX S-1500i microwave power generator with a maximum power of 1.5 kW and a frequency of 2.45 GHz. This equipment is best known for its MPECVD quality. It enables unprecedented control over deposition parameters and helps in varying a wide range of process parameters [131]. The schematic of the apparatus along with the microwave power generator is shown in Figure 5.1. The reactor consists of a double walled water-cooled chamber of 5.78 inches diameter and 13 inches height. The chamber is made up of 300 series electro polished stainless steel.

The microwave power generator has a variable output from 20% to 100% of its rating 1.5 kW. The forward and reflected powers are read out in the digital display with a resolution of ±1W. The microwave power is coupled by a symmetric plasma coupler and is focused onto the substrate in the presence of the reactive gases through a 4.75 inch quartz window. The microwave power ionizes the reactive gases and a plasma ball is formed at or slightly above the substrate surface. The gas flow systems and the control systems used for the reactive gases are described in detail in the next section. The

substrate holder provides a motorized Z-motion position control for raising or lowering the substrate to alter the proximity of the sample to the plasma. A graphite susceptor is placed on top of the substrate holder; a graphite disc on which the substrate is kept during growth is placed onto this graphite susceptor. The substrate is loaded into the reactor through the 2.06 in x 4.13 in door in front of the reactor.

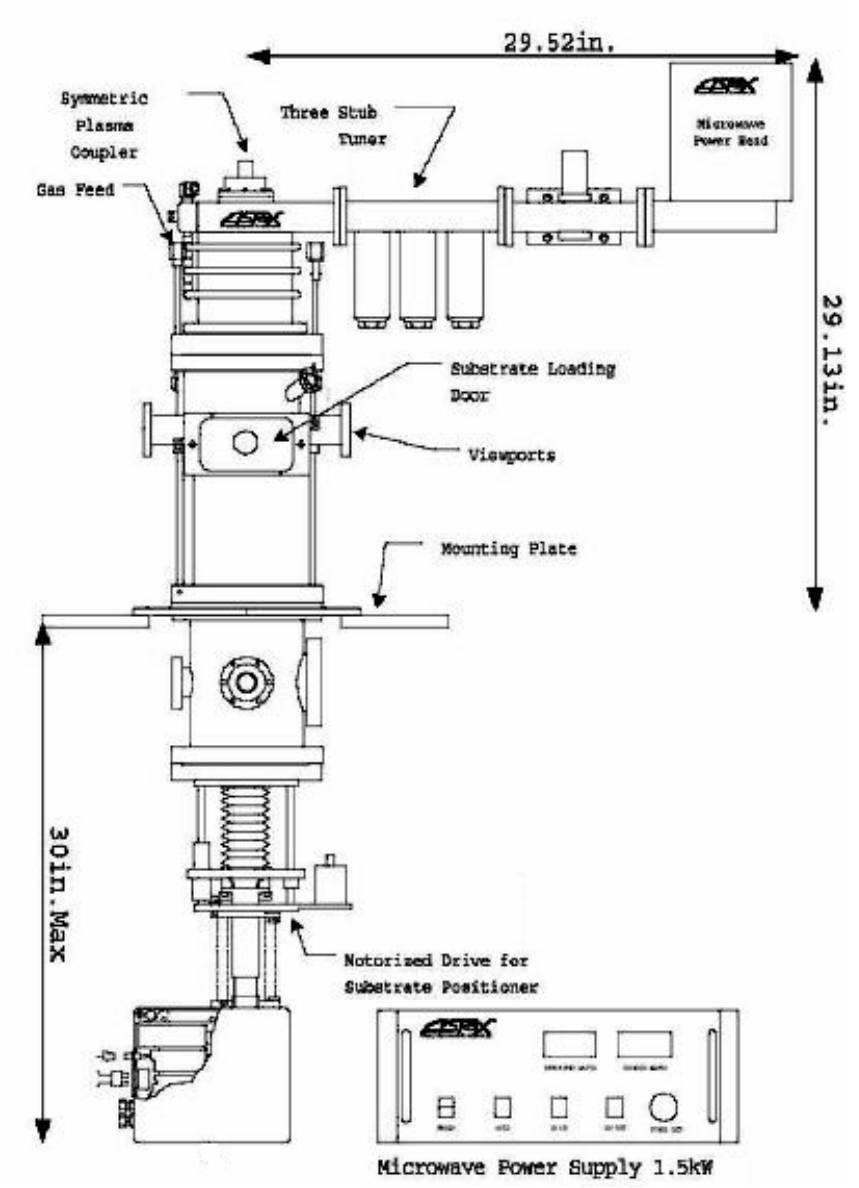

Figure 5.1: Schematic of a Microwave Plasma Enhanced CVD reactor [131]

The system is also equipped with an option of a Shenzen Mastech DC power supply (HY3020) for supplying a negative voltage to the substrate and positive voltage to the reactor chamber. The voltage can be varied from 0 - 30 V and the current from 0 - 20 A. Also, the reactor is provided with another option of a substrate heater assembly which can heat the substrate upto 1200°C in ultra high vacuum (UHV). The heater used is obtained from Heatwave Labs Inc. (Model No. 101491). Unless specifically mentioned, this research did not use the option of the biasing the substrate with a negative voltage or external heating applied to the substrate through the heater.

The stainless steel chamber has two sapphire viewports apart from the viewport in the door for in situ optical diagnostics. The substrate temperature is constantly monitored using a Williamson Dual wavelength optical pyrometer. The pyrometer is focused on to the substrate through the sapphire viewports. The pyrometer has four narrow bands of spectral filters of different wavelengths and it determines the temperature of objects without contact with the help of infrared temperature sensors. The sensors work on the principle that the energy emitted by an object is proportional to its temperature. The signal received by the sensor from viewing the object is converted into desired temperature output by sensor electronics and is displayed in a digital meter. Moreover the sensors are placed in rugged enclosures to protect them from hostile operating conditions. The model of the Williamson dual wavelength pyrometer used in the experimental setup is TEMPMATIC 8220S-C-T series.

5.2 Gas Flow System and Control system

The flow rate of the reactive gases and controlling their flow is handled by the gas flow and control systems. They consists MKS type 247C mass flow meters along with

MKS type 1159B mass flow controllers, MKS type 250C pressure/flow controller, a MKS type 127 Baratron pressure transducer, valves and necessary tubing. The stainless steel chamber is connected to a mechanical pump (Alcatel) and is capable of taking the chamber pressure to ~10^{-2} Torr. The reactive gases used in this study are methane (CH_4), hydrogen (H_2) and nitrogen (N_2). Ultra high pure (UHP) grade of H_2 and N_2 are used and chemically pure (CP) grade CH_4 is used.

The reactive gases are pumped into the reaction chamber and the MKS type 250C pressure controller [132] facilitates in controlling the chamber pressure. It has multiple functions, namely to control the flow valves to accurately maintain a set pressure, it can accept input values from a variety of pressure transducers and it can be used for gas ratio control. The front panel facilitates in the selection of the input range, controlling loop tuning and controlling automatic and manual valve. Correct flow rates of gases are obtained taking into consideration the compensation needed because of gas being removed by the pump.

Thus the pressure controller maintains the required pressure in the chamber and the pressure in the system is monitored by the MKS type 127 Baratron pressure transducer [133]. The pressure transducer has a sensor, a signal conditioner and power supply and constantly monitors the pressure in the reaction chamber and reports to the pressure controller. The pressure transducer has an accuracy of ±0.15% and the pressure controller has ±0.25%. The flow rates of the reactive gases are controlled by the MKS type 247C mass flow meters [134] coupled with the MKS type 1159B mass flow controllers [135]. The mass flow meter consists of a power supply, four signal conditioning channels, four set point circuits and a digital panel display meter. They are

used to monitor and provide set point levels for the mass flow controllers. The mass flow controllers in turn allow a rationed quantity of the reactive gases as instructed to them through the set point in the mass flow meters. In other words, the mass flow controller accurately measures and controls the mass flow rates of reactive gases.

A photograph of the experimental set up is shown in Figure 5.2. This chapter gives only the brief outline of the instruments and equipments used. Details and specifications of the various equipments and instruments used are given in the Appendix.

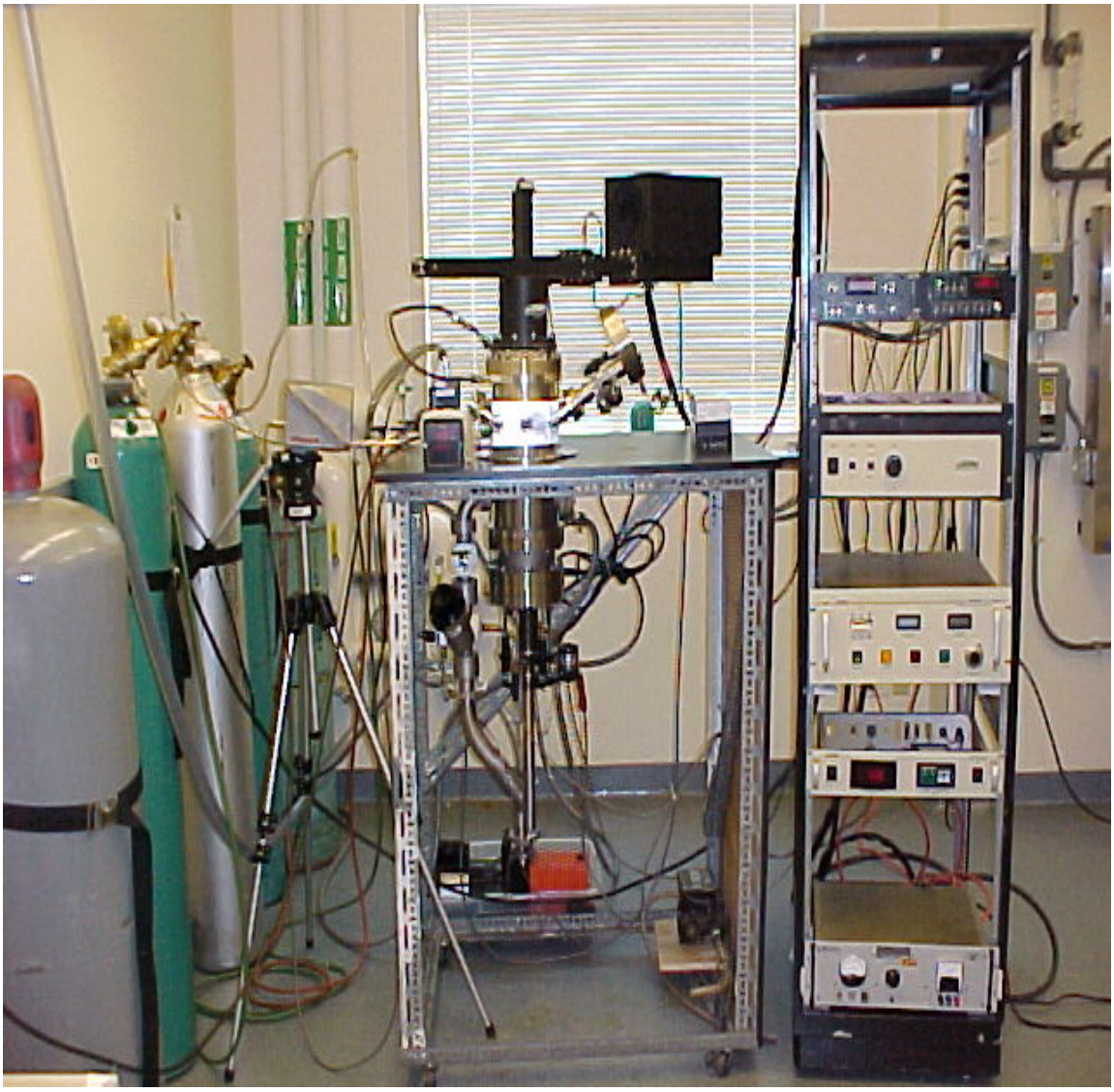

Figure 5.2. Photograph of Microwave Plasma Enhanced CVD experimental setup

5.3 Methodology

A detailed description of the methodology of growing carbon nanotubes using a colloidal form of iron oxide as a catalyst is given in this section. It describes the substrate preparation and cleaning, catalyst coating and the carbon nanotube deposition and growth procedure.

5.3.1 Substrate Preparation and Cleaning

Cleaning substrates using various chemicals is one of the most important methods of substrate treatment to improve adhesion of the coating. Chemicals are used to remove the contaminants from the surface to clean the surface. Chemicals also react with substrate materials to make chemical changes in the surface and make it react with coating and enhance the adhesion. Most of the substrate treatment process with chemicals involves the treatment of the substrates with hydroxides, water and acid. Cleaning may include chemical degreasing, electrolytic degreasing or treatment with an oxidizing agent.

In order to clean the silicon substrates they are placed in an acetone bath and ultrasonicated for 5-15 mins. This helps in removing the impurities from the substrate and facilitates in better adhesion of the catalyst film to the substrate. Ultrasonication in acetone cleans the substrate reasonably well. But if the cleansing action is not adequate then, the cleaning process developed by Fleming *et al* [136] should be used. In this investigation the silicon substrates are ultrasonicated in acetone for 15 mins.

5.3.2 Catalyst coating

The catalyst – the colloidal form of iron oxide needs to be applied onto the silicon substrate before growth of nanotubes as it is an essential element for nanotube growth. The catalyst solution used in this study is a mineral oil based solution with an average particle size of 100Å (10 nm). 10 ml of the catalyst solution is diluted with 90 ml of isopropyl alcohol and is used as a catalyst precursor solution. Unless otherwise stated the catalyst solution has this concentration and for convenience this solution will be called the standard catalyst solution. The catalyst solution is applied onto the silicon wafer substrates by four methods.

1. By squirting using an atomized spray bottle.
2. A small droplet of the catalyst is placed onto the substrate using a Pasteur pipette.
3. The catalyst solution is dropped onto the substrate and spin coated using a dremel hand grinder.
4. A measured quantity of the catalyst solution is dropped onto the substrate using a Pasteur pipette. Then a microscope cover glass is placed on top of it and evenly smeared all over the substrate so that a thin film of the catalyst coating is evenly applied over the entire substrate.

The catalyst coated substrate is loaded into the CVD reactor for the growth of nanotubes. The process gases used in this study are methane (CH_4), hydrogen (H_2) and nitrogen (N_2). Carbon nanotubes are formed on the substrates following a deposition procedure which is described in the next section.

5.3.3 Carbon Nanotube Deposition Procedure

The deposition procedure for the growth of carbon nanotubes is as follows:

- The mass flow meter and the pressure transducer readout are switched on first for warm up.
- Cooling water supply for the reactor and the process gas cylinders are opened.
- The substrate coated with the catalyst material is placed on a graphite plate and placed in the reactor on top of the graphite susceptor.
- The chamber is closed and the vacuum pump is turned on until the pressure is ~10^{-2} torr. Then the desired pressure is set which is normally between 5-25 Torr.
- The hydrogen gas is switched on and the flow rate is controlled using the MKS mass flow meter. It normally varies from 0-100 sccm.
- The microwave power is switched on and the hydrogen plasma is formed and the reflected watts are reduced by adjusting the knobs.
- Immediately, nitrogen flow rate is started which is also varied from 0-90 sccm.
- The sample is plasma pretreated in the H_2-N_2 plasma for a given time according to the requirement.
- The methane flow rate is switched on and it usually varies between 2.5-30 sccm and after the required growth time, the methane flow rate is switched off.
- Hydrogen gas flow is also turned off and nitrogen is normally allowed during the cool down process.
- Nitrogen gas flow is shut off and the substrate is allowed to anneal in the chamber for ~5 mins with the vacuum pump still running. Then the vacuum pump is shut off.

- The substrate is removed from the chamber after venting the chamber and it is now ready for characterization.

5.4 Characterization

The carbon nanotubes deposited on top of the substrate with are characterized using scanning electron microscopy (SEM), transmission electron microscopy (TEM), atomic force microscopy (AFM), and μ-Raman spectroscopy. The detailed description of the characterization techniques and the equipments are described in the next chapter.

CHAPTER 6

CHARACTERIZATION TECHNIQUES USED

6.1 Introduction

The carbon nanotubes grown are characterized by various methods. Characterization of nanotubes provides information that enables better understanding of how well the nucleation and growth of nanotubes have taken place, their quality, the density of growth or the yield of the nanotubes, their microstructure and morphology. They can also help in classifying the tubes grown under different categories, such as SWNTs or MWNTs, metallic or semiconducting. It becomes really important to do characterization on the deposited materials because carbon has different allotropes, namely graphite, diamond, fullerenes, and nanotubes. Apart from the allotropes there is also amorphous carbon. In most of the cases, the deposition is black in color and in order to clearly state that the deposited material is carbon nanotubes and not any other form of carbon, characterization is very important. Therefore it is a necessity to differentiate these forms of carbon and identify techniques to characterize them. Also, it becomes important to characterize the nanotubes in order to validate and tell that they are either MWNTs or SWNTs. The characterization also helps us to find out whether the deposited nanotubes are aligned vertically or aligned locally or non-aligned.

Jung *et al* [137] synthesized carbon nanotubes using plasma enhanced HFCVD and they used a systematic procedure for characterizing the nanotubes produced.

- First the morphology of the catalyst coating and the nanotubes grown are characterized using a scanning electron microscope (SEM).
- Transmission electron microscopy (TEM) is used to study the detailed morphology of the nanotubes. It provides a better idea of the walls of the nanotubes, the bamboo structure or the inside tube morphology, the catalyst particle at the tip. Also, diameter of the tube and surface defects can be analyzed using TEM.
- In order to specifically state the elemental composition of the nanoparticle at the tip of the nanotubes and also to find out the intensity of the carbon content, Electron dispersive X-ray Spectroscopy (EDS) peaks was used.
- The nanotubes can be multiwalled or single walled and in order to validate their presence apart from TEM, μ-Raman spectroscopy was used. It shows the corresponding peaks for single and multi-walled nanotubes and by this way we can authenticate the type of nanotube.

Similar to Jung *et al* [137] other researchers [138, 139] have been following a specific protocol for characterizing the tubes synthesized in order to have a better understanding. Apart from above mentioned characterization techniques one other frequently used technique is AFM which is used by Jang *et al* [140]. The AFM helps in determining the average diameter of the nanotubes. Also, it can be used to analyze the surface morphology of the nanotubes. It can be used as a tool for analyzing the surface defects and kinks in the nanotubes. A variety of techniques are employed by various researchers

for the purpose of characterization apart from those mentioned above such as Auger Electron Spectroscopy (AES), X-ray Diffraction (XRD), Low Energy Electron Diffraction (LEED). Scanning Electron Microscopy (SEM) is extensively used in this study for characterization. Also Scanning Transmission Electron Microscopy (STEM), Atomic Force Microscopy (AFM), Energy Dispersive Spectra (EDS) and μ-Raman Spectroscopy are also used during this research. These techniques are discussed elaborately in the ensuing sections.

6.2 Electron Microscopy

Carbon nanotubes after synthesis are subjected to characterization to observe and study the growth morphology. An extensive examination using a Scanning Electron Microscope (SEM) is first done. The great depth of field and high resolution of the SEM compared with the optical microscope, and its capability for determining elemental compositions by means of associated x-ray analysis facilities, have made SEM the premier instrument utilized in the study of synthesized nanotubes. When more detailed information about the morphology and the microstructure is required, a transmission electron microscope (TEM) is employed. In both SEM and TEM, an electron beam is directed onto the specimen to be examined. The electron specimen interaction signals are depicted in Figure 6.1. Through control of the incident electron beam, unique information can be obtained regarding specimen surface topography, crystal structure and lattice defects, elemental composition etc. An appropriate detection system is required to properly harness the various interaction signals emerging out from the specimen [141].

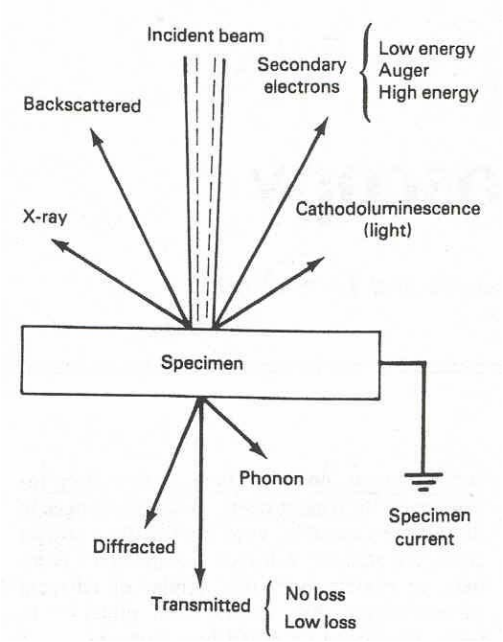

Figure 6.1 Electron Specimen Interaction signals [141]

6.2.1 SEM and TEM instruments

Schematic drawing illustrating the basic configurations of SEM and TEM are shown in Figure 6.2 (a) and (b) respectively. Both instruments employ an illumination system consisting of an electron gun and subsequent electromagnetic lenses to project an approximately focused or collimated beam of electrons onto the specimen. In TEM, additional lenses below the specimen are provided for image formation and magnification. Suitably located apertures are employed to define the beam along with coils for beam alignment, astigmatism correction and beam scanning. A vacuum environment is required for both microscopes to limit scattering by gas molecules.

The most common source of electrons in both instruments is a heated tungsten filament, although a single crystal lanthanum hexaboride (LaB_6) emitters and tungsten field emission tips are gaining in popularity. These two sources are substantially brighter

than the tungsten filament, as much as 10^2 times for the LaB_6 source and 10^4 for the tungsten field emission source. In general, they provide improved resolution, analytical capabilities, and greater operational life but cost is higher and more sophisticated vacuum system is required. The electrons are accelerated through a potential that is established by an applied voltage between the filament and anode. SEM accelerating voltages typically range from about 100 V to 30 kV.

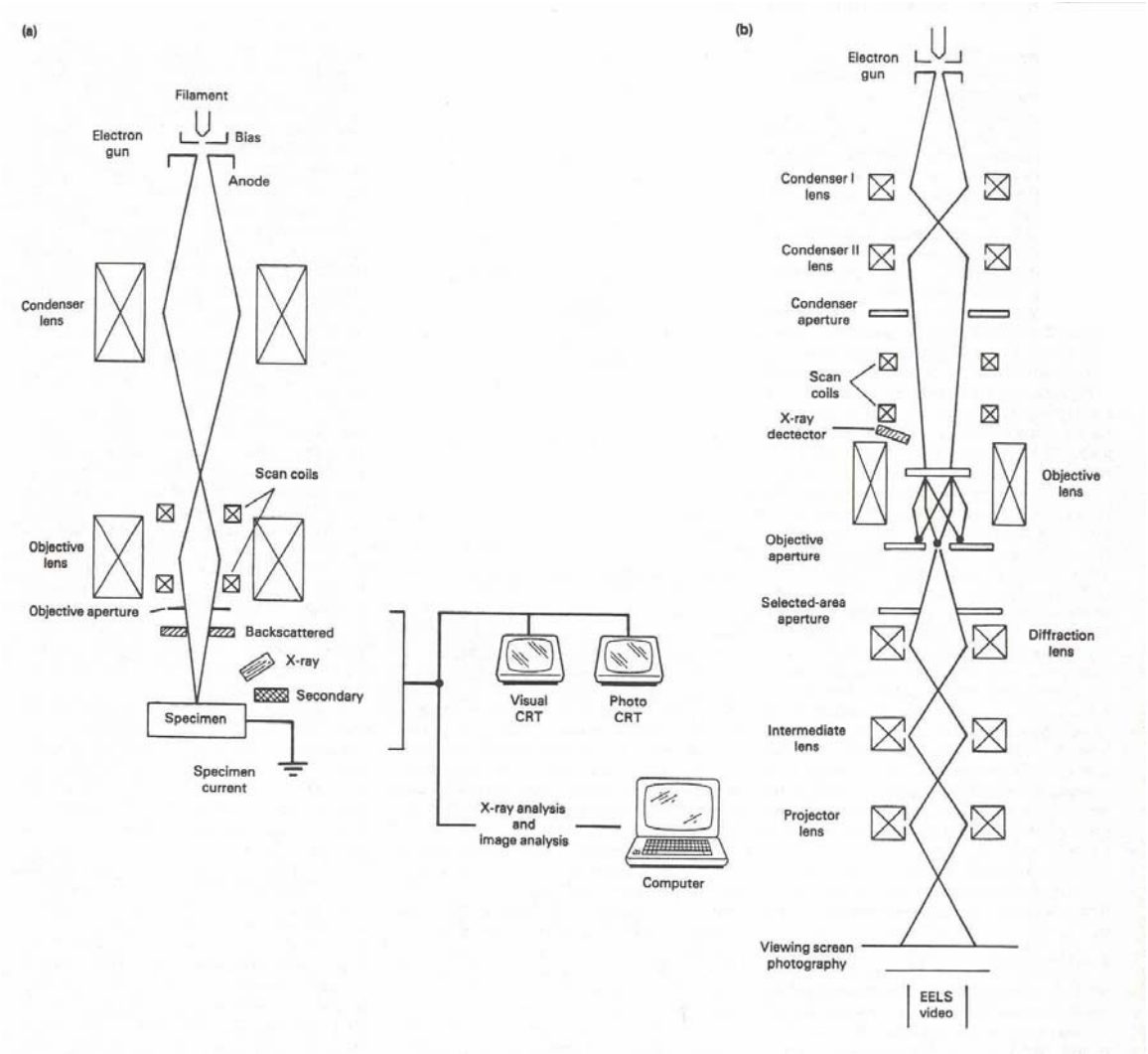

Figure 6.2 Schematic configurations of (a) SEM and (b) TEM

TEM is available at 3 different accelerating voltage ranges. The most commonly used ones are about 120 kV, but allow selection of voltages as low as 20 kV. The

maximum voltage is typically between 200 kV and 400 kV. High-voltage instruments are capable of operating at 10^6 V and higher voltages. In general, higher accelerating voltage permits penetration of thicker specimen and provides improved resolution.

In SEM, the specimen is normally located below the final lens in the illumination system. For improved resolution some instruments provide a second position within the final lens. The electron beam is focused onto a small spot and scanned serially over the specimen to form a rectangular raster. Secondary electrons are collected to provide a signal that is amplified and used to modulate the intensity of the electron beam in a CRT. The magnification of the image is determined by the ratio of the distance scanned on the specimen to the corresponding image displayed on the CRT. Resolution is determined to a first approximation by the diameter of the beam incident on the specimen. The diameter of the beam is controlled by the type of filament, the excitation of the condenser lenses, the final aperture size, and the working distance. In actual operation, the nature of the specimen and the signal source (secondary electrons, x-rays and so on) usually plays a limiting role in determining resolution [141].

TEM is significantly different from SEM and here the specimen is illuminated by a relatively broad, nearly parallel, stationary beam of electrons. Transmitted and diffracted electrons that have lost little or no energy and that do not deviate too far from the optical axis are focused by the objective lens. Subsequent lenses provide additional magnification and allow observation of the either the image or a diffraction pattern. The image and diffraction pattern can be viewed directly on a fluorescent screen, photographed, or displayed by means of a TV system [141]. TEM are also modified and

designed to function in the scanning mode. They are commonly referred to as Scanning Transmission Electron Microscope (STEM).

A JEOL JSM-6400 SEM is used in this present investigation. The SEM has a secondary electron resolution of 3.5 nm at 8 mm working distance and 10 nm at 39 mm working distance. The accelerating voltage of the SEM ranges from 0.2 to 40 kV which can be varied as desired. The voltage from 0.2 to 5 kV is variable in steps of 0.1 kV and from 5 to 40 kV is variable in steps of 1 kV. The specimen stage can be tilted from -5° to 90° and the specimen stage can be rotated 360° endless. The specimen movement range is 50 mm in x-axis, 70 mm in y-axis and 40 mm in z-axis. Magnifications from 10X to 300,000X can be obtained at a working distance of 39 mm. Other working distances available are 8, 15, 25, 39 and 48 mm. The images can be seen in the CRT display equipped in the instrument. The SEM is equipped with a CCD camera coupled to a computer for taking digital pictures of the images. For this purpose, an image analysis software by EVEX called Evex Nanoanalysis and digital imaging (version 2.0.925) is used [142].

The JSM-6400 scanning microscope is a state-of-the-art high resolution scanning electron microscope with a modern digital image processing system and it also assures high performance and lower noise at low accelerating voltages and high quality secondary electron images. The JSM-6400 can be used as an electron probe x-ray microanalyzer by adding an energy dispersive spectrometer or wavelength dispersive spectrometers, allowing accurate and efficient nondestructive elemental analysis. Figure 6.3 shows the photograph of JEOL JSM-6400 SEM.

Figure 6.3 JEOL JSM-6400 Scanning Electron Microscope (SEM)

The other electron microscope used in this investigation is JEOL 100 CX II Scanning Transmission Electron Microscope (STEM). The specimen chamber works on the basis of airlock mechanism and it has a loading capacity for 6 specimens. The resolution of the STEM is 0.2 nm. The accelerating voltages available are 20, 40, 60, 80 and 100 kV. In low magnification mode it can magnify samples for 100 X, 200 X, 400 X and 600 X. In wide field-high contrast mode it can magnify from 340 X to 300,00 X in 23 steps and in standard mode it can magnify from 1000 X to 850,000 X in 23 steps. The high resolution mode is 1.04 times that of the standard. The magnified image is formed onto a 75 mm x 85 mm fluorescent screen. After the required image is focused and seen on the fluorescent screen, the image can also be exposed onto a camera film using an inbuilt Polaroid camera. The STEM is provided with an option for adding a CCD camera device to view the images digitally and take pictures using image analysis software. The STEM is employed in this study to characterize the carbon nanotubes and classifying

them as SWNT or MWNT. It also facilitates to find the diameter of the nanotubes and also the surface morphology of the tubes by clearly depicting the kinkiness in the tubes. Figure 6.4 shows the picture of the JEOL 100 CX II STEM.

Figure 6.4 JEOL 100 CX II STEM

6.3 Atomic Force Microscopy (AFM)

The atomic force microscope (AFM) works similar to a stylus profiler. The only difference between the AFM and the stylus profiler is that the probe forces applied on the surface in AFM are much smaller compared to that in a surface profiler. Because of this reason higher resolution image can be obtained in AFM than in surface profiler. In an AFM a probe constantly raster scans across the surface and a constant force is applied between the probe and the sample. A 3D image of the sample is formed by monitoring

the raster scans of the probe on the sample. The force applied is constantly monitored and in order to maintain a constant force a feedback mechanism is equipped. This facilitates to control the position of the Z piezoelectric ceramic. Figure 6.5 shows the components of a light level atomic force microscope (AFM). The resolution of the pictures obtained by the AFM normally depends on the geometry of the probes. Sharper probes are found to give better resolution as they can map even small crevices with ease [144].

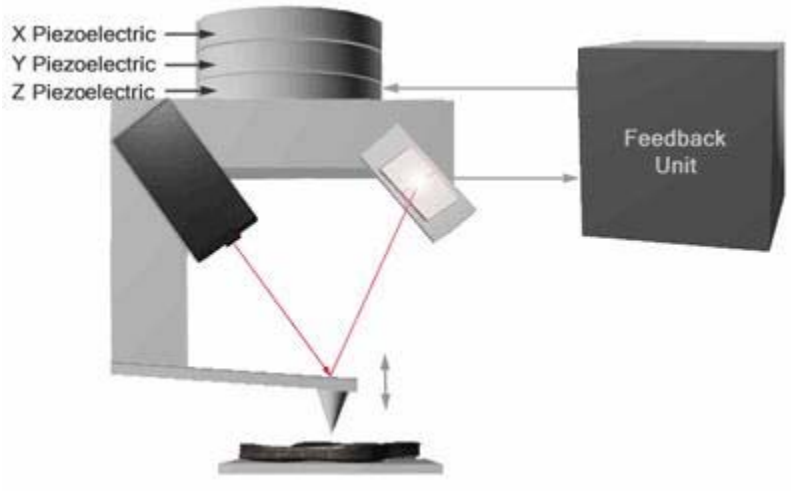

Figure 6.5 Components of a "light level" AFM [144]

Dimension™ 3100 series digital scanning probe microscope (AFM/STM) is used in this study to characterize the synthesized carbon nanotubes. This equipment is capable of imaging the surface using scanning mode as well as tapping mode [145]. Also it can be used as a Scanning Tunneling Microscope (STM). Figure 6.6 shows the image of the Dimension™ 3100 series digital scanning probe microscope.

The AFM is used in order to better understand the surface morphology of the nanotubes grown and surface defects can be identified. Apart from surface defects study, AFM is also used to measure the outside diameter of the nanotubes and it can be used to obtain the average diameter of a nanotube with varying diameters. Also this allows in

determining the average diameters of the tubes scanned by averaging out all the individual diameters over a given length of nanotubes.

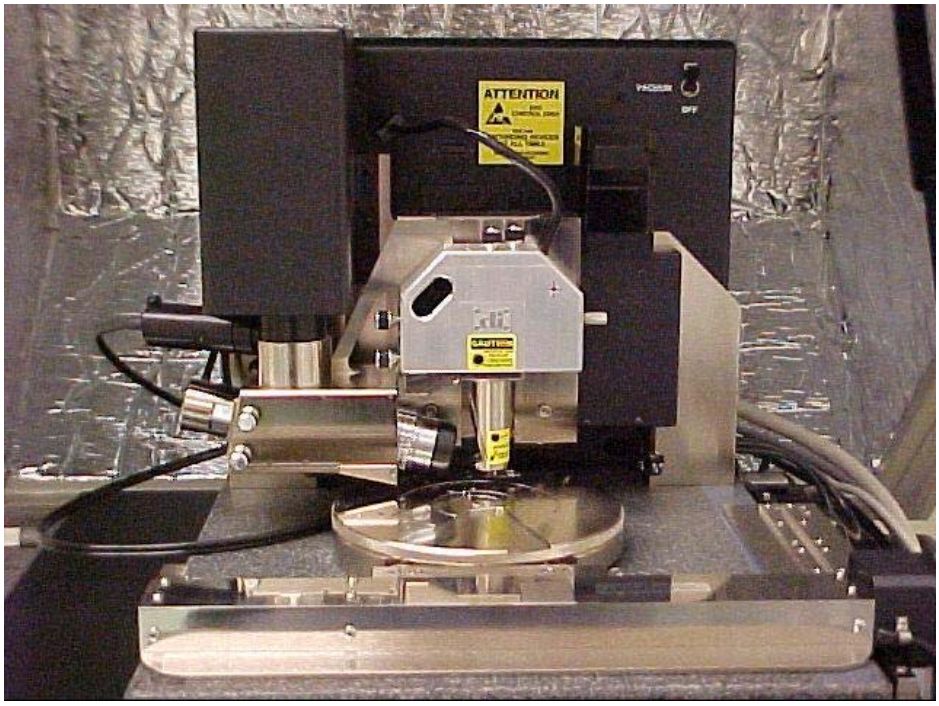

Figure 6.6 Dimension™ 3100 series digital scanning probe microscope (AFM/STM)

6.4 μ-Raman Spectroscopy

Raman spectroscopy is the most commonly used tool for decisively saying whether the tubes are SWNTs or MWNTs depending on their characteristic peaks being generated. Photons of light or laser are allowed to interact inelastically with molecules of materials and the energy change is measured in this technique. When a sample is irradiated the incident radiation can be absorbed, transmitted, reflected or scattered. The strongest form of scattering among the elastic scattering is Rayleigh scattering, in which the electrons and nuclei are displaced in opposite directions by the radiation. Monochromatic radiation may be scattered inelastically by a molecule, when incident and scattered photons do not have the same energy [146]. This effect was experimentally

demonstrated by Sir C V Raman and hence the name μ-Raman Spectroscopy. This effort fetched him a Nobel prize in physics in 1930. A SPEX 500M μ-Raman Spectrometer is used in this study which is as shown in Figure 6.7.

Figure 6.7 SPEX 500 M μ-Raman Spectrometer

The deposition formed on the silicon wafer after CVD might be containing not only carbon nanotubes but also various allotropes of carbon such as diamond, graphite, fullerene, carbon fibers etc. So it is better to characterize the deposited coating and for which the μ-Raman Spectrometer works handy.

These characterization thus facilitate to optimize the experiments based on the results obtained and can be useful in analyzing and understanding the results. The results of characterization in this study and discussion are dealt elaborately in the ensuing chapters.

CHAPTER 7

RESULTS

Experiments were conducted to study the role of pretreatment and its effect with pretreatment time. Tests were conducted by growing carbon nanotubes by varying the method of catalyst coating thereby optimizing the pretreatment time for best yield and alignment of nanotubes. Also, experiments were conducted by varying the growth time to investigate the nucleation density and yield of carbon nanotubes with respect to growth time. Similarly, the chamber pressure was varied to determine the optimum pressure when vertically aligned nanotubes are grown. The methane flow rate was varied to obtain vertically aligned tubes with as fewer impurities as possible. Growing tubes with fewer impurities facilitate various applications of this material easily without the need for further purification.

7.1 Results

7.1.1 Importance of Plasma Pretreatment

As previously pointed out the standard catalyst solution has 90% isopropyl alcohol and 10% catalyst solution which is mineral-oil based. When the standard catalyst solution is coated onto the substrates, the liquid portion of the catalyst solution covers the substrate in the form of a thin continuous film of catalyst layer. Also, the nanoparticles of the catalyst are dispersed evenly along with the liquid. The carrier fluid along with the

diluting alcohol forms a thin film which is quite large in area compared to the average particle size of the catalyst (~10 nm). Continuous film of catalyst layer is not helpful for the growth of nanotubes. This film has to be broken down into nanosized catalyst islands which help in the nucleation of carbon nanotubes. The task of breaking down the continuous thin catalyst film into nanosized particles is done by plasma pretreatment. Thus plasma pretreatment plays an important role of creating a conducive environment for nanotubes growth by making nanosized particles from the continuous film. The plasma pretreatment is done in H_2/N_2 plasma. Experiments were conducted to understand the importance of plasma pretreatment. The standard catalyst solution is coated onto a cleaned silicon wafer. Tests were conducted to distinguish the growth of CNTs between no pretreatment and plasma pretreatment. The plasma pretreatment is done for ~5 mins in H_2/N_2 plasma. The conditions for pretreatment are chamber pressure: 15 torr, microwave power: 500 watts and the flow rates of H_2 and N_2: 40 sccm and 50 sccm, respectively. Figures 7.1 and 7.2 show the SEM micrographs of a sample with no plasma pretreatment and 5 min pretreatment, respectively.

7.1.2 Effect of variation of plasma pretreatment

The duration for which the sample is plasma pretreated is as important as the plasma pretreatment process itself. From Figure 7.1 and Figure 7.2, the importance of plasma pretreatment can be clearly seen. Similarly, there is an optimum pretreatment time when there is a good growth and better alignment.

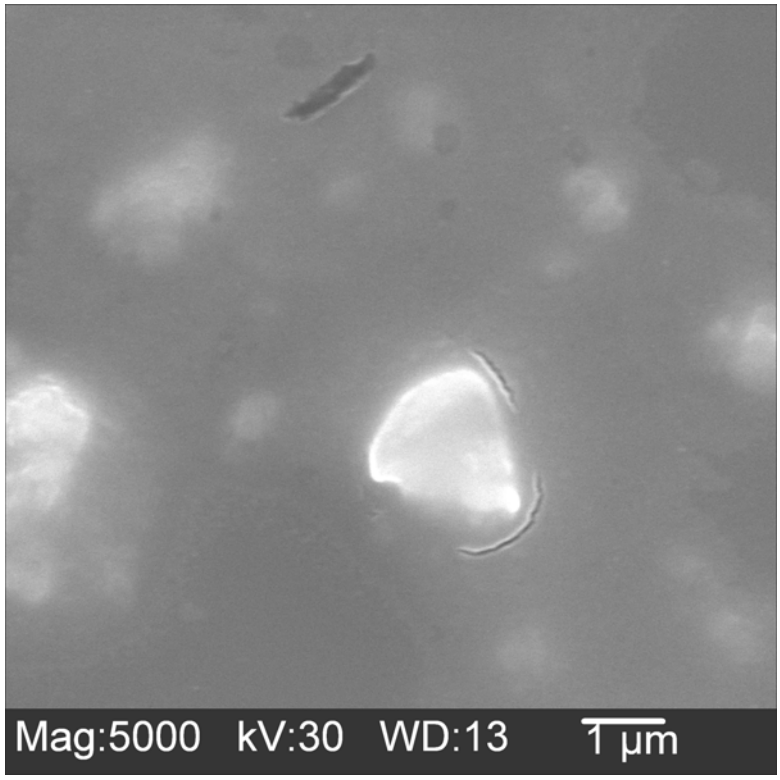

Figure 7.1 SEM micrograph of a thin film of catalyst on a silicon substrate with no pretreatment

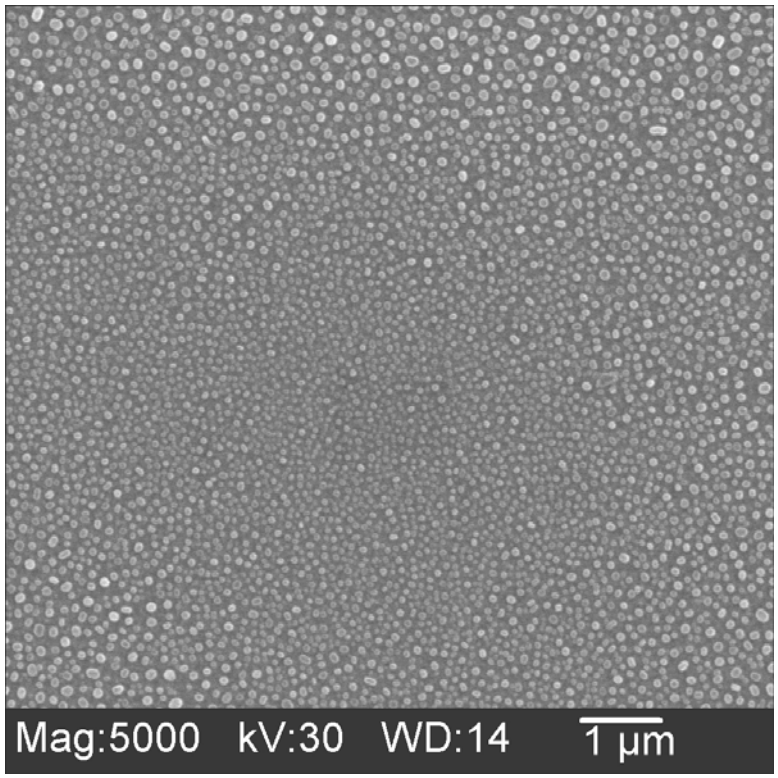

Figure 7.2 SEM micrograph of a sample 5 min pretreatment showing nanoparticles

Experiments were conducted at various plasma pretreatment times namely, 0, 3, 5, 10 and 15 mins. The pretreatment is done in a H_2/N_2 environment and after the pretreatment time, CH_4 is introduced to start the growth of CNTs. The experimental parameters employed during the variation of pretreatment time are given in Table 7.1. The catalyst was coated onto the substrate using an atomized spray bottle by squirting. Figures 7.3 to 7.7 are the SEM micrographs for the variation of plasma pretreatment for 0, 3, 5, 10 and 15 mins respectively. It is clear from the corresponding SEM micrographs that the nucleation density of the nanotubes slowly increases with the pretreatment time. Also, the nanotubes locally align themselves with increase in the pretreatment time. It is found that 10 min pretreatment is optimum where good nucleation density, better degree of alignment as well as lesser amorphous carbon and terminating clusters are obtained.

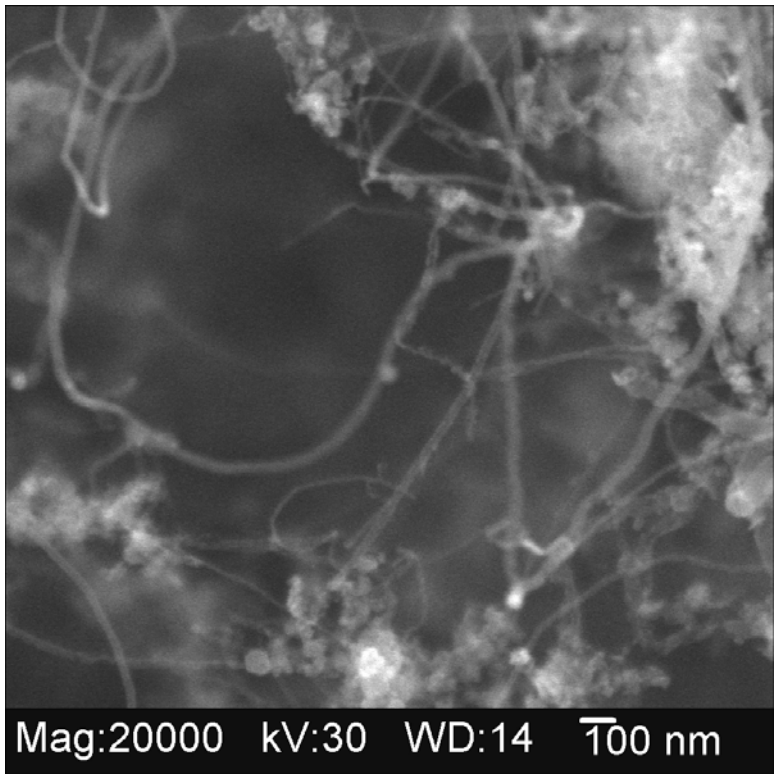

Figure 7.3 SEM micrograph of nanotubes grown on silicon without pretreatment

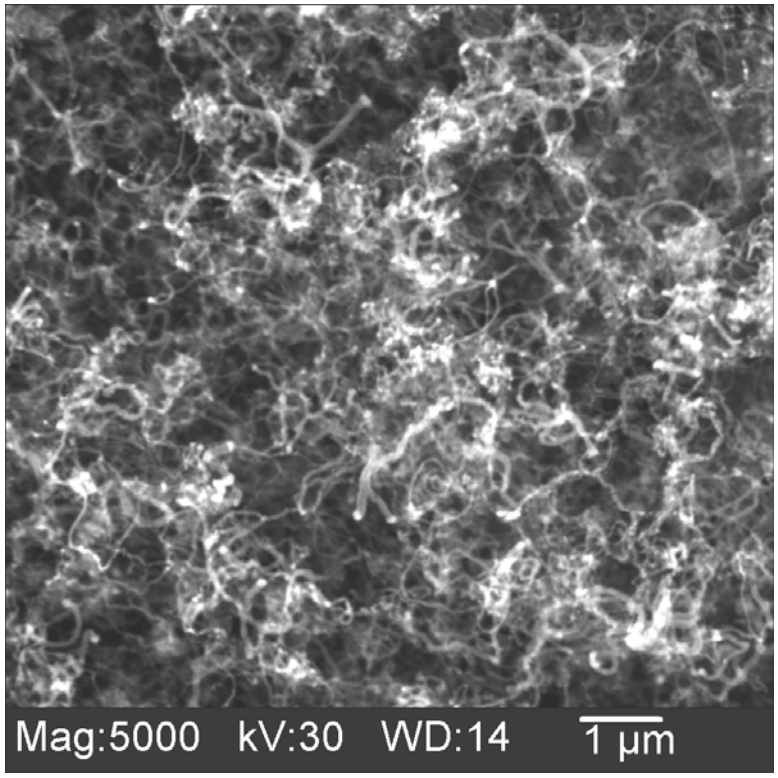

Figure 7.4 SEM micrograph of nanotubes on silicon with 3 mins pretreatment

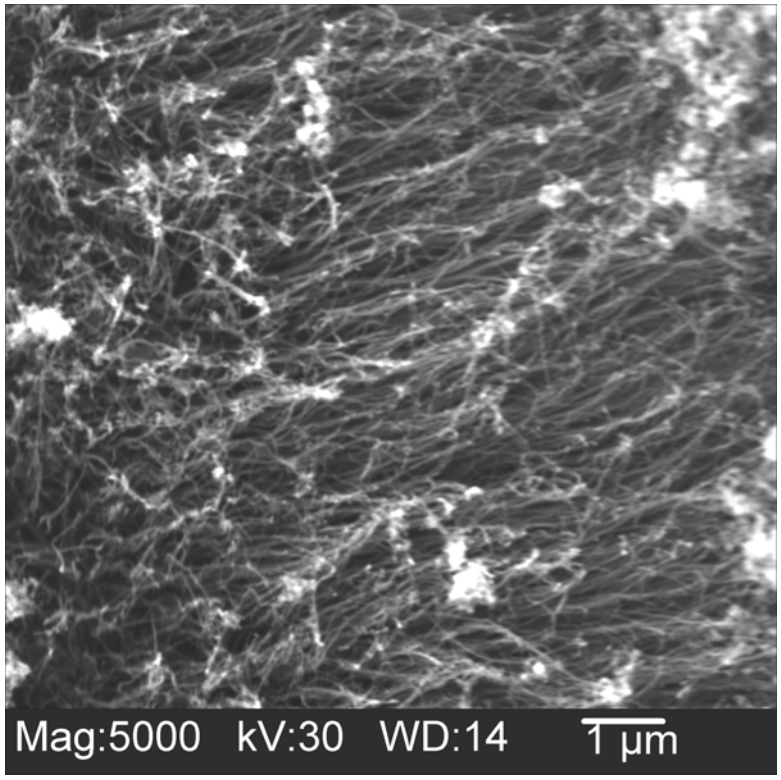

Figure 7.5 SEM micrograph of nanotubes on silicon with 5 mins pretreatment

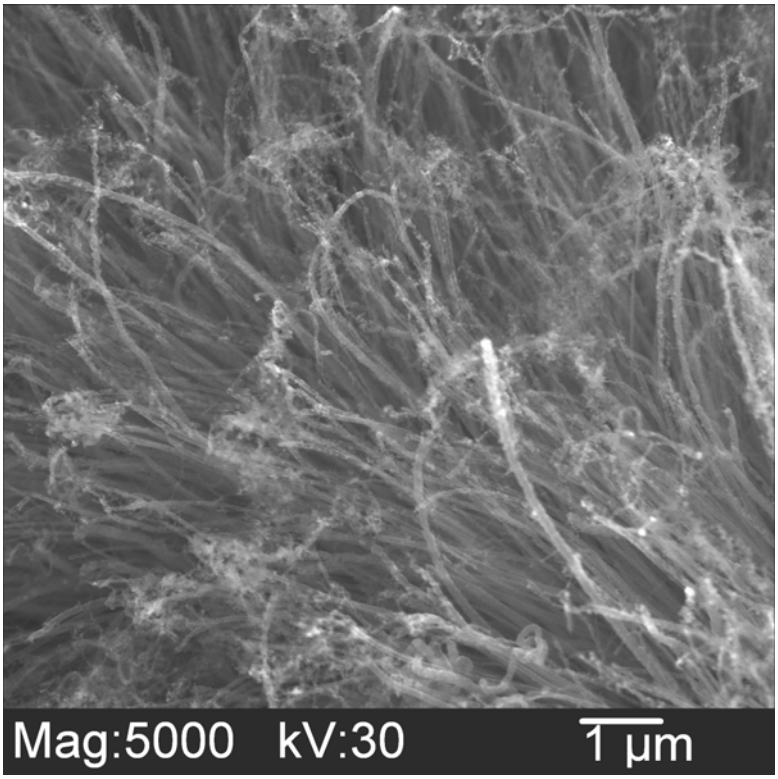

Figure 7.6 SEM micrograph of nanotubes on silicon with 10 mins pretreatment

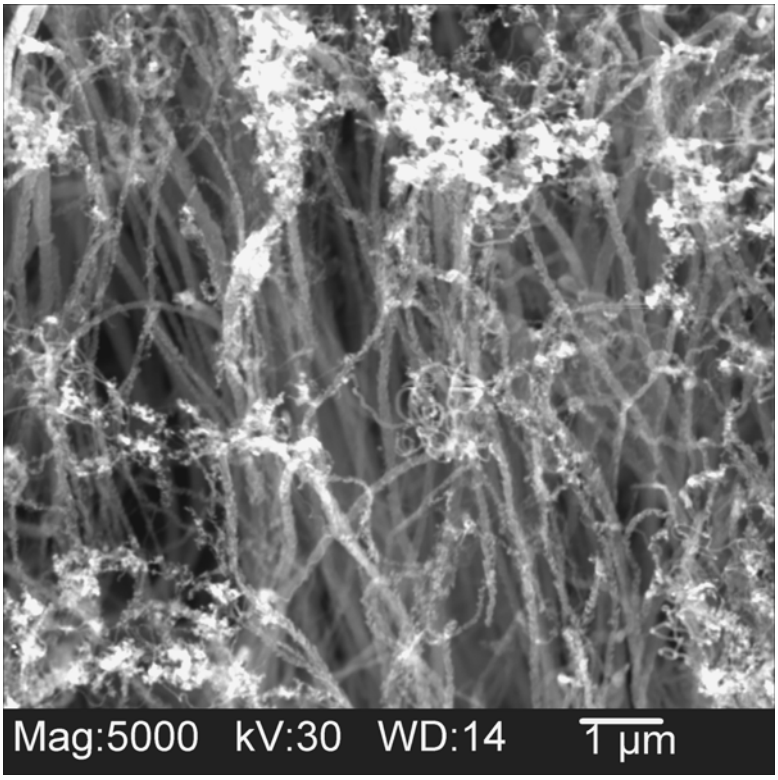

Figure 7.7 SEM micrograph of nanotubes on silicon with 15 mins pretreatment

Table 7.1 Process parameters used in the study of the effect of plasma pretreatment

Catalyst coating	2 squirts of atomized spray
Pretreatment time (variable), mins	**0, 3, 5, 10 and 15**
Microwave power, watts	500
Chamber pressure, torr	15
Growth time, mins	30
Flow rates of $H_2/N_2/CH_4$, sccm	40/50/10

7.1.3 Effect of catalyst concentration with pretreatment time

Tests were conducted to study the effect of growth of carbon nanotubes by varying the catalyst concentration coated onto the substrate and pretreatment time. The former is varied by the number of squirts (2 squirts and 5 squirts) applied onto the substrate and the latter for 0 min and 10 mins. The process parameters used in this study are given in Table 7.2.

Table 7.2 Process parameters for effect of catalyst concentration with pretreatment

	Pretreatment (0 min)	**Pretreatment (10 mins)**
Catalyst coating (variable)	**2 squirts, 5 squirts**	**2 squirts, 5 squirts**
Microwave power, watts	500	500
Chamber pressure, torr	15	15
Growth time	30 mins	30 mins
Flow rates of $H_2/N_2/CH_4$, sccm	40/50/10	40/50/10

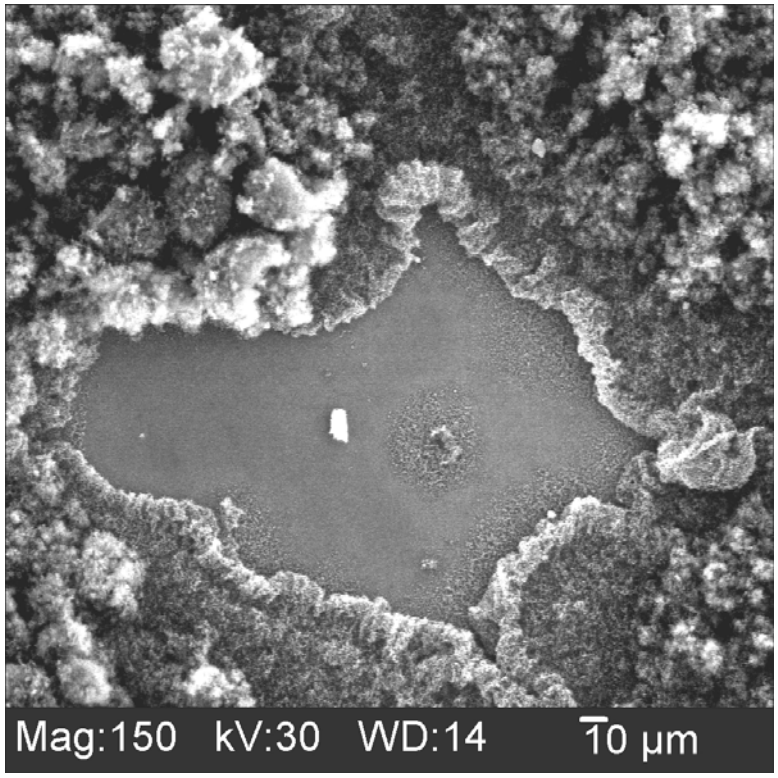

Figure 7.8 SEM micrograph of 0 min pretreatment and 2 squirts catalyst

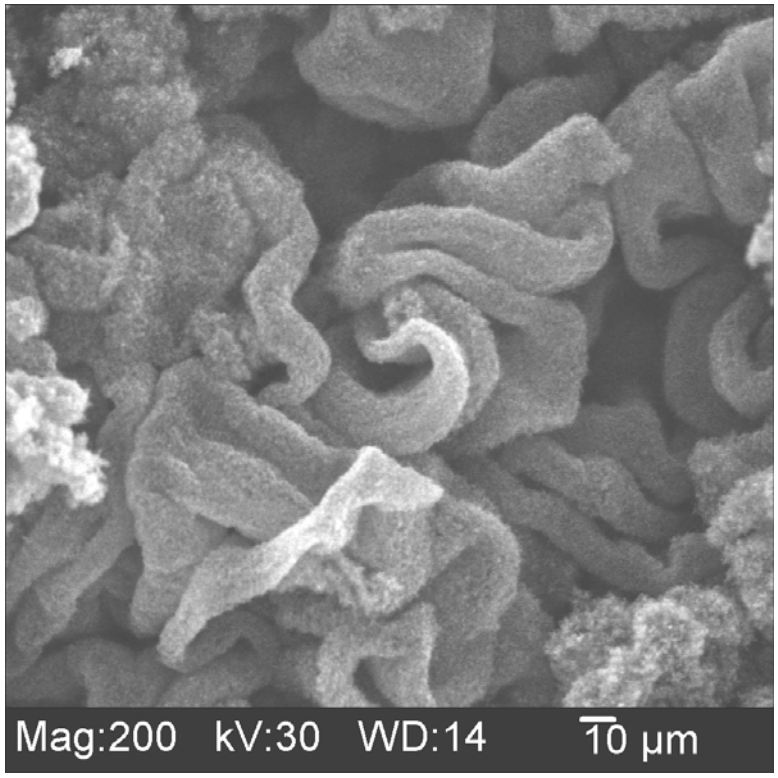

Figure 7.9 SEM micrograph of 0 min pretreatment and 5 squirts catalyst

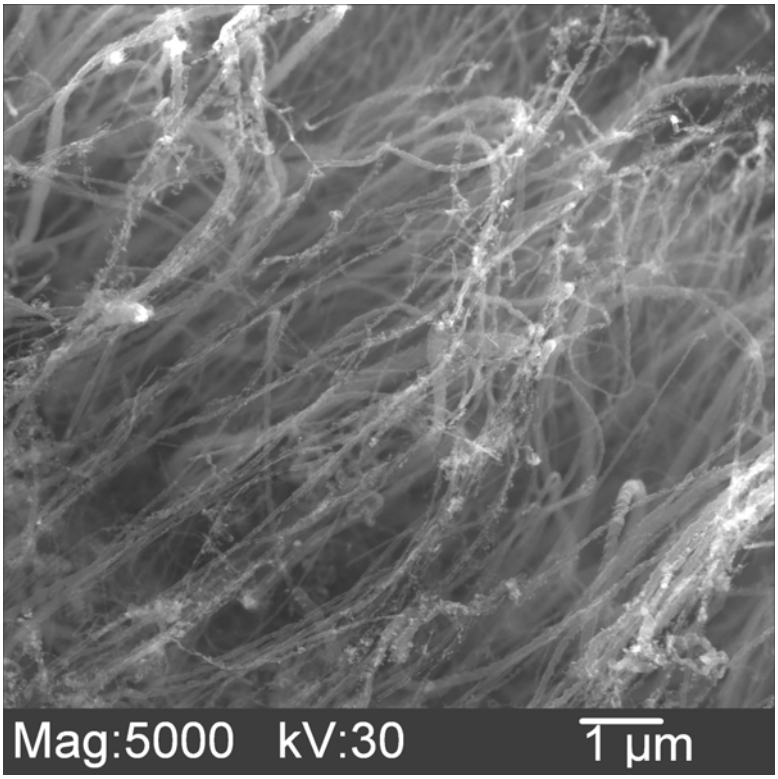

Figure 7.10 SEM micrograph of 10 mins pretreatment and 2 squirts catalyst

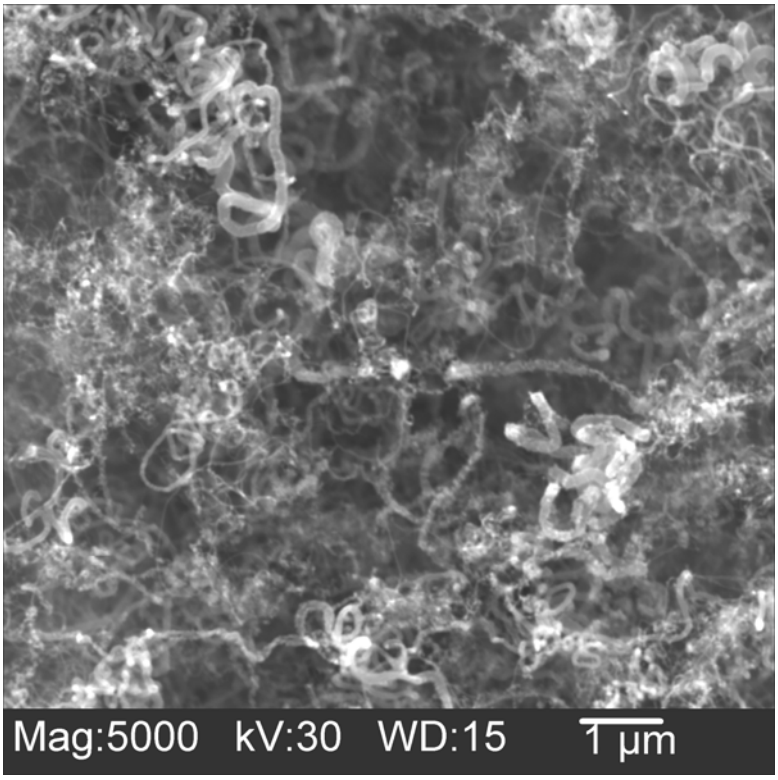

Figure 7.11 SEM micrograph of 10 mins pretreatment and 5 squirts catalyst

The SEM micrographs of the test results of the variation of catalyst concentration with pretreatment time are seen from Figures 7.8 to Figure 7.11. The deposition on 0 min pretreatment for both 2 squirts and 5 squirts formed carbonaceous deposits, but the nanotube growth is very sparse in both cases as seen in Figure 7.3. In the nanotubes grown for 10 mins pretreatment, more aligned and better tubes are formed for 2 squirts as compared to the tangled and coiled tubes for 5 squirts.

7.1.4 Effect of variation of the method of catalyst application

The catalyst can be applied onto the substrate by various methods. Based on the method and the way by which optimum catalyst coating is applied, better yield and alignment of the tubes are obtained. Four different methods are used to apply the catalyst.

- The catalyst is squirted on the sample by an atomized spray bottle.
- A drop of the catalyst is placed onto the substrate by using a Pasteur pipette.
- The catalyst is spin coated on the substrate by applying drops of catalyst solution while rotating the sample using a hand grinding machine.
- A measured quantity of catalyst is placed on the substrate and a microscope cover glass is placed on top and carefully smeared it all over the substrate.

The SEM micrographs for the test results are shown in Figures 7.12 to 7.15. It can be seen that smearing has better effect than other methods of catalyst application. Even though the squirting atomized spray and the spin coating produces aligned tubes, the tubes produced by smearing the catalyst is found to be better and more cleaner without impurities. Also the tubes are lengthier in case of smearing.

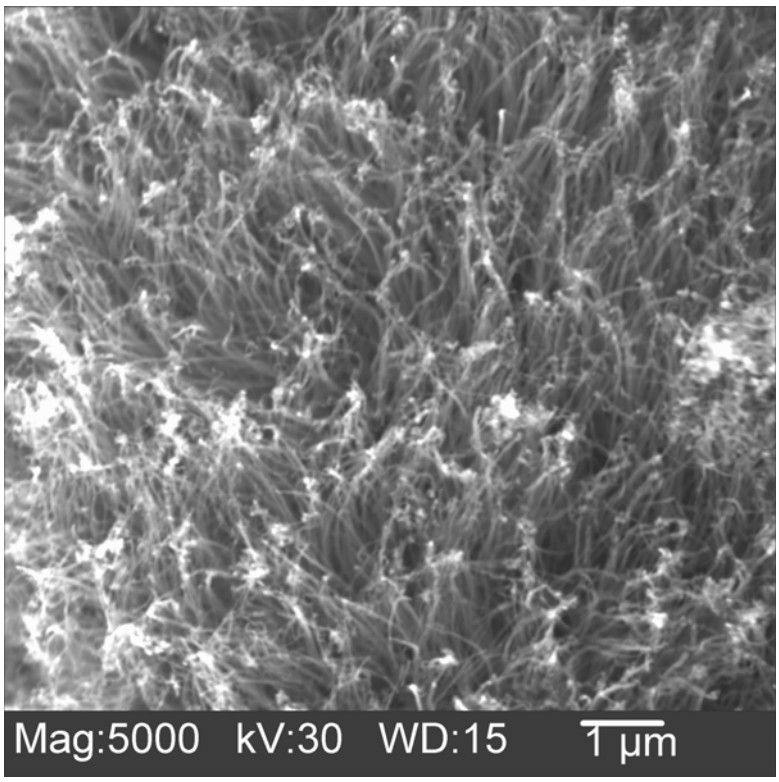

Figure 7.12 – Nanotubes grown by squirting catalyst material

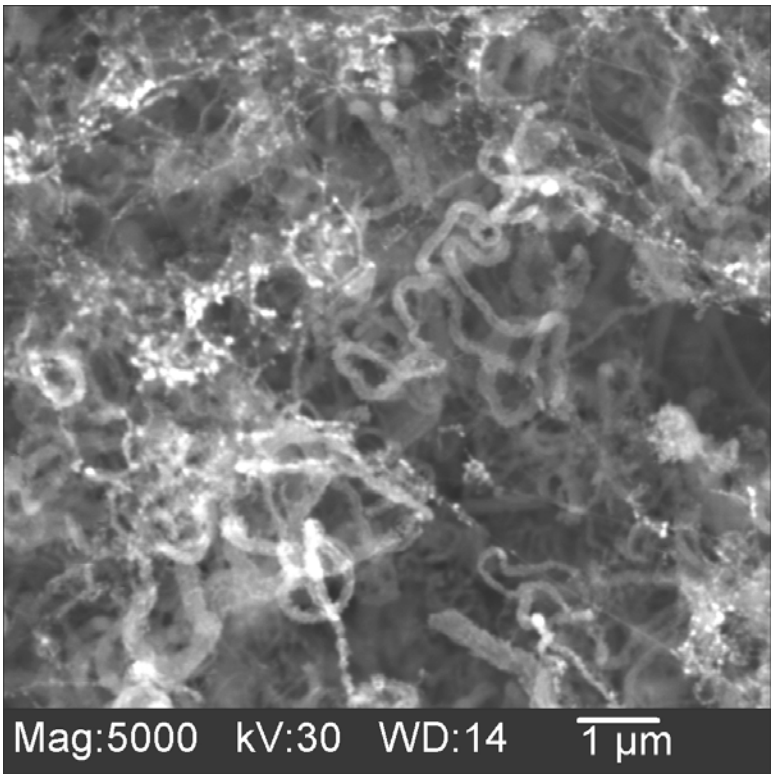

Figure 7.13 – Nanotubes grown by placing a catalyst drop on the substrate using Pasteur pipette

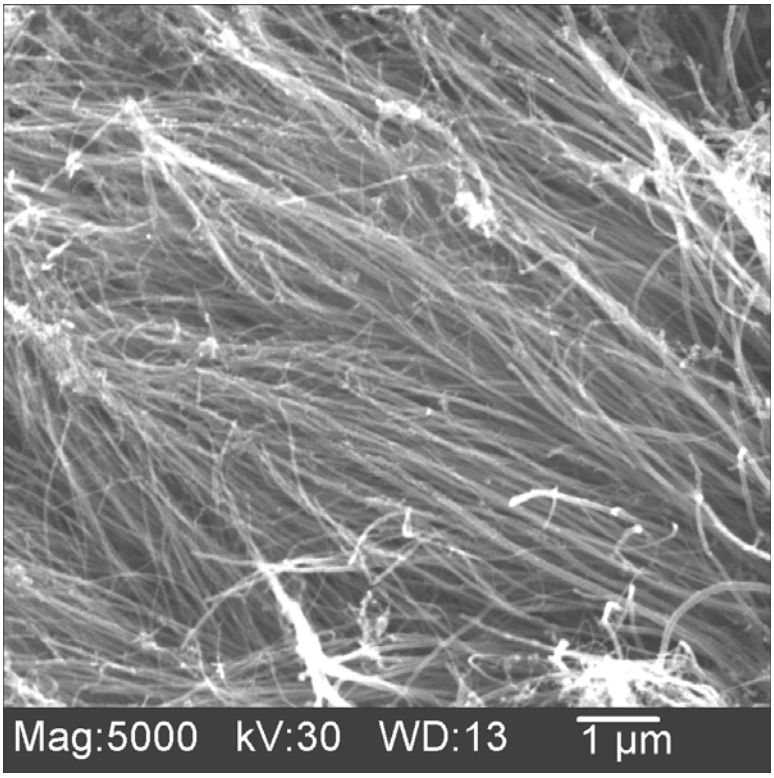

Figure 7.14 – Nanotubes grown by spin coating the substrate with catalyst

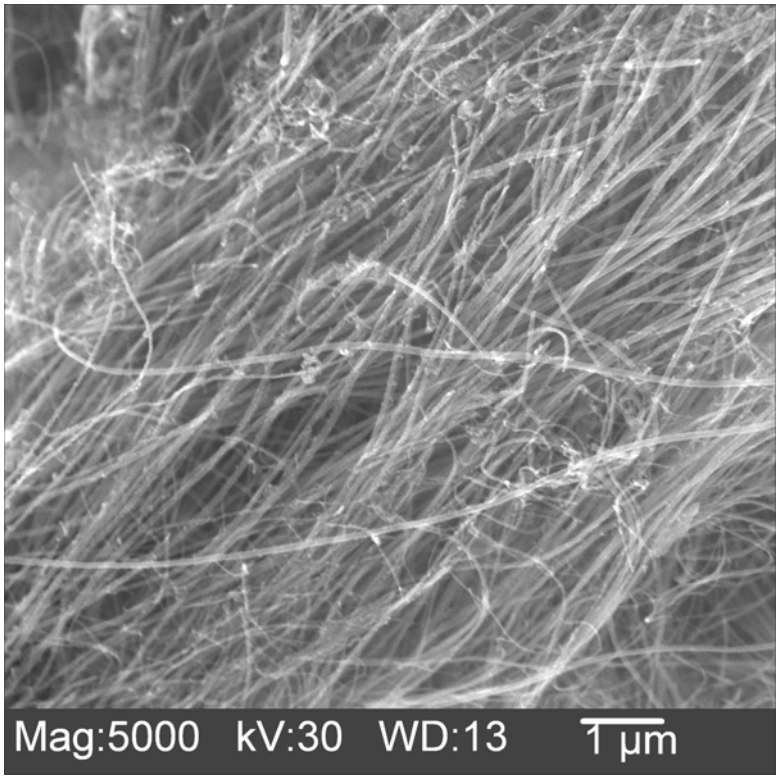

Figure 7.15 – Nanotubes grown by smearing the substrate with catalyst

7.1.5 Effect of variation of growth time

Another important criterion that needs to be studied apart from the pretreatment time and its importance is the effect of growth time on carbon nanotubes. Experiments were conducted at different growth times namely 30, 15, 10, 5, 3, and 1 min. Figures 7.16 to 7.21 show the SEM micrographs of carbon nanotubes grown for 30, 15, 10, 5, 3 mins and 1 min, respectively and Table 7.3 gives the process parameters used. It can be seen that even for 1 min growth time there is deposition and carbon nanotube growth (Figure 7.21). However, the tubes grown are not fully developed and the catalyst islands are not fully utilized for growth. Though tubes form at all the growth times, the tubes grown for 1, 3, and 5 mins are found to be tangled and curled while the tubes grown for 10, 15, and 30 mins are aligned. These tubes are aligned locally and the alignment of the tubes is either parallel to the substrate surface or at an angle to the substrate. As can be seen from Figure 7.22, 10 mins growth was found to be the optimum growth time

Table 7.3 Process parameters used to study the effect of growth time

Catalyst coating	1 drop - smeared
Pretreatment time, mins	5
Microwave power, watts	500
Chamber pressure, torr	15
Growth time (variable), mins	**30, 15, 10, 5, 3, 1**
Flow rates of $H_2/N_2/CH_4$, sccm	40/50/10

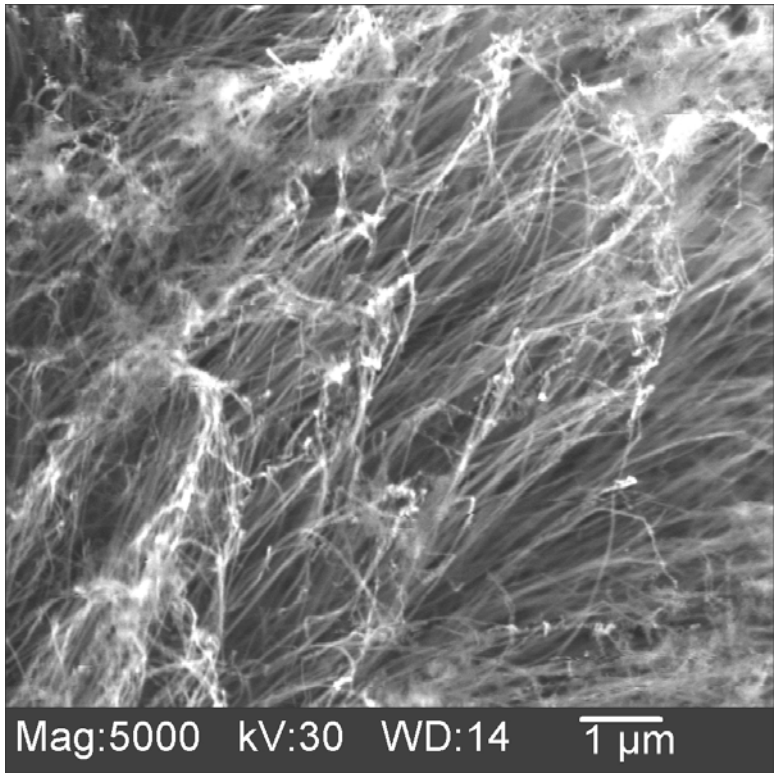

Figure 7.16 SEM micrograph of nanotubes grown for 30 mins

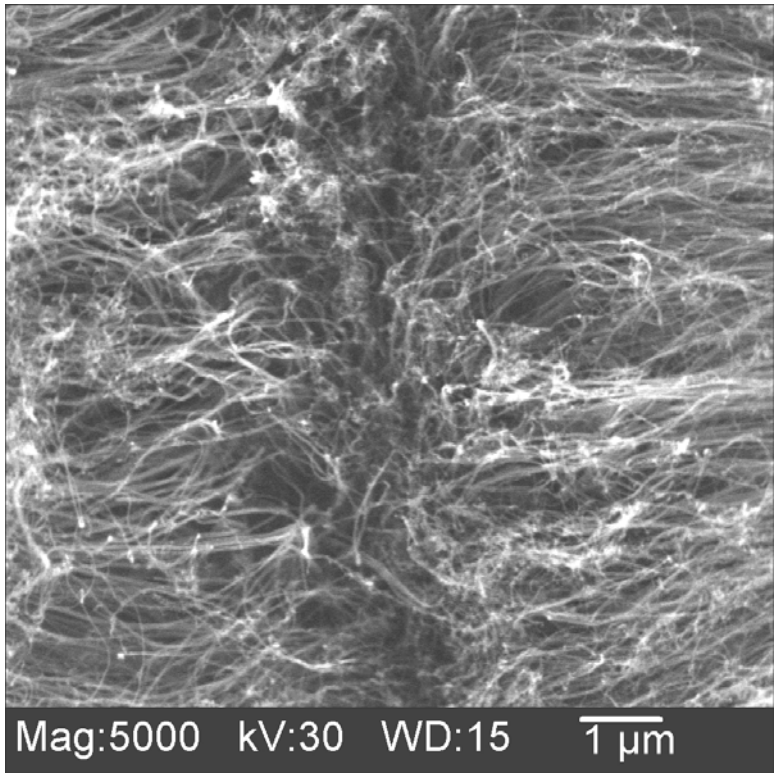

Figure 7.17 SEM micrograph of nanotubes grown for 15 mins

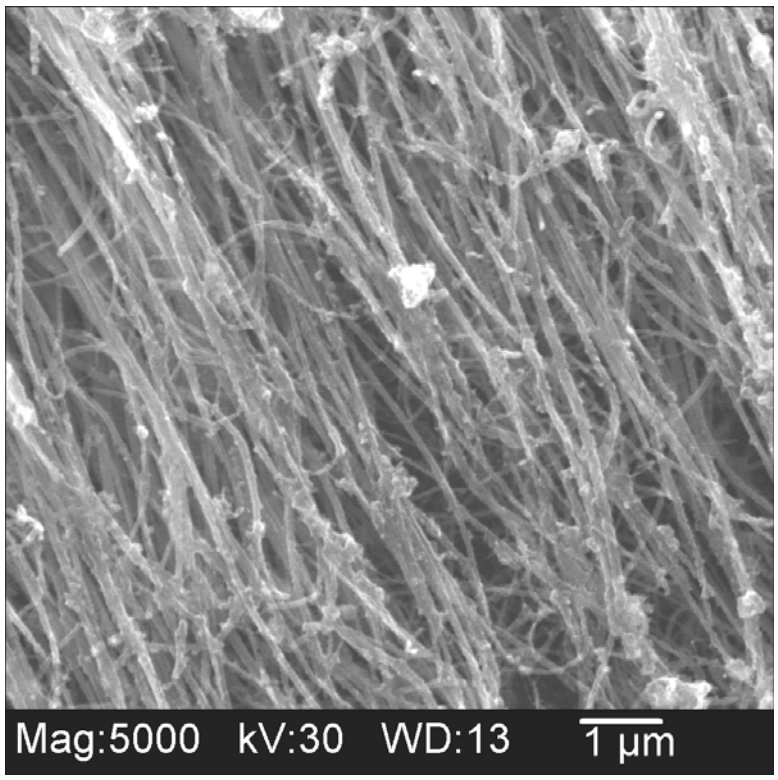

Figure 7.18 SEM micrograph of nanotubes grown for 10 mins

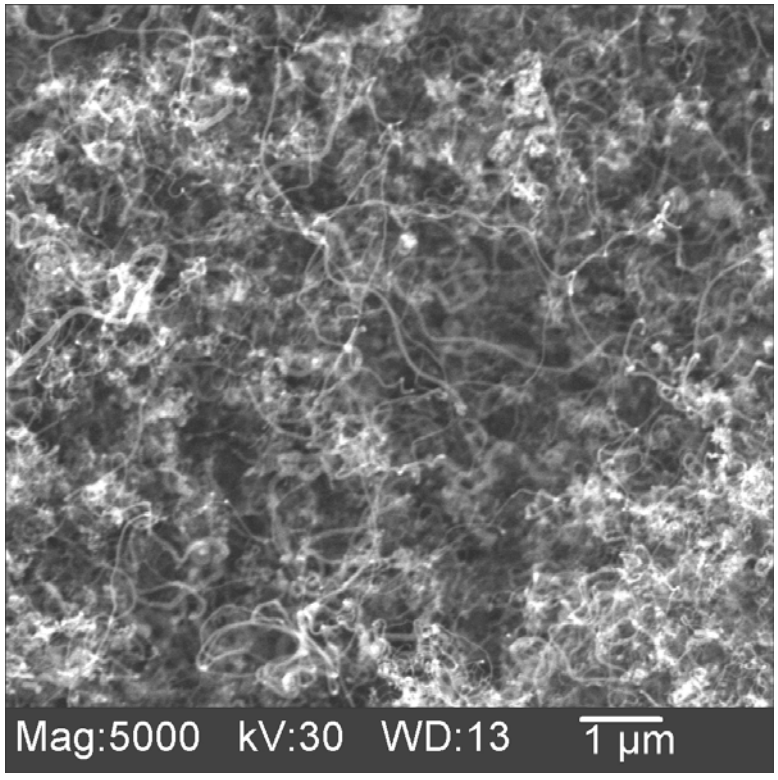

Figure 7.19 SEM micrograph of nanotubes grown for 5 mins

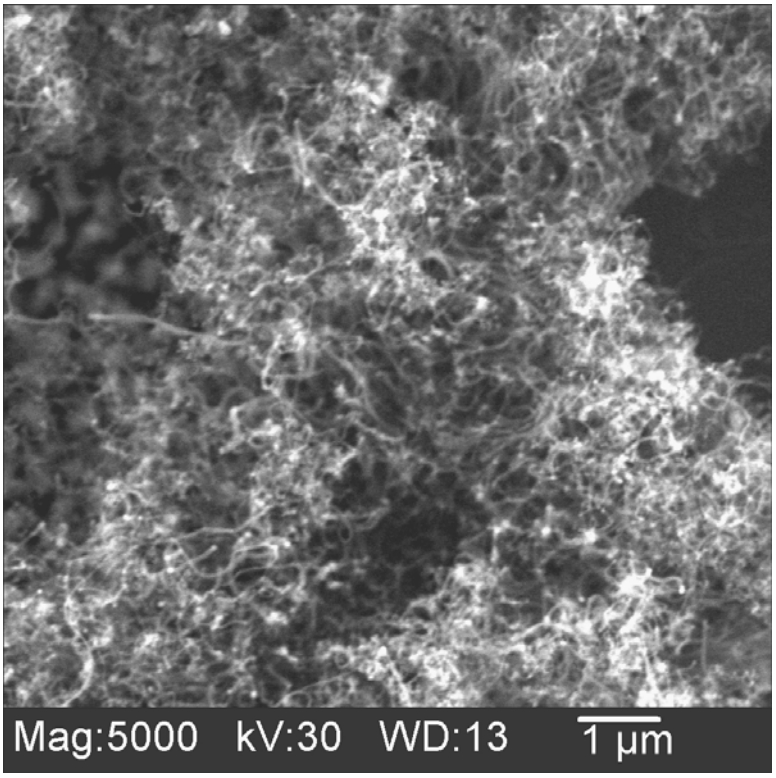

Figure 7.20 SEM micrograph of nanotubes grown for 3 mins

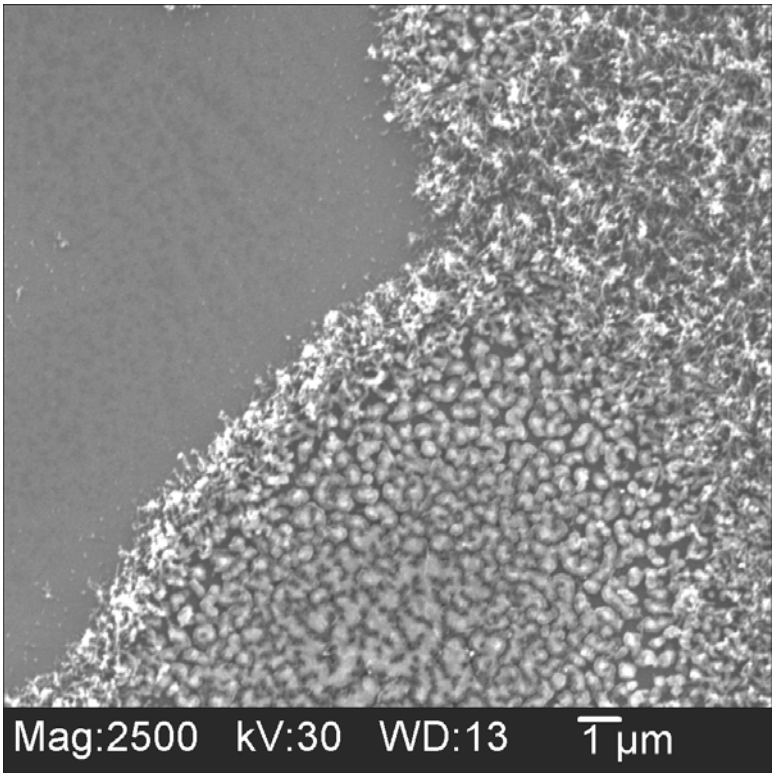

Figure 7.21 SEM micrograph of nanotubes grown for 1 min

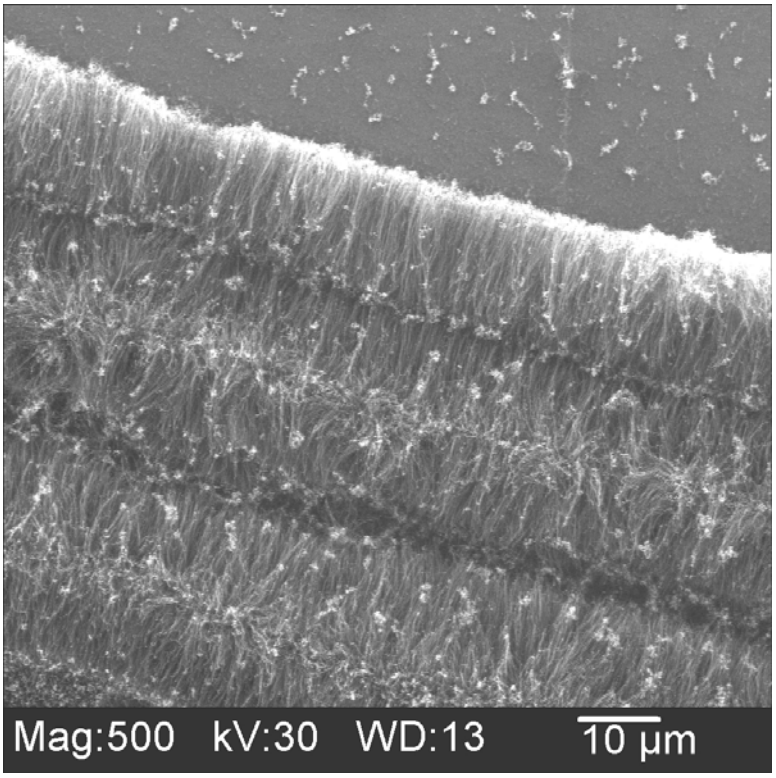

Figure 7.22 Low magnification image of nanotubes grown for 10 mins

From the results of variation of growth time as well as the variation of pretreatment time it is evident that 10 mins of growth time and 10 mins of pretreatment time are the optimum conditions for growing nanotubes in these conditions. Better yield of tubes with local alignment is obtained, but the focus now should be to obtain better vertical alignment and increased nucleation density and yield of the tubes. Carbon nanotubes are grown by varying the pressure and results are analyzed in the following.

7.1.6 Effect of variation of chamber pressure

In order to better understand the effect of growth pressure and also to synthesize tubes that can be grown vertically, experiments were conducted at different pressures of 10, 12.5, 15, 17.5 and 20 torr and the results are studied. Figures 7.23 to 7.27 are SEM micrographs showing the results of these tests. 20 torr was found to be the optimum

pressure having high yield density. Also the nucleation density as well as the vertical alignment were found to increase with increase in pressure. Table 7.4 gives the process parameters used in this study. Figures 7.28 and 7.29 show the vertical alignment seen at 17.5 torr and 20 torr, respectively.

Table 7.4 Process parameters used to study the effect of chamber pressure

Catalyst coating	1 drop - smeared
Pretreatment time, mins	10
Microwave power, watts	500
Chamber pressure (variable), torr	**10, 12.5, 15, 17.5, 20**
Growth time, mins	10
Flow rates of $H_2/N_2/CH_4$, sccm	40/50/10

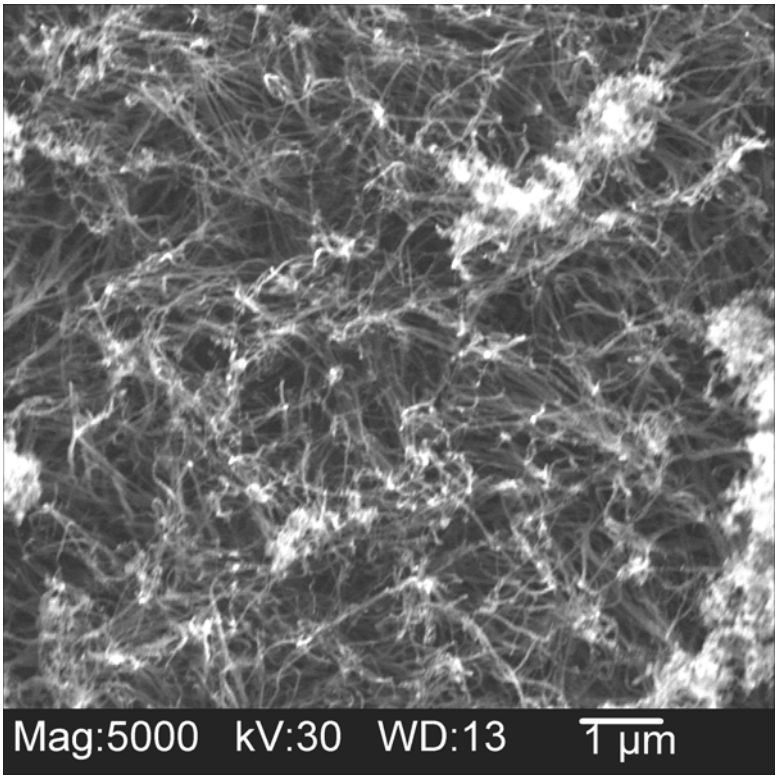

Figure 7.23 SEM micrograph of nanotubes grown at 10 torr

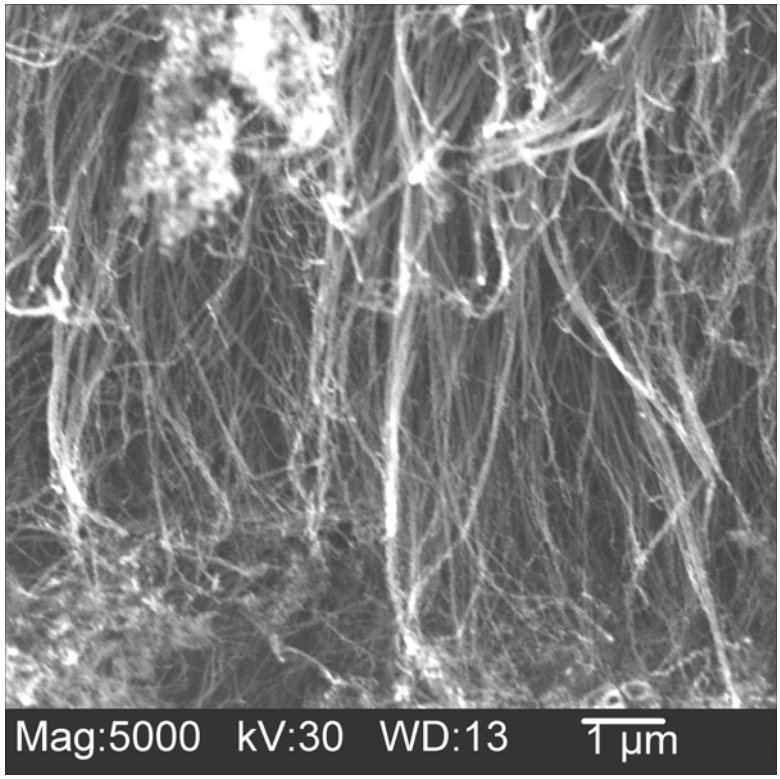

Figure 7.24 SEM micrograph of nanotubes grown at 12.5 torr

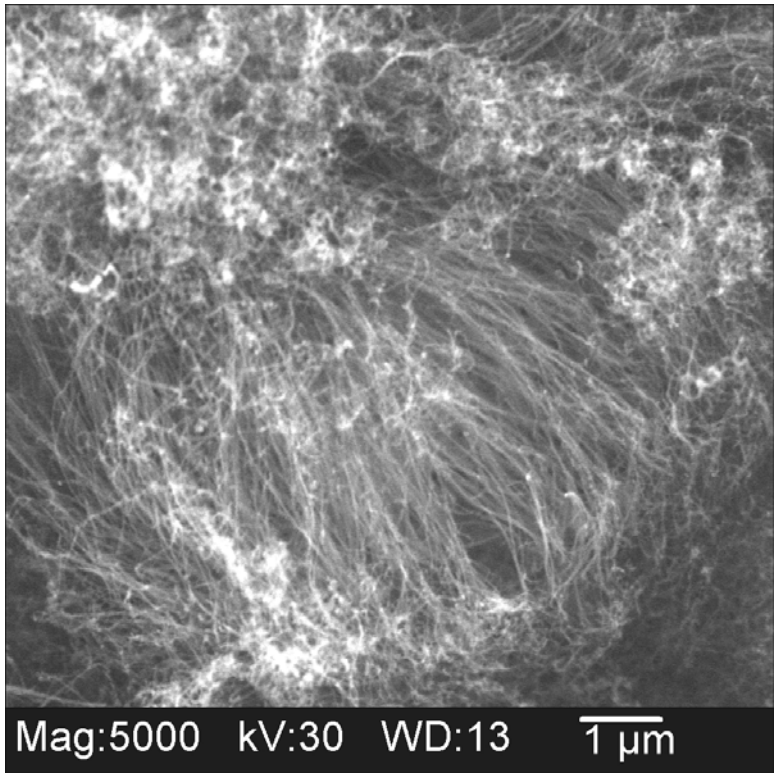

Figure 7.25 SEM micrograph of nanotubes grown at 15 torr

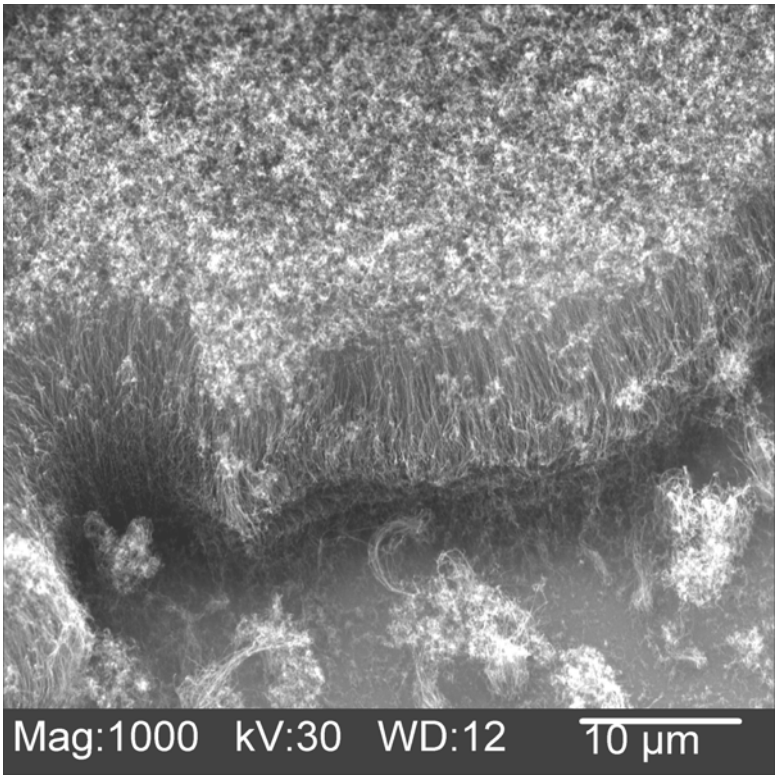

Figure 7.26 SEM micrograph of nanotubes grown at 17.5 torr

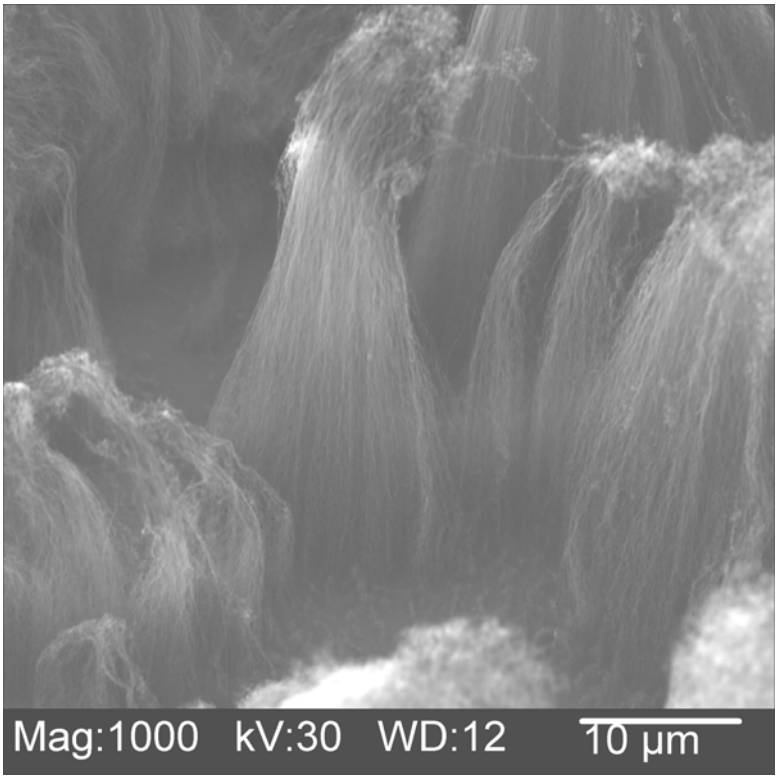

Figure 7.27 SEM micrograph of nanotubes grown at 20 torr

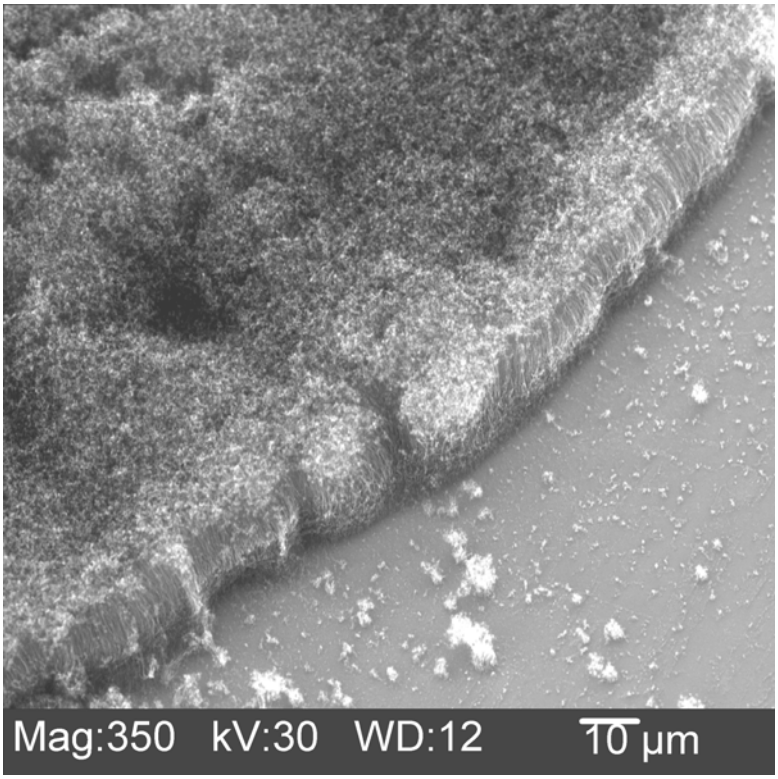

Figure 7.28 Low magnification image of vertically aligned tubes grown at 17.5 torr

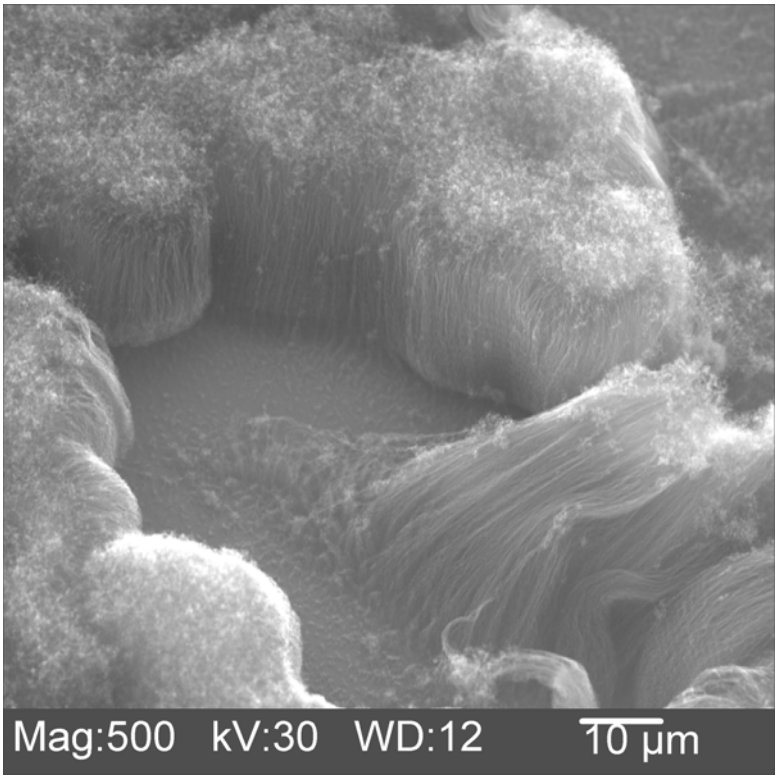

Figure 7.29 Low magnification image of vertically aligned tubes grown at 20 torr

7.1.7 Effect of variation of methane flow rate

Methane being the carbon source gas for the synthesis of CNT, it will have a significant influence on the growth. Experiments were conducted at various flow rates of methane namely 2.5, 5, 10, 15, and 20 sccm to investigate the nucleation behavior and alignment of CNTs. Since vertically aligned tubes were obtained for a chamber pressure of 20 torr, these tests were also carried out at 20 torr. Table 7.5 lists the process parameters used for the variation of methane flow rate. Figures 7.30 to 7.34 are the SEM micrographs of the results showing the effect of variation of methane flow rate for 2.5, 5, 10, 15, and 20 sccm, respectively. From figures 7.30 and 7.31, it is clear that there is no nucleation when methane flow rate is 2.5 sccm or 5 sccm. The nanotubes grow for 10, 15 and 20 sccm and the tubes grow vertically normal to the substrate. The nucleation density was also found to increase with increase in methane flow rate. The carbon nanotubes were characterized in the SEM by scraping a portion of the deposit with a sharp tweezer. A methane flow rate of 20 sccm was found to be optimum for production of vertically aligned nanotubes with fewer impurities.

Table 7.5 Process parameters used to study the effect of methane flow rate

Catalyst coating	1 drop - smeared
Pretreatment time, mins	10
Microwave power, watts	500
Chamber pressure, torr	20
Growth time, mins	10
Flow rates of $H_2/N_2/$**CH_4 (variable)**, sccm	40/50/**(2.5, 5, 10, 15, 20)**

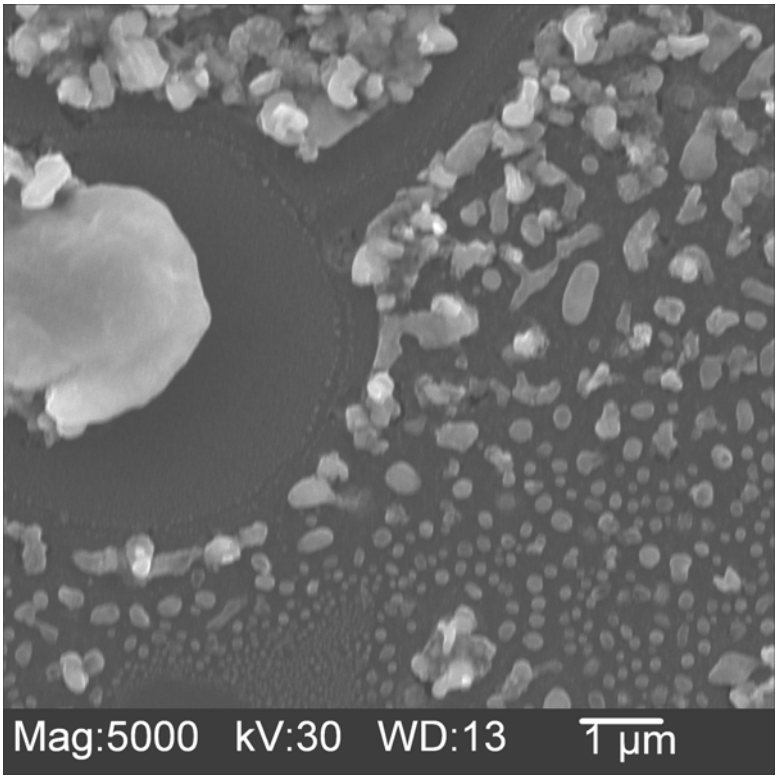

Figure 7.30 SEM micrograph revealing no tube growth for 2.5 sccm of methane

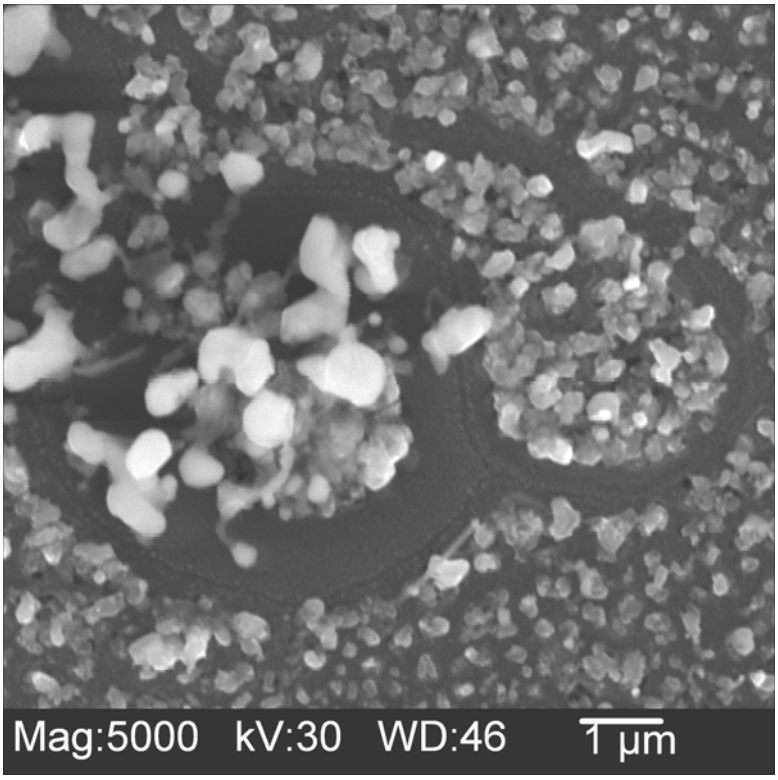

Figure 7.31 SEM micrograph indicating initiation of CNTs at 5 sccm of methane

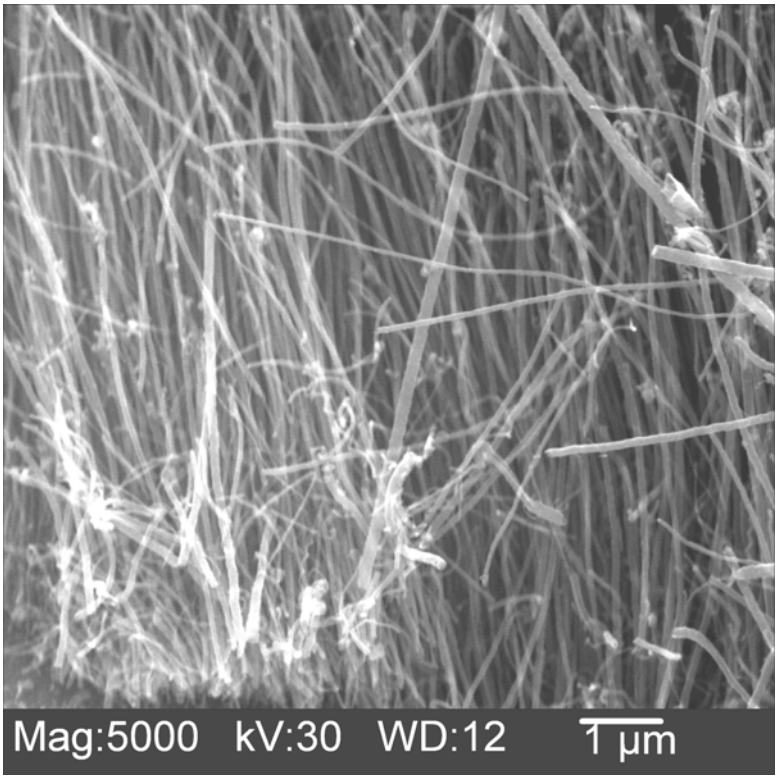

Figure 7.32 SEM micrograph of aligned nanotubes grown at 10 sccm of methane

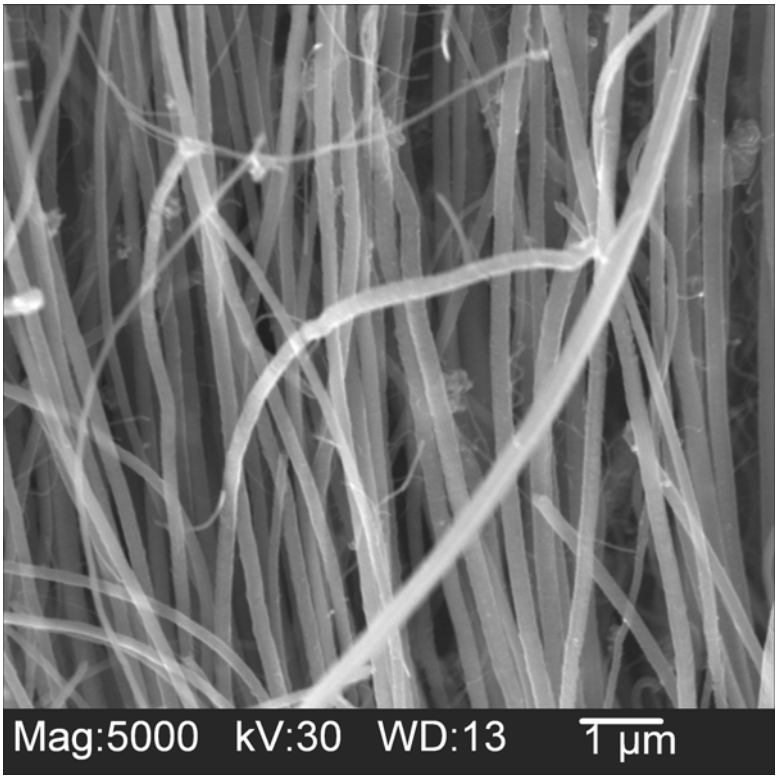

Figure 7.33 SEM micrograph of aligned nanotubes grown at 15 sccm of methane

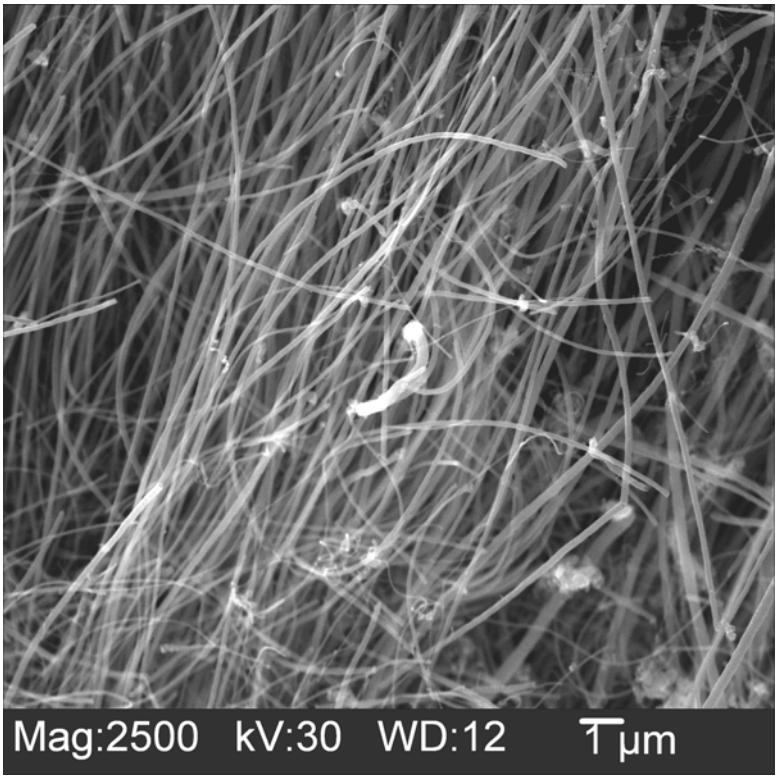

Figure 7.34 SEM micrograph of aligned nanotubes grown at 20 sccm of methane

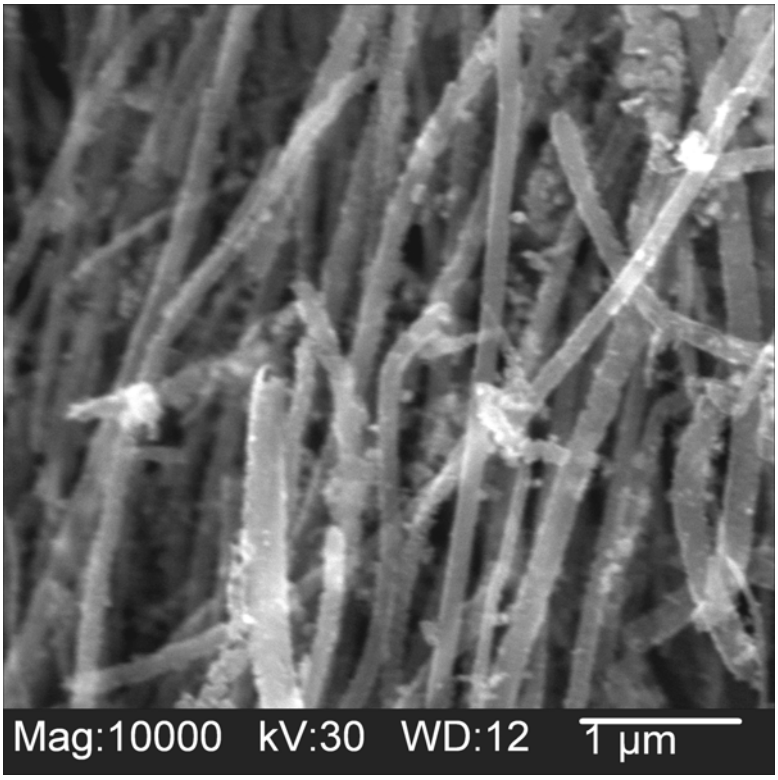

Figure 7.35 Impurities sticking to nanotubes grown at 10 sccm of methane

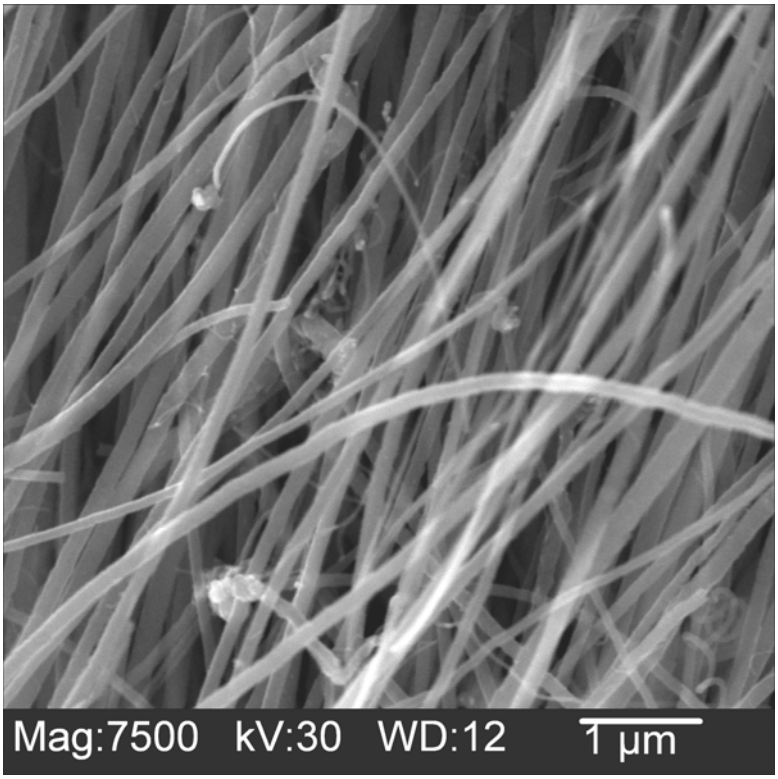

Figure 7.36 Nanotubes grown with rarely any impurity at 20 sccm of methane

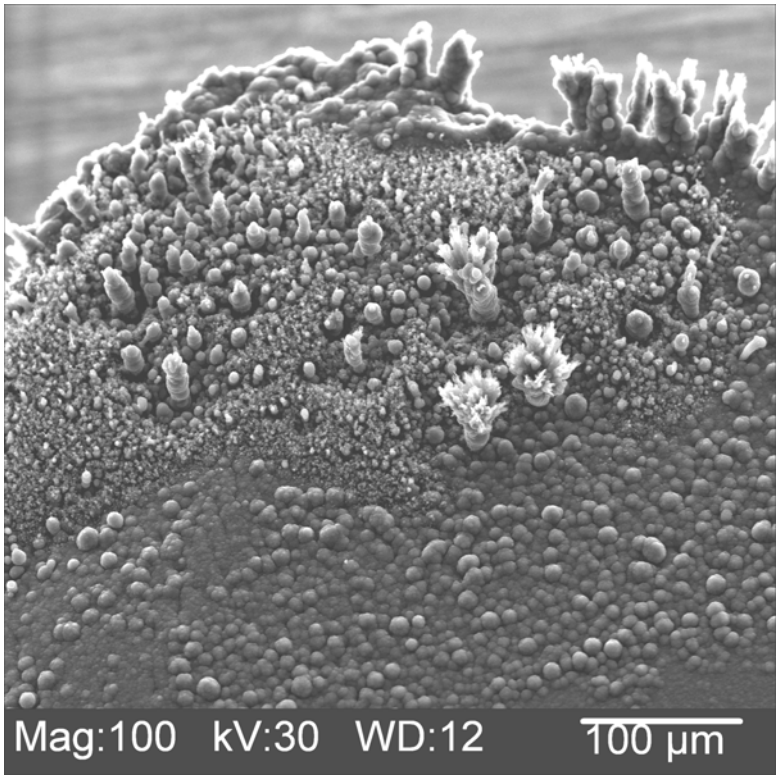

Figure 7.37 SEM micrograph of amorphous carbon deposits on the corner

The higher magnification of SEM images taken at 10 sccm and 20 sccm revealed that nanotubes grown at 10 sccm have some impurities associated with the tubes whereas the tubes grown at 20 sccm are more pure, as shown in Figures 7.35 and 7.36, respectively. However, due to the higher increase in the methane flow rate there are amorphous deposits formed on the corners of the wafer which can be seen in Figure 7.37.

7.2 Characterization using Scanning Transmission Electron Microscope (STEM)

STEM is used in this study to characterize the nanotubes synthesized using microwave plasma enhanced CVD. STEM analysis should facilitate in the identification of the nature of the tubes synthesized, i.e. single walled or multiwalled. Moreover, it can show the internal morphology of the tubes synthesized. The diameter of the tubes, wall thickness, and the defects in the outer walls such as kinks can be analyzed. Also the STEM micrographs facilitate in finding out whether the tubes have catalyst particle in their tips or the tip is closed without any particle. The location of the catalyst particle in the tube can shed light on the growth mechanism involved in the synthesis.

For the STEM analysis, the synthesized nanotubes are scrapped using a sharp tweezer. These tubes are then suspended in methanol and ultrasonicated using an ultrasonic cleaner for 15 mins to properly disperse the nanotubes in methanol. A small quantity of these dispersed nanotubes is carefully taken using a micro pipette. They are then placed on to a TEM grid coated with formvar. Care is taken not to use carbon coated grid as researchers were mislead due to the carbon coating in the grid. The TEM grid with the nanotubes is placed in the STEM sample holder and the nanotubes are analyzed.

7.2.1 Multiwalled nanotubes

The STEM micrographs showed that nanotubes synthesized using colloidal form of iron oxide as catalyst were multiwalled. The tubes have either a hollow core or a bamboo shaped internal morphology. Bamboo structured tubes have a linear chain of hollow compartments and they are spaced nearly at equal intervals. The mechanism of the bamboo shaped tube is explained by Saito [106]. According to him, the dissolved carbon diffuses into the bottom side of the catalyst and the carbon segregates to form nanotubes. The catalyst particle is pushed out due to the stress force created in the graphitic sheath due to segregation of carbon from the inside of the sheath. Figure 7.38 is a micrograph showing bamboo shaped nanotubes synthesized using colloidal iron oxide as catalyst, where the carbon has diffused on top of the catalyst rather than at the bottom. Apart from the bamboo shaped tubes, tubes with hollow core are also grown which is shown in Figure 7.39. These two figures also convey that the tubes are multiwalled.

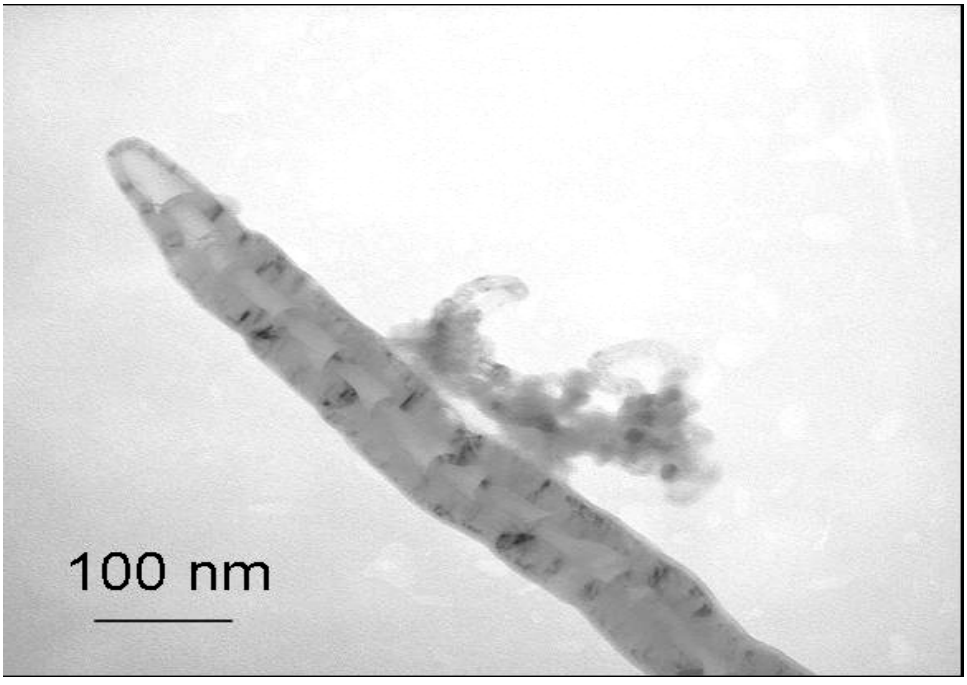

Figure 7.38 STEM micrograph of a nanotube with a bamboo structure

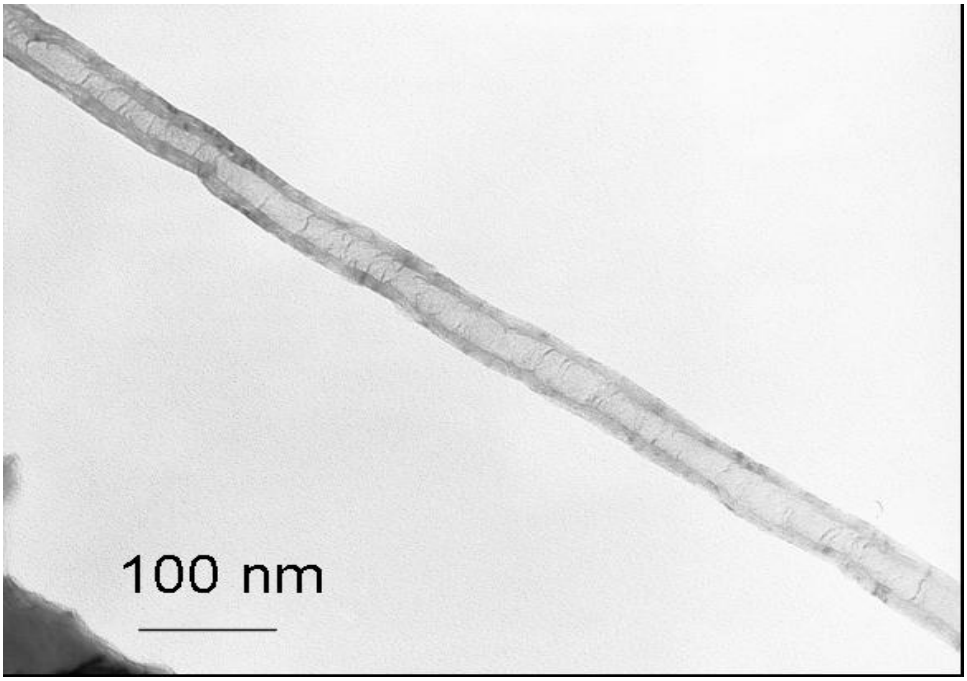

Figure 7.39 STEM micrograph of a nanotube with hollow core

7.2.2 Effect of variation of chamber pressure

STEM analysis was also done on nanotubes synthesized to study the effect of chamber pressure. Figures 7.40 to 7.42 show STEM micrographs of carbon nanotubes grown at 15, 17.5, and 20 torr, respectively. These results enabled the determination of the average tube diameters at various pressures.

7.2.3 Effect of variation of methane flow rate

The nanotubes synthesized by varying the flow rate of methane are also analyzed in STEM to investigate the variation in wall thickness as the methane flow rate increases. The STEM micrographs of nanotubes grown at 10, 15, and 20 sccm are shown in Figures 7.43 to 7.45, respectively. It was found that wall thickness increases with the increase in methane flow rate.

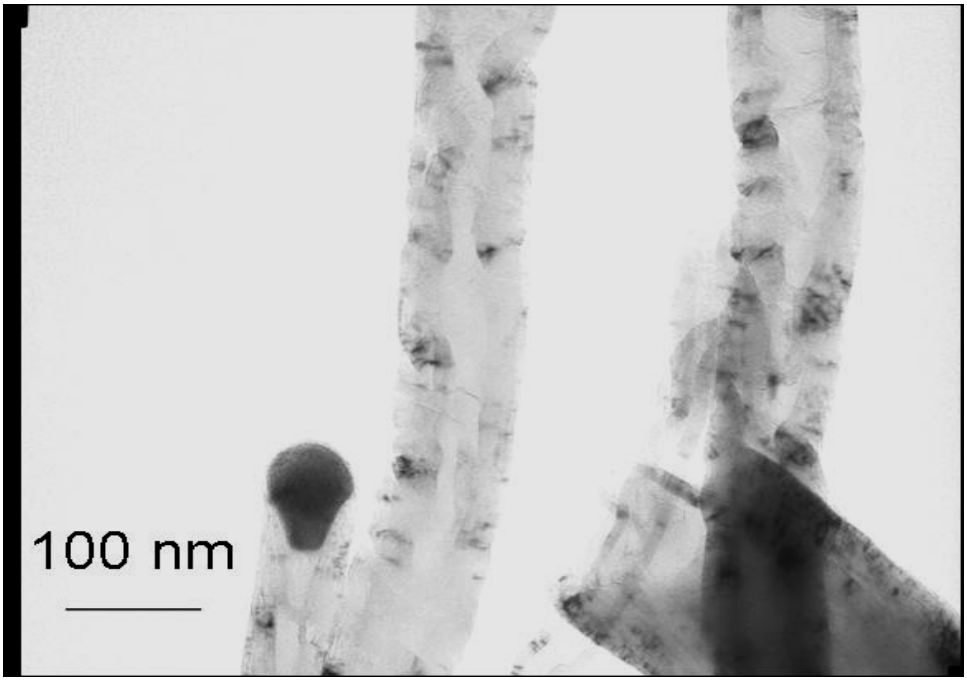

Figure 7.40 STEM micrograph of nanotubes grown at a pressure of 15 torr

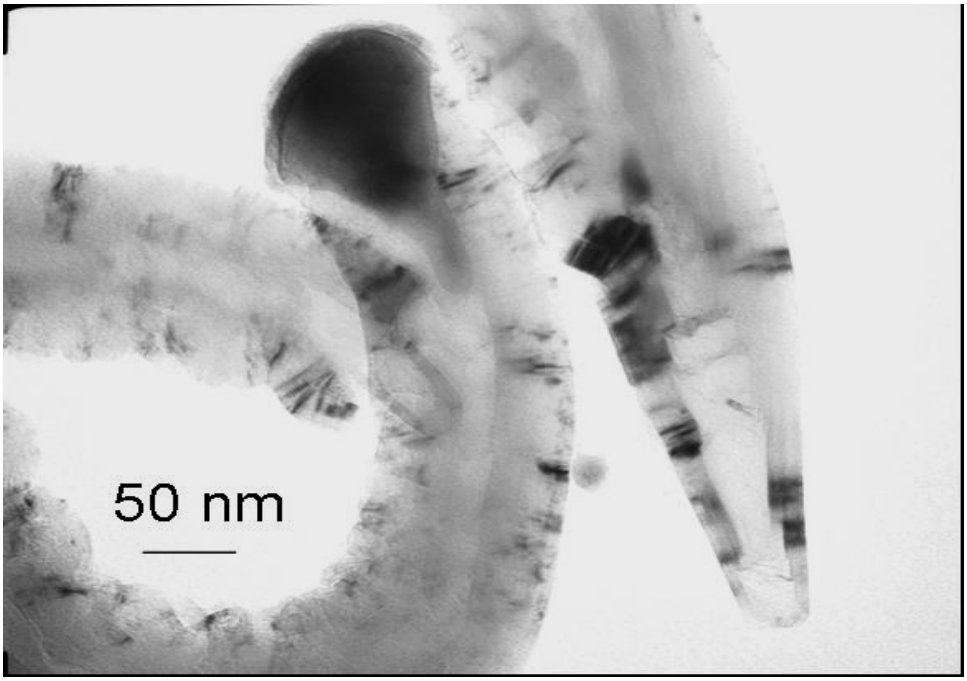

Figure 7.41 STEM micrograph of nanotubes grown at a pressure of 17.5 torr

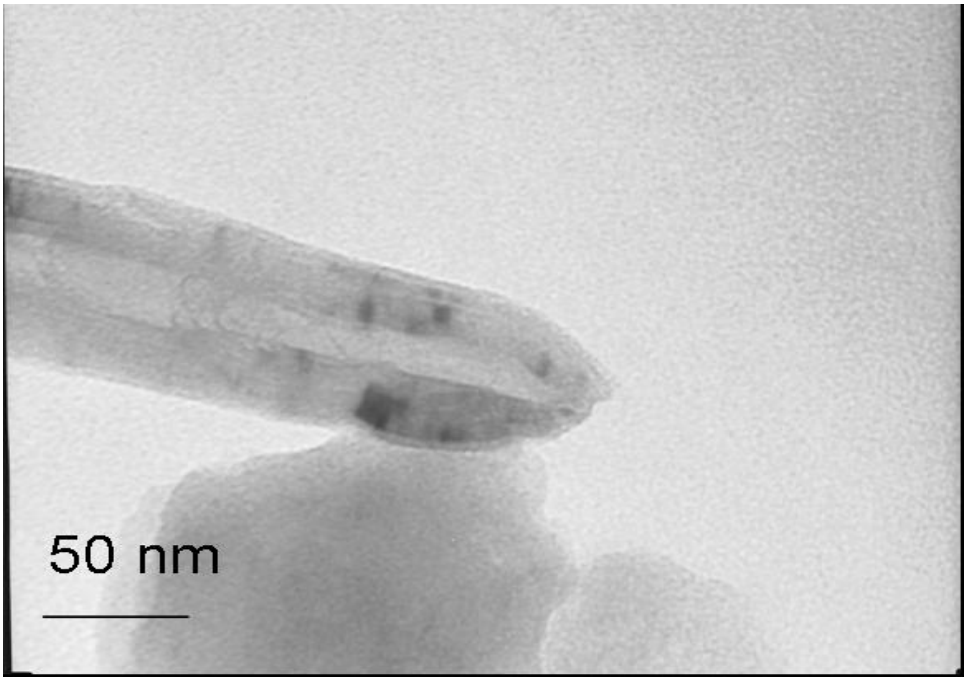

Figure 7.42 STEM micrograph of nanotube grown at a pressure of 20 torr

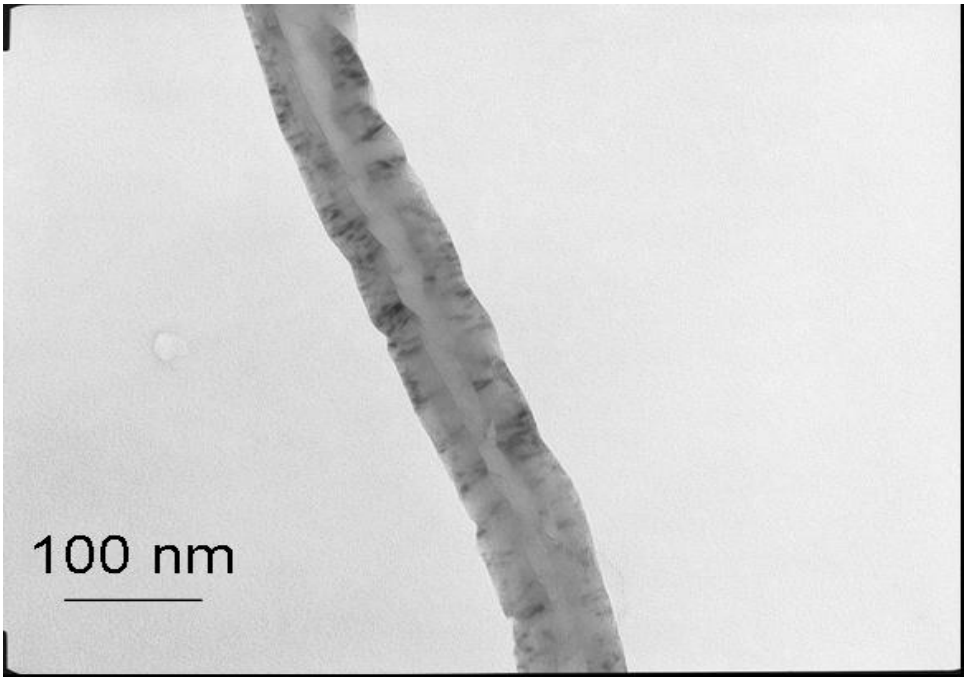

Figure 7.43 STEM micrograph of a nanotube grown at a methane flow rate of 10 sccm

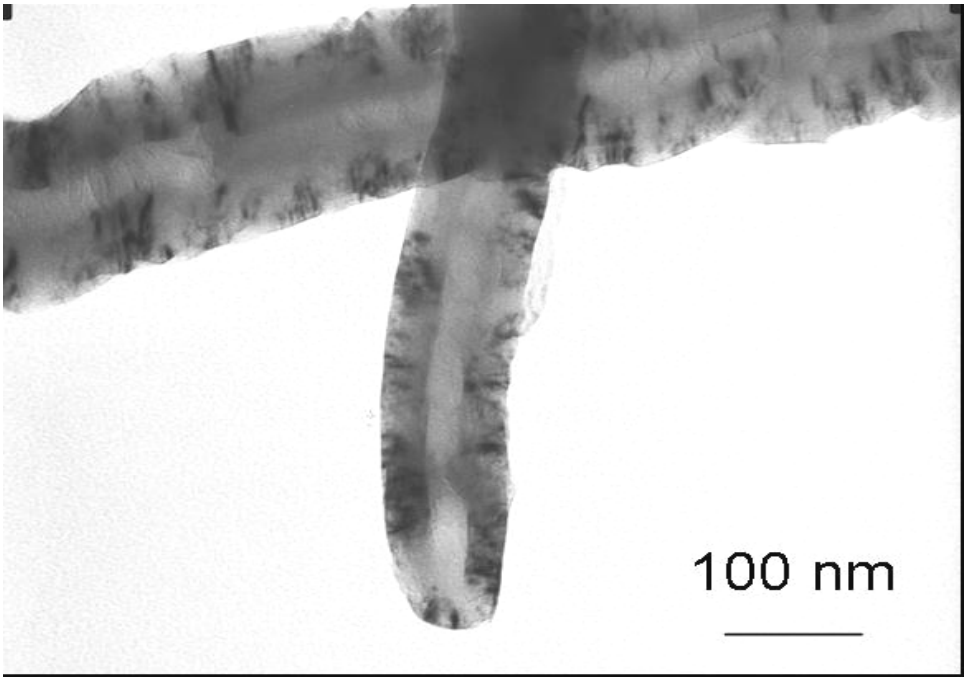

Figure 7.44 STEM micrograph of nanotubes grown at a methane flow rate of 15 sccm

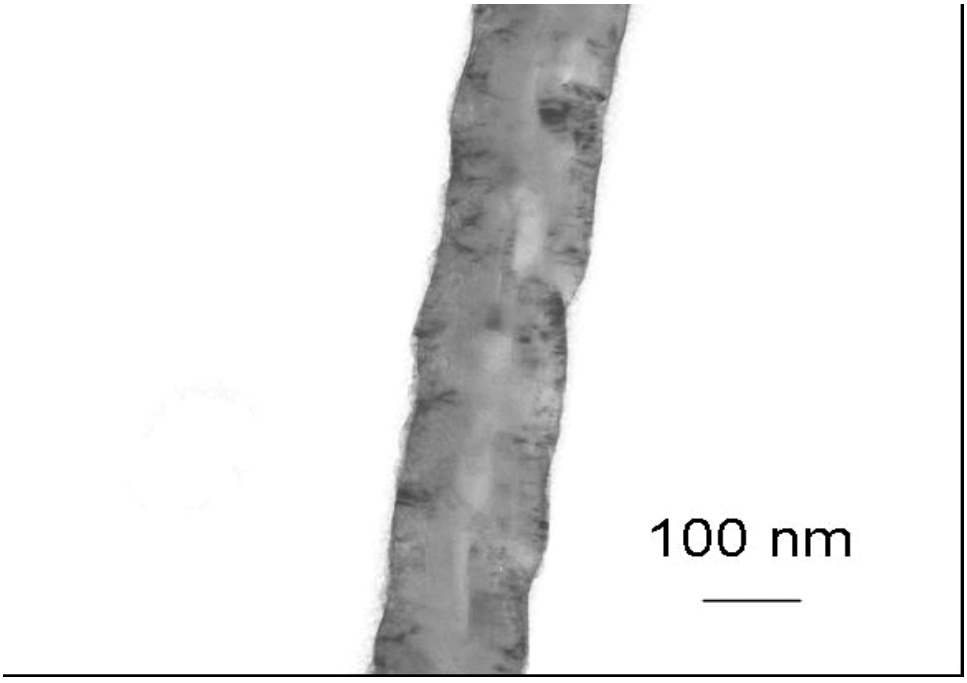

Figure 7.45 STEM micrograph of a nanotube grown at a methane flow rate of 20 sccm

7.3 Characterization using Atomic Force Microscopy (AFM)

The sample preparation for AFM is quite similar to TEM. The nanotubes are suspended in methanol and ultrasonicated for 15 mins. These dispersed nanotubes are placed on a microscope cover glass and is taken for analysis under AFM. AFM can be used to study the diameter variation in the nanotubes. Also, it enables identification of the surface deformities found on the outside wall of the nanotubes.

Figure 7.46 shows an AFM image of a carbon nanotube grown from colloidal iron oxide catalyst. From this the diameter of the nanotube can be estimated. The AFM image also enables analysis of the surface defects as shown in Figure 7.47. The section analysis option of the AFM can be used to determine the diameter of the tube as shown in Figure 7.48 or the average diameter over a given length of the nanotube as shown in Figure 7.49.

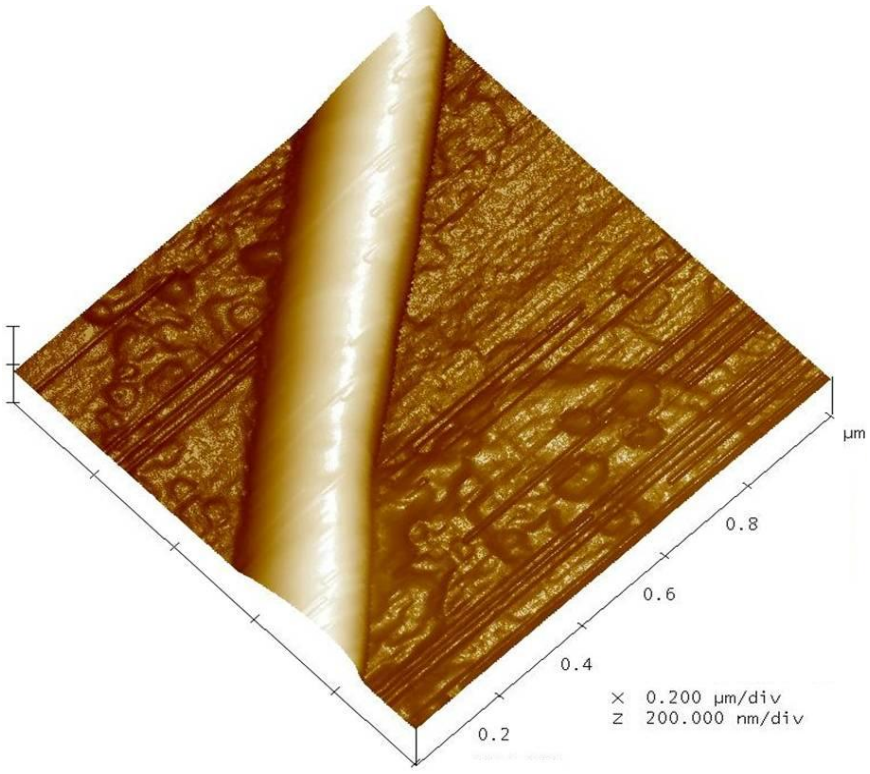

Figure 7.46 AFM micrograph of a carbon nanotube

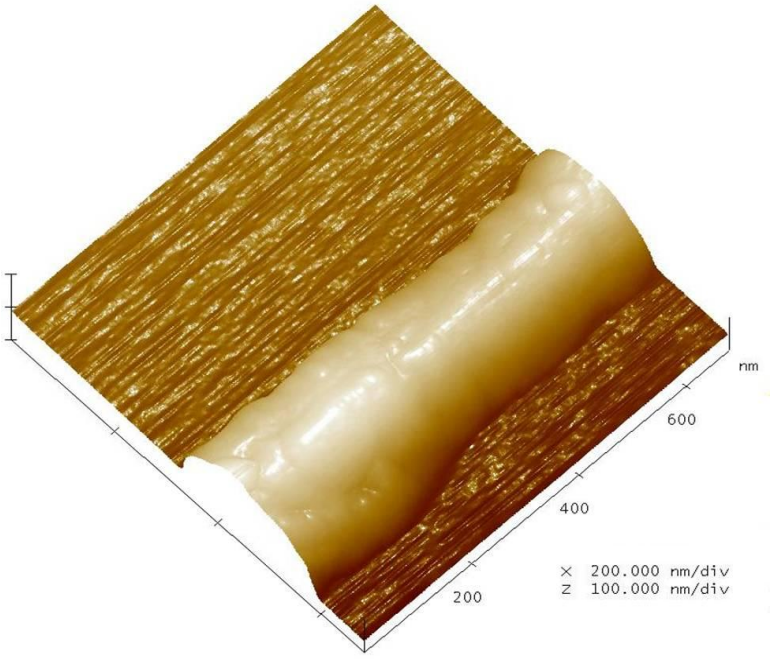

Figure 7.47 AFM micrograph of a nanotube showing the surface defects

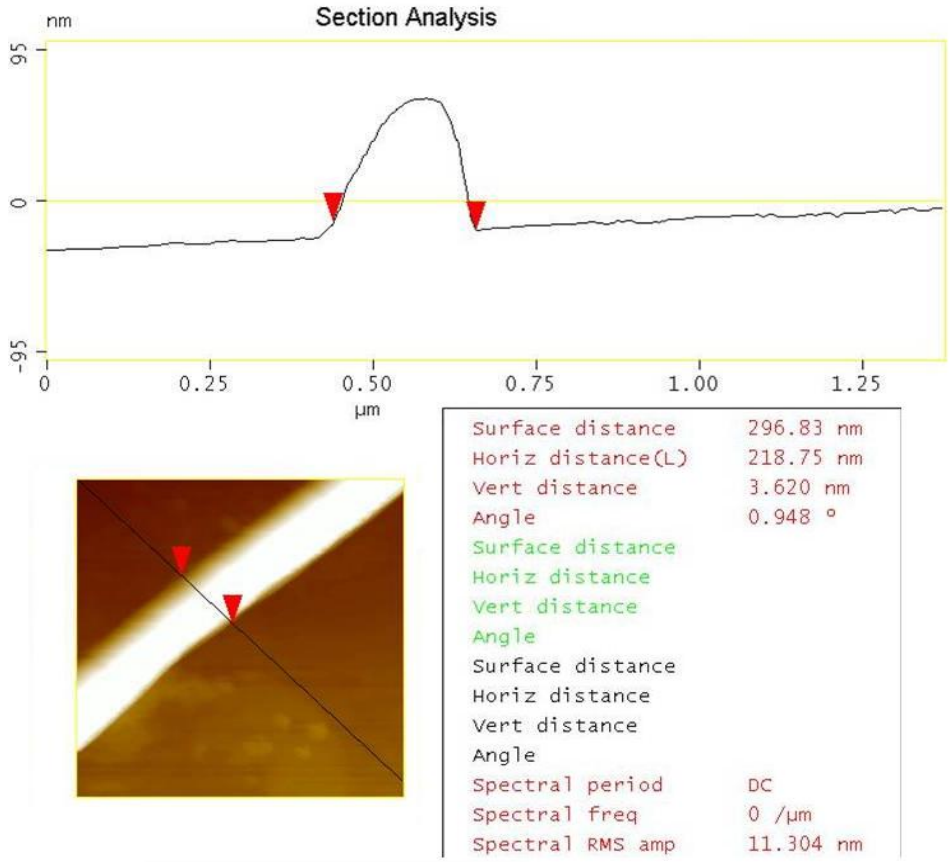

Figure 7.48 Section analysis of a carbon nanotube to determine the diameter

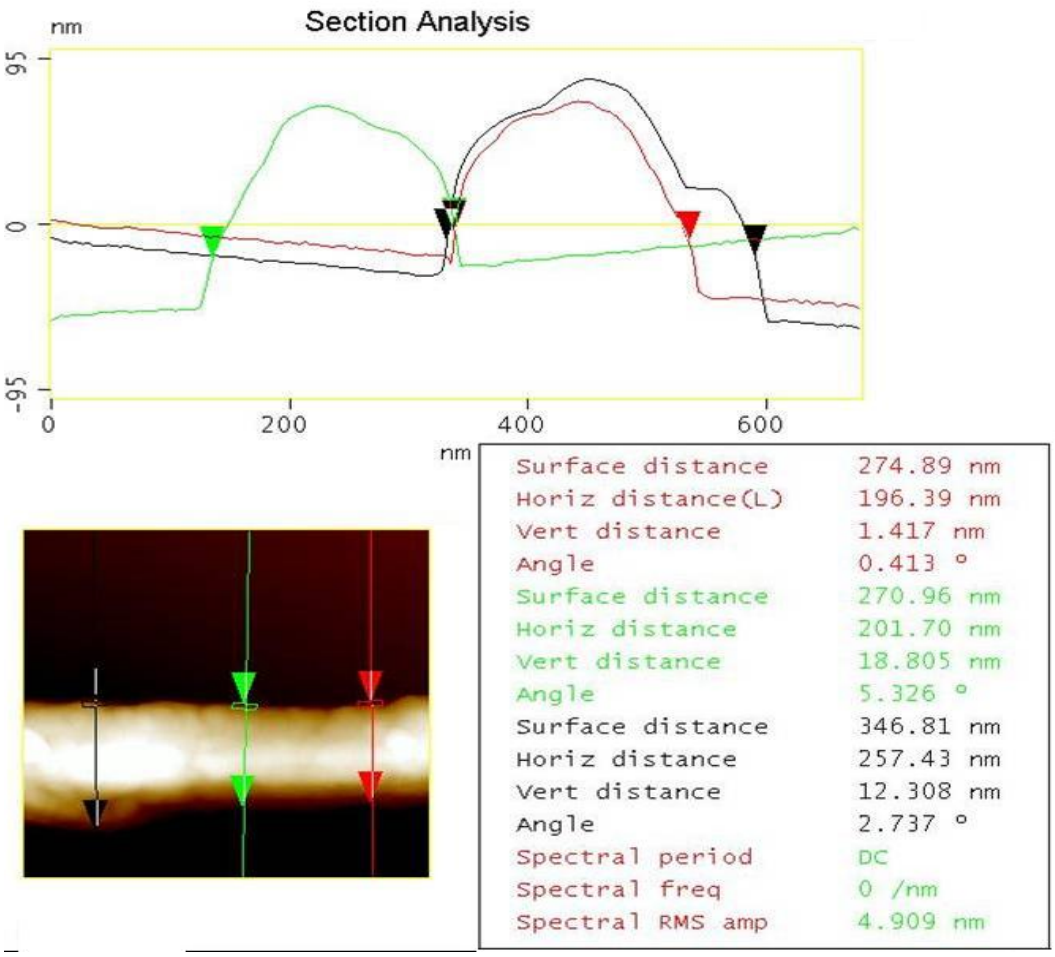

Figure 7.49 Section analysis to determine diameter over a given length of a nanotube

7.4 Elemental analysis using Energy Dispersive Spectra (EDS)

Elemental analysis of the deposited sample gives an idea about the various elements present in the deposit. Figure 7.50 shows the EDS spectra of the sample revealing the presence of C, Fe, and Si peaks. The carbon peak corresponds to the grown carbon nanotubes, the iron to the reduced iron catalytic particles from the colloidal iron oxide and since the substrate used here is silicon we can also see peaks for silicon.

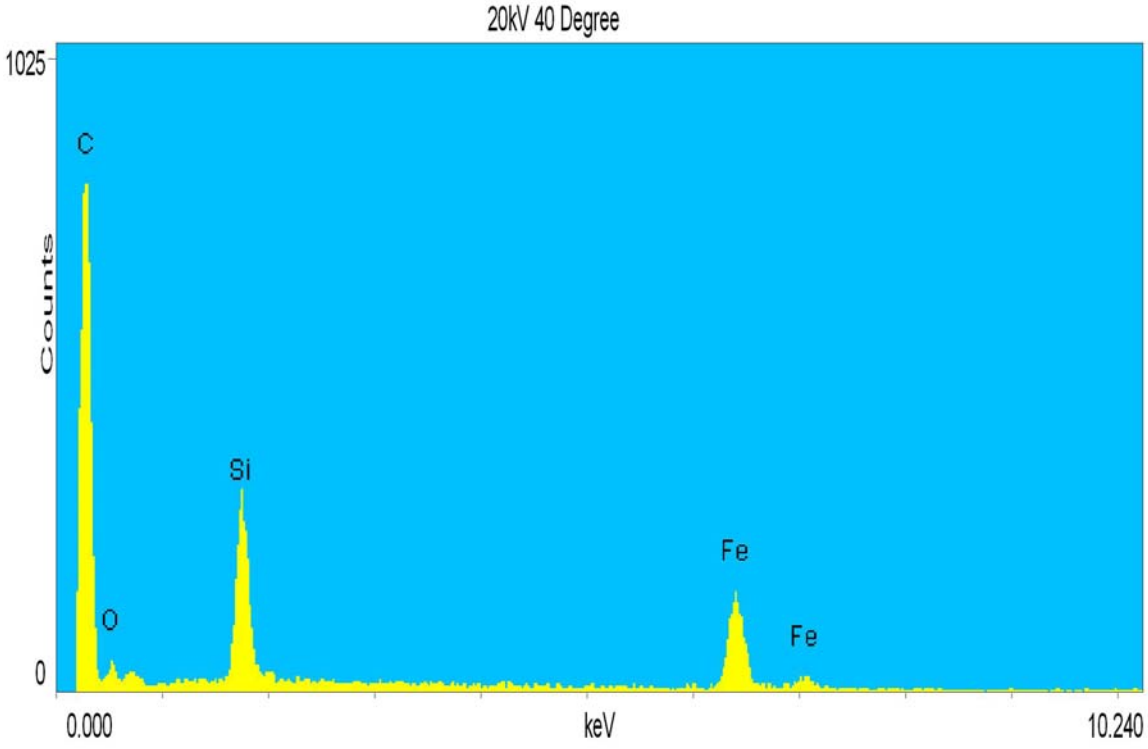

Figure 7.50 Energy Dispersive Spectra (EDS) showing C, Fe and Si peaks

7.5 Phase purity determination using μ-Raman spectroscopy

Though TEM analysis of nanotubes showed that grown carbon nanotubes are multiwalled, phase purity analysis was done on the nanotubes using μ-Raman spectroscopy in order to complement the results from TEM. Multiwalled carbon nanotubes have characteristic Raman peaks called the D and the G peaks at ~ 1350 cm^{-1} and 1580 cm^{-1}, respectively. Figures 7.51 and 7.52 show the Raman peaks obtained from the locally aligned and vertically aligned nanotubes grown from colloidal iron oxide catalyst showing these peaks.

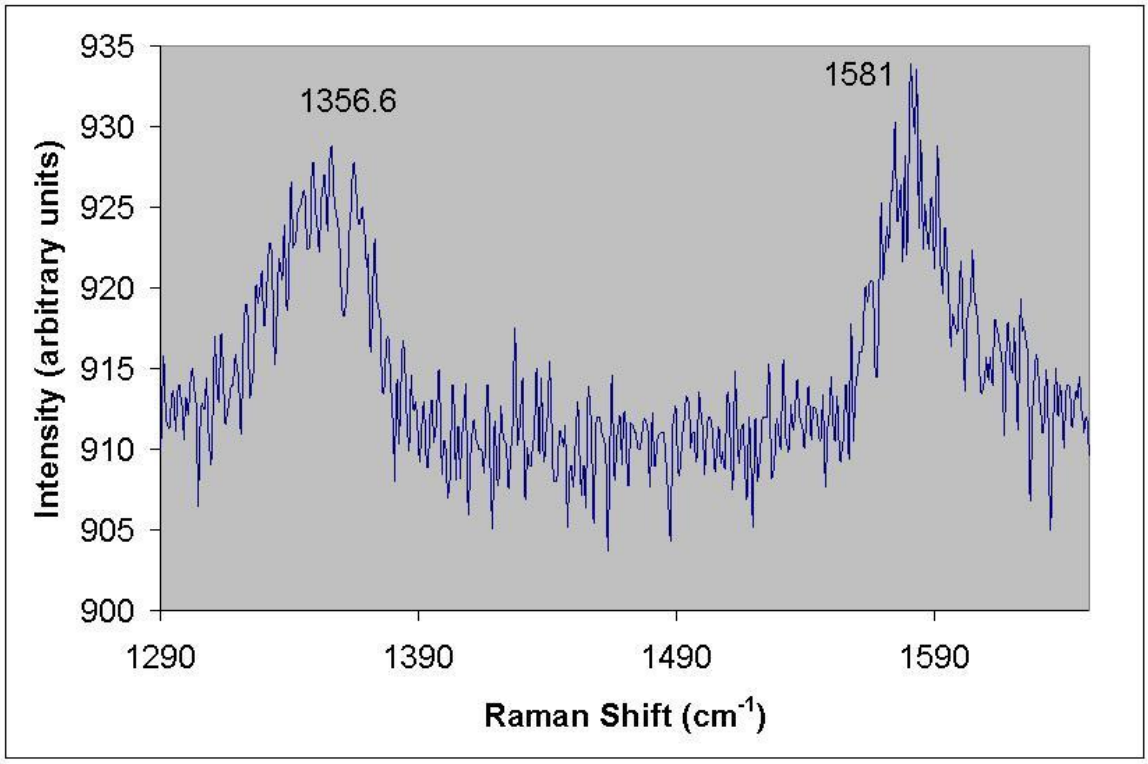

Figure 7.51 μ-Raman spectra on locally aligned carbon nanotubes

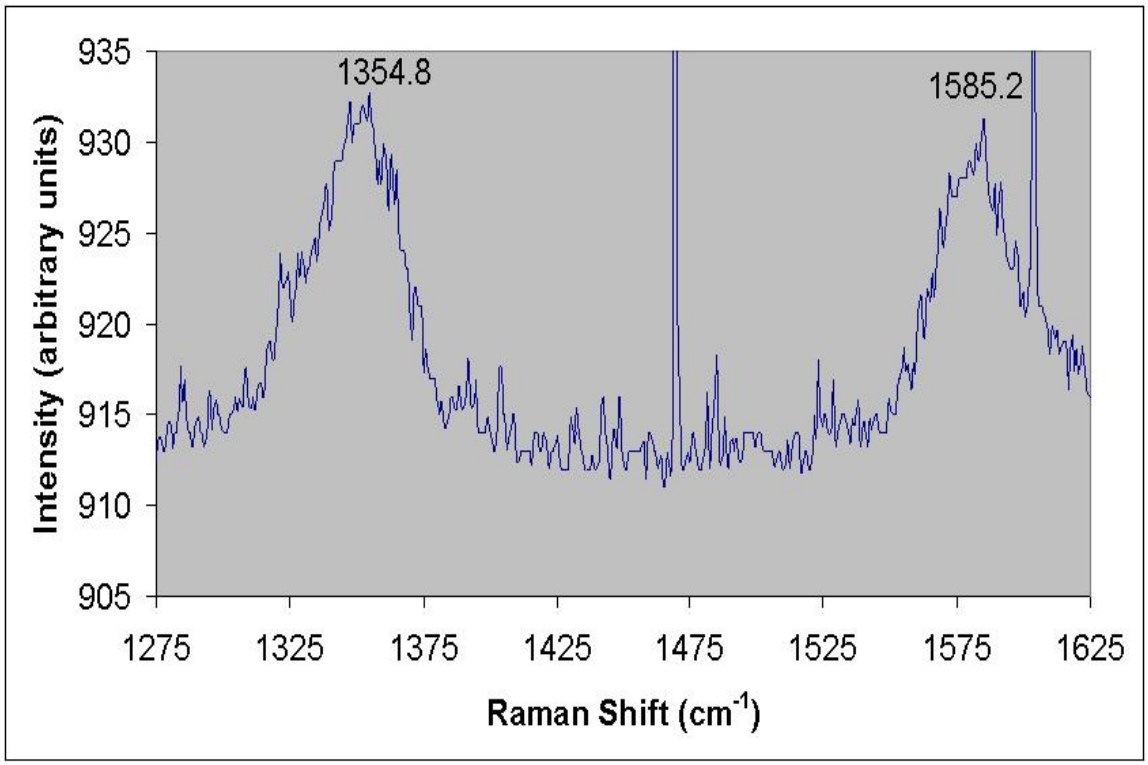

Figure 7.52 μ-Raman spectra on vertically aligned carbon nanotubes

CHAPTER 8

DISCUSSION

This chapter discusses elaborately the results obtained by conducting various experiments. The importance of plasma pretreatment and variation of pretreatment time to study the optimum growth parameters is analyzed. Variations of growth time, chamber pressure and the flow rate of methane in discussed to arrive at optimum growth time, chamber pressure and methane flow rate to obtain vertically aligned carbon nanotubes with fewer impurities.

8.1 Importance of plasma pretreatment

Plasma pretreatment is a very crucial and important step involved in the synthesis of nanotubes. This treatment breaks down the thin continuous catalyst film into nanosized catalyst particles. Figures 7.1 and 7.2 clearly show how the catalyst film breaks up into nano particles due to plasma pretreatment. These broken down catalyst nanoparticles act as seeds for the nucleation and growth of nanotubes. The thin continuous film has a large area compared to the size of the nanoparticles. This does not help the carbon to diffuse through and form nanotubes. But the carbon radicals find it easy to diffuse through the catalyst nanoparticles and forms nanotubes. The diameter of the nanotubes is determined by the size of the catalyst nanoparticles created.

8.2 Effect of variation of plasma pretreatment

The plasma pretreatment time also plays a vital role in the synthesis of carbon nanotubes. Good growth of nanotubes with better alignment is obtained only under optimum pretreatment time. We know from Section 7.2.1 that the pretreatment breaks up the continuous catalyst film into nanosized particles. This is true only until an optimum time. Beyond that optimum pretreatment time, due to prolonged exposure to plasma the catalyst islands start melting together and forms a melt pattern as shown in Figure 3.30. The agglomeration of the catalyst particle will also not result in better yield of nanotubes.

Figures 7.3 to 7.7 show SEM micrographs of nanotubes grown at pretreatment times of 0, 3, 5, 10, and 15 mins, respectively. Figure 7.3 shows that there are very few nanotubes obtained from 0 min or no pretreatment sample. The nucleation density is sparse and there is no alignment of the tubes. Figure 7.4 shows tangled and curly nanotubes with varying diameters. Figure 7.5 shows nanotubes grown from 5 mins pretreatment. The tubes seem to have the same diameters and there is considerable localized alignment and the tubes are short. The 10 mins pretreated sample (See Figure 7.6) shows greater alignment and the tubes are considerably longer. The tubes are bigger in diameter than the one for 5 min pretreatment and they are of uniform diameter. The alignment in this sample is much better than in the 5 min pretreatment sample. The 15 mins pretreatment sample though producing aligned nanotubes is also forming many terminating clusters and impurities. So, the optimum pretreatment time was found to be 10 mins for producing long tubes with better alignment.

8.3 Effect of catalyst concentration with pretreatment time

The growth of carbon nanotubes with catalyst concentration and pretreatment time was investigated. It can be seen from Figures 7.8 and 7.9, that it is very difficult for the nucleation of carbon nanotubes to take place at 0 min or no pretreatment time. The figures show carbonaceous deposits similar to a curled up cloth, but it is very difficult to find nanotubes grown amongst these deposits. Though there are some nanotubes that are formed as shown in Figure 7.3, the nucleation density is very low. This indicates that pretreatment time is essential for growing nanotubes. Also, it can be seen that for a pretreatment of 10 mins and 2 squirts of catalyst, tubes with some sort of local alignment is formed, whereas coiled and tangled tubes form for 10 mins pretreatment and 5 squirts of catalyst. This indicates that 2 squirts of catalyst is better than 5 squirts, suggesting that there is an optimum concentration of catalyst beyond which the yield and alignment of tubes are rather poor.

8.4 Effect of variation of the method of application of catalyst coating

A study of the variation in the method of application of catalyst coated facilitates in finding the method which gives optimum results in the yield of better nanotubes. From SEM micrographs shown in Figures 7.12 to 7.15, tubes form in all the cases. The tubes formed due to squirting results in locally aligned tubes which are of uniform diameter, short, and with considerable terminating clusters. The tubes formed by placing the catalyst using a Pasteur pipette are more coiled and tangled, non-uniform in diameter with considerable terminating clusters. The tubes grown with spin coating as well as

smearing yield tubes with better alignment and yield. But the tubes obtained from smearing are found to be better than the spin coated sample. Also, the spin coated sample has more terminating clusters compared to smeared sample. The yield and nucleation density in the case of smeared sample are found to be more than the spin coated sample. Thus smearing of catalyst was found to be the best method of catalyst coating yielding superior quality tubes.

8.5 Effect of variation of growth time

The growth time of the nanotubes similar to pretreatment time plays an important role in obtaining tubes with better alignment and more yield. The growth time was varied (30, 15, 10, 5, 3, and 1 min) and corresponding SEM micrographs are shown in Figures 7.16 to 7.21. A some what surprising result is that nanotubes form even for 1 min of growth. Figure 7.21 shows few tubes formed. It can also be seen that there are considerable number of catalyst islands which are unused. Since the deposition time was just 1 min not every catalyst island is utilized and the growth was abruptly terminated here. The tubes grown for 3 and 5 mins seem to be not aligned and also there are many terminating clusters. The nanotubes grown for 10, 15, and 30 mins are all locally aligned. They are either aligned parallel to the substrate as shown in Figure 7.17 or aligned at a particular angle to the substrate as shown in Figures 7.16 and 7.18. The tubes grown for 10 mins growth time seem to have better alignment. Also, the yield and nucleation density for 10 mins growth is good. This can be seen from the low magnification micrograph for 10 mins grown sample as shown in Figure 7.22. It shows four rows of locally aligned nanotubes and the increased nucleation density can be clearly seen. These

results suggests that the best growth time that yields good nanotubes with better alignment and nucleation density is 10 mins.

8.6 Effect of variation of chamber pressure

Since good nucleation density is obtained with above mentioned processing conditions; it would be better to still further increase the nucleation density and also obtain tubes with vertical alignment. In order to obtain better nucleation density, the concentration of the radicals involved in the chemical kinetics of the reaction should be increased. This could be achieved by increasing the chamber pressure. At higher pressures the creation of reactive radicals is more as the gas molecules collide more. Experiments were conducted at various chamber pressures of 10, 12.5, 15, 17.5, and 20 torr and their corresponding SEM micrographs of CNTs are shown in Figures 7.23 to 7.27. It can be seen that the tubes grown at 10 torr are randomly oriented and the nucleation density is not significant. The tubes grown at 12.5 and 15 torr though are locally aligned, they do not have good nucleation density. The tubes grown at increased pressures of 17.5 and 20 torr produce vertically aligned nanotubes with good nucleation density. Another important factor to note is that the tubes grown at 17.5 and 20 torr are considerably small in diameter compared to tubes grown at other pressures. This is another factor that can be correlated to increase in nucleation density other than the pressure. The low magnification micrographs of tubes grown at 17.5 torr (Figure 7.28) seem to be shorter than the tubes grown at 20 torr (Figure 7.29). Also, the tubes grown at 20 torr after a certain length tend to bend over. Thus 20 torr seem to be the optimum pressure for the growth of vertically aligned nanotubes with increased nucleation density.

Incidentally it was also shown that 20 torr was the optimum pressure for the nucleation of diamond which is another form of carbon using hot-filament CVD [147]. Literature study on the growth of aligned nanotubes using plasma enhanced CVD is covered by Nidadavolu [149].

8.7 Effect of variation of methane flow rate

Since nanotubes with better nucleation density and vertical alignment are obtained with the above process parameters, the focus can be shifted to obtaining vertical tubes with more nucleation but fewer impurities. Since further purification of nanotubes will result in some loss of nanotubes. Synthesis of nanotubes with fewer impurities would be preferable for use in applications directly. Tests were conducted at varying methane concentrations (2.5, 5, 10, 15, and 20 sccm). Figures 7.30 to 7.34 show the SEM micrographs of CNT samples for varying methane concentrations. It was found that at low methane flow rates (2.5 and 5 sccm) no nanotubes were formed. The tubes obtained for 10, 15, and 20 sccm are found to be vertically aligned. The high magnification images of tubes grown at 10 sccm as seen in Figure 7.35 show considerable impurities attached to the walls of the nanotubes, whereas the high magnification image of tubes grown at 20 sccm are free of such impurities. However, from Figure 7.37 it is clear that though pure tubes are formed in the deposited region, amorphous carbon particles are also formed in the corners and edges of the sample. Thus, a flow rate of 20 sccm of methane was found to be the optimum yielding vertically aligned nanotubes with fewer impurities.

8.8 Characterization using Scanning Transmission Electron Microscope (STEM)

The STEM analysis on the carbon nanotubes (Figures 7.38 and 7.39) reveals that the tubes formed are multiwalled nanotubes. It can be seen from Figure 7.38 that internal morphology of the nanotube is a bamboo structure, whereas the internal morphology of the nanotube in Figure 7.39 is a hollow core. In the bamboo growth shown in Figure 7.38, the carbon has diffused on the upper part of the catalyst compared to lower part as suggested by Saito [106].

The STEM micrographs are also used to determine diameter of the nanotubes synthesized. Figures 7.40 to 7.42 show STEM micrographs of tubes grown at different pressures namely, 15, 17.5, and 20 torr, respectively. From the micrographs it can be seen that the tubes grown at 15 torr have an average diameter ranging from 80 – 120 nm, the tubes grown at 17.5 torr ranges from 100 – 130 nm and the tubes grown at 20 torr has an average diameter ranging from 70 – 100 nm. This complements the results obtained from SEM studies (Figures 7.23 to 7.27). Even though the tubes grown at 15 torr have lower average diameter than the tubes at 17.5 torr, due to vertical alignment there is more nucleation density in case of 17.5 torr. Similarly, in case of 17.5 torr and 20 torr tubes, both having vertical alignment, the sample from 20 torr has more nucleation density as its average tube diameter is lesser than the average tube diameter of tubes grown at 17.5 torr.

The flow rate of methane was varied (10, 15, and 20 sccm) and Figures 7.43 to 7.45 show the results of corresponding STEM micrographs. The average wall thickness of the nanotubes grown at 10 sccm is ~60 nm, at 15 sccm is ~70 nm and at 20 sccm is ~110 nm. From these results it can be seen that as the methane flow rate is increased, more carbon radicals become available. This results in the carbon diffusing into the

catalyst to form more walls of the tubes. Thus as the methane flow rate is increased the wall thickness of the nanotubes increases.

From the STEM micrographs (Figures 7.40 to 7.42) it can be seen that at the closed ends of some of the nanotubes catalyst particles are present, whereas others do not have any catalyst particle in the tips. If the catalyst particle is in the tip, the nanotube uses a tip growth mechanism where the carbon diffuses on the lower side of the catalyst. If there is no catalyst particle at the tip of the nanotube, then it follows a base growth mechanism where the carbon diffuses on the upper side of the catalyst. Figure 7.41 shows STEM micrographs of two nanotubes from the same sample, one with catalyst at the tip and the other without any catalyst at the tip. The tip growth mechanism or base growth mechanism is also determined by the strength of bonding between the catalyst and the substrate. If the bonding between the substrate and the catalyst is weak, it results in tip growth and if the bonding is strong, it results in base growth mechanism. Review of literature on the growth mechanisms is covered by Ramakrishnan [148].

8.9 Characterization using Atomic Force Microscopy (AFM)

AFM can be used to further supplement the diameter measurement by having accurate values. Figure 7.46 shows the AFM image of a nanotube and from the scale it can be calculated that the average tube diameter is ~220 nm. AFM is a powerful tool for analyzing the surface deformities of the nanotubes as shown in Figure 7.47. It can be seen that the tube has more kinks and bulges on the surface. Rather than calculating the diameter of the tubes from the scale on the micrograph, diameters can be exactly measured by a section analysis as shown in Figure 7.48. The horizontal distance

calculated is the diameter of the nanotube. In case of the diameter of the nanotube varying over a given length, diameter calculation at various sections of the tube can also be done using section analysis as shown in Figure 7.49. All the horizontal distances can be averaged to get the average tube diameter. The diameter of the tube in Figure 7.49 varies from 196 to 257 nm, with the average diameter of the tube being 218 nm.

8.10 Elemental analysis using Energy Dispersive Spectra (EDS)

The EDS analysis to determine the elemental composition of the deposited nanotubes is shown in Figure 7.50. It can be seen from the figure that a peak is obtained for carbon corresponding to the nanotube deposits. Apart from the carbon peak, a peak for silicon which is the substrate is also seen. Plasma pretreatment reduces the colloidal iron oxide coating applied into nanosized iron particles. The peaks obtained for iron correspond to these nanoparticles.

8.11 Phase purity determination using μ-Raman spectroscopy

μ-Raman spectroscopy was performed on the locally aligned and vertically aligned nanotubes synthesized through microwave plasma enhanced CVD. Figure 7.51 shows the Raman spectra of the locally aligned nanotubes and Figure 7.52 shows the Raman spectra of vertically aligned nanotubes. The peaks obtained from the Raman spectra further substantiates that the synthesized tubes are multiwalled nanotubes. The characteristic D and G peak for multiwalled nanotubes are seen in both figures.

CHAPTER 9

CONCLUSIONS AND FUTURE WORK

9.1 Conclusions

A systematic study was conducted to assess the effect of various process parameters in the synthesis of vertically aligned, multiwalled carbon nanotubes using a colloidal form of iron oxide as catalyst. The following conclusions that may be drawn from this study:

1. Microwave plasma enhanced CVD can be used as an effective means for the synthesis of multiwalled carbon nanotubes with fewer impurities using a colloidal form of iron oxide as a catalyst.
2. The plasma pretreatment of the catalyst coating is an essential and important step in the synthesis of the carbon nanotubes. This enables the break down of thin film of iron oxide catalyst into nanosized iron particles.
3. The nanosized iron particles act as seeds for the nucleation and growth of carbon nanotubes.
4. Various methods of application of the catalyst onto the sample were investigated and it was found that smearing a droplet of catalyst using microscope cover glass was found to be the best method yielding nanotubes with better alignment.

5. Though smearing works for this case, the catalyst concentration after coating is not uniform and varies over the sample.
6. 10 mins of pretreatment time was found to be optimum yielding longer, aligned tubes with fewer terminating clusters.
7. The growth time on the synthesis of the nanotubes was analyzed and 10 mins of growth time was found to be optimum yielding superior aligned nanotubes with higher nucleation density.
8. As the chamber pressure is increased, the vertical alignment of the nanotubes, the nucleation density, and yield of the nanotubes were found to increase. It was found that 20 torr was the optimum chamber pressure for the experimental conditions used.
9. By varying the flow rate of methane, it was found that the vertically aligned tubes with fewer impurities were formed with methane flow rate of 20 sccm. The corners of the substrate though had deposits of amorphous carbon and care should be taken while synthesis to find ways for eliminating it so that pure nanotubes can be formed.
10. It can be seen from the STEM micrographs that the wall thicknesses of the CNTs increase with flow rate of methane.
11. The STEM micrographs showed that the nanotubes grown were multiwalled.
12. The nanotubes grown were found to have either a bamboo structure or hollow core morphology.
13. Based on the location of the catalyst particle in the carbon nanotubes, the growth mechanism can be verified. If the catalyst particle is located at the tip, then it

follows the tip growth mechanism. If the tip of the nanotube is closed with no particle, then it follows a base growth mechanism. The strength of bonding between the catalyst particle and the substrate determines the growth mechanism.

14. The Raman spectra on the nanotubes further substantiated that the nanotubes grown were multiwalled.

9.2 Future Work

1. Substrate heater was not used during this study. By using the substrate heater, it is possible to control the temperature of the synthesis. This will facilitate in a better control of the synthesis.
2. The option of biasing the substrate was also not used in this study. The substrate holder can be given a negative biasing and from the literature it appears that can lead to the formation of better aligned vertical nanotubes.
3. A better method for catalyst coating should be used. Commercially available vacuum spin coaters help in coating the liquid catalyst of required thickness evenly over the entire substrate. Also ultrasonic nebulizer can be used to coat a thin layer of catalyst mist evenly over the entire substrate.
4. Other process parameters such as microwave power, flow rate of hydrogen, flow rate of nitrogen or the use of other reactive gases such as acetylene and ammonia need to be investigated.
5. The incorporation of the nanotubes for a specific application needs to be investigated.

REFERENCES

1. Kroto, H.W., Heath, J.R., O'Brien, S.C., Curl, R.F., and R.E. Smalley, "C_{60}-Buckministerfullerene," Nature **318** (1985) 162-163.
2. Kratschmer, W., Lamb, L. D., Fostiropoulos, K., and D. R. Huffman, "Solid C_{60} – a new form of carbon," Nature **347** (1990) 354-358.
3. Iijima, S., "Helical microtubules of graphitic carbon," Nature **354** (1991) 56-58.
4. Iijima, S., and T. Ichihashi, "Single-shell carbon nanotubes of 1-nm diameter," Nature **363** (1993) 603–605.
5. Harris, P.J.F., "Carbon nanotubes and Related Structures – New materials for the Twenty-first Century," Cambridge University Press, Cambridge (1999).
6. Dresselhaus, M.S., Dresselhaus, G., and R. Saito, "Carbon fibers based on C60 and their symmetry," Physical Review B **14** (1992) 6234-6242.
7. Dresselhaus, M.S., Dresselhaus, G., and R. Saito, "Physics of carbon nanotubes," Carbon **33** (1995) 883-891.
8. Dai, H., "Carbon nanotubes: Opportunities and challenges," Surface Science **500** (2002) 218-241.
9. Ebbesen, T.W., and P.M. Ajayan, "Large-scale synthesis of carbon nanotubes," Nature **358** (1992) 220-222.

10. Saito, Y., Nishikubo, K., Kawabata, K., and T. Matsumoto, "Carbon nanocapsules and single-layered nanotubes produced with platinum-group metals by arc-discharge," Journal of Applied Physics **80** (1996) 3062-3067.

11. Chernozatonskii, L.A., Kosakovskaja, Z.J., and E.A. Fedorov, "Nanofilament carbon structures," JETP Letters **56** (1992) 26.

12. Ge, M., and K. Sattler, "Vapor-condensation generation and STM analysis of fullerene tubes," Science **260** (1993) 515-518.

13. Ge, M., and K. Sattler, "Scanning tunneling microscopy of single-shell nanotubes of carbon," Applied Physics Letters **65** (1994) 2284-2286.

14. Guo, T., Nikolaev, P., Rinzler, A.G., Tomanek, D., Colbert, D.T., and R.E. Smalley, "Self assembly of tubular fullerenes," Journal of Physical Chemistry **99** (1995), 10694-10697.

15. Eklund, P.C., Pradhan, B.K., Kim, U.J., and Q. Xiong, "Large Scale production of single walled carbon nanotubes using ultrafast pulses from a free electron laser," Nanoletters **2** (2002) 561-566.

16. Bolshakov, A.P., Uglov, S.A., Saveliev, A.V., Konov, V.I., Gorbunov, A.A., Pompe, W., and A. Graff, "A novel CW laser-powder method of carbon single-walled nanotubes production," Diamond and Related Materials **11** (2002) 927-930.

17. Endo, M., Takeuchi, K., Igarashi, S., Kobori, K., Shiraishi, M., and H.W. Kroto, "The production and structure of pyrolytic carbon nanotubes," Journal of Physics and Chemistry of Solids **54** (1993) 1841-1848.

18. Sarkar, A., Kroto, H.W., and M. Endo, "Hemi-toroidal networks in pyrolytic carbon nanotubes," Carbon **33** (1995) 51-55.

19. Endo, M., Takeuchi, K., Kobori, K., Sarkar, A., Kroto, H.W., and H.W. Takahashi, "Pyrolytic carbon nanotubes from vapor-grown carbon fibers," Carbon **33** (1995) 873-881.

20. Vander Wal, R.L., and T.M. Ticich, "Comparative flame and furnace synthesis of single-walled carbon nanotubes," Chemical Physics Letters **336** (2001), 24-32.

21. Hsu, W.K., Hare, J.P., Terrones, M., Kroto, H.W., Walton, D.R.M., and P.J.F. Harris, "Condensed phase nanotubes," Nature **377** (1995) 687-689.

22. Hsu, W.K., Hare, J.P., Terrones, M., Kroto, H.W., Walton, D.R.M., and H. Terrones, "Electrolytic formation of carbon nanostructures", Chemical Physics Letters **262** (1996) 161-166.

23. Nikolaev, P., Michael, P., Bronikowski, J., Bradley, R.K., Rohmund, F., Colbert, D.T, Smith, K.A., and R.E. Smalley, "Gas-phase catalytic growth of single-walled carbon nanotubes from carbon monoxide," Chemical Physics Letters **313** (1999) 91-97.

24. Tibbetts, G.G., Bernardo, C.A., Gorkiewicz, D.W., and R.L. Alig "Role of sulfur in the production of carbon fibers in the vapor phase", Carbon **32** (1994) 569-576.

25. Resasco, D.E., Alwarez, W.E., Pompeo, F., Balzano, L., Herrera, J.E., Kitiyanan, B., and A. Borgna, "A scalable process for production of single-walled carbon nanotubes (SWNTs) by catalytic disproportionation of CO on a solid catalyst," Journal of Nanoparticle Research **4** (2002) 131-136.

26. Dresselhaus, M.S., Dresselhaus, G., and Ph. Avouris, Topics in Applied Physics, "Carbon nanotubes – Synthesis, structure, properties and applications," Springer (2000).

27. Cassell, A.M., Raymakers, J.A., Kong, J., and H. Dai, "Large Scale CVD Synthesis of Single-Walled Carbon Nanotubes," Journal of Physical Chemistry B **103** (1999) 6484-6492.

28. Andrews, R., Jacques, D., Rao, A.M., Derbyshire, F., Qian, D., Fan, X., Dickey, E.C., and J. Chen, "Continuous production of aligned carbon nanotubes: a step closer to commercial realization," Chemical Physics Letters **303** (1999) 467-474.

29. Okazaki, T., and H. Shinohara, "Synthesis and characterization of single-wall carbon nanotubes by hot filament assisted chemical vapor deposition," Chemical Physics Letters **376** (2003) 606-611.

30. Chaisitsak, S., Yamada, A., and M. Konagai, "Hot filament enhanced CVD synthesis of carban nanotubes by using a carbon filament," Diamond and Related Materials **13** (2004) 438-444.

31. Delzeit, L., McAninch, I., Cruden, B.A., Hash, D., Chen, B., Han, J., and M. Meyyappan, "Growth of multiwall carbon nanotubes in an inductively coupled plasma reactor", Journal of Applied Physics **91** (2002) 6027-6033.

32. Yu, W., Zhang, J., Liu, X., and W. Xi, "Spinose carbon nanotubes grown on graphitized DLC film by low frequency plasma-enhanced chemical vapor deposition," Diamond and Related Materials **12** (2003) 2203-2207.

33. Huang, Z.P., Xu, J.W., Ren, Z.F., Wang, J.H., Seigal, M.P., and P.N. Provencio, "Growth of highly oriented carbon nanotubes by plasma-enhanced hot filament chemical vapor deposition," Applied Physics Letters **73** (1998) 3845-3847.

34. Qin, L.C., Zhou, D., Krauss, A.R., and D.M. Gruen, "Growing carbon nanotubes by microwave plasma-enhanced chemical vapor deposition," Applied Physics Letters **72** (1998) 3437-3439.

35. Choi, Y.C., Bae, J.D., Lee, Y.H., Lee, B.S., Park, G.S., Choi, W.B., Lee, N.S., and J.M. Kim, "Growth of carbon nanotubes by microwave plasma-enhanced chemical vapor deposition at low temperature," Journal of Vacuum Science Technology A **18** (2000) 1864-1868.

36. Sung, S.L., Tsai, S.H., Tseng, C.H., Chiang, F.K., Liu, X.W., and H.C. Shih, "Well aligned carbon nitride nanotubes synthesized in anodic alumina by electron cyclotron resonance chemical vapor deposition," Applied Physics Letters **74** (1999) 197-199.

37. Chen, C.M., Chen, M., Leu, F.C., Hsu, S.Y., Wang, S.C., Shi, S.C., and C.F. Chen, "Purification of multiwalled carbon nanotubes by microwave digestion method," Diamond and Related Materials **13** (2004) 1182-1186.

38. Wang, Z., Ba, D., Lei, F., Cao, P., Yang, T., Gu, Y., and H. Gao, "Synthesis and characterization of large area well-aligned carbon nanotubes by ECR-CVD without substrate bias," Vacuum **77** (2005) 139-144.

39. Miyauchi, Y., Chiashi, S., Murakami, Y., Hayashida, Y., and S. Maruyama, "Fluorescence spectroscopy of single-walled nanotubes synthesized from alcohol," Chemical Physics Letters **387** (2004) 198-203.

40. Floro, J.A., Rossnagel, S.M., and R.S. Robinson, "Ion-bombardment-induced whisker formation on graphite", Journal of Vacuum Science and Technology A **1** (1983) 1398-1402.

41. Laplaze, D., Bernier, P., Maser, W.K., Flamant, G., Guillard, T., and A. Loiseau, "Carbon nanotubes: the solar approach," Carbon **36** (1998) 685-688.

42. Edison, T.A., "Manufacture of filaments for incandescent lamps", US Patent No 470,925 dated June 21, 1888.

43. Schutzenberger, P., and L. Schutzenberger, Compt. Rendue Acad. Science **111** (1890) 774.

44. Pelabon, C.H., Compt. Rendue Acad. Science **137** (1905) 706.

45. Bacon, R., "Growth, structure and properties of graphitic whiskers," Journal of Applied Physics **31** (1960) 283-290.

46. Moore, A.W., Ubbelohde, A.R., and D.A. Young, "An induction furnace for operations upto 3400°C using well oriented graphite," British Journal of Applied Physics **13** (1962) 393-398.

47. Saito, R., Dresselhaus, G., and M.S. Dresselhaus, "Physical properties of carbon nanotubes," Imperial College Press (1998).

48. Smalley, R.E., DoD Workshop in Washington, DC (December 1990).

49. Huffman, D.R., DoD Workshop in Washington, DC (December 1990).

50. Dresselhaus, M.S., DoD Workshop in Washington, DC (December 1990).

51. Fowler, P.W., "Carbon cylinders: a new class of closed-shell clusters," Journal of Chemical Society **86** (1990) 2073-2077.

52. Mintmire, J.W., Dunlap, B.I., and C.T. White, “Are fullerene tubules metallic?,” Physical Review Letters **68** (1992) 631-634.

53. Saito, R., Fujita, M., Dresselhaus, G., and M.S. Dresselhaus, "Electronic structure of graphene tubules based on C-60," Physical Review B **46** (1992) 1804-1811.

54. Bethune, D.S., Kiang, C.H., DeVries, M.S., Gorman, G., Savoy, R., and R. Beyers, “Cobalt-catalyzed growth of carbon nanotubes with single-atomic-layer-walls,” Nature **363** (1993) 605-607.

55. Thess, A., Lee, R., Nikolaev, P., Dai, H.J., Petit, P., Robert, J., Xu, C.H., Lee, Y.H., Kim, S.G., Rinzler, A.G., Colbert, D.T., Scuseria, G.E., Tomanek, D., Fischer, J.E., and R.E. Smalley, “Crystalline Ropes of Metallic Carbon Nanotubes,” Science **273** (1996) 483-487.

56. Li, W.Z., Xie, S., Qian, L.X., Chang, B.H., Zou, B.S., Zhou, W.Y., Zhao, R.A., and G. Wang, “Large-scale synthesis of aligned carbon nanotubes,” Science **274** (1996) 1701-1703.

57. Ebbesen, T.W., Lezec, H.J., Hiura, H., Bennett, J.W., Ghaemi, H.F., and T. Thio, “Electrical-conductivity of individual carbon nanotubes,” Nature **382** (1996) 54-56.

58. Treacy, M.M.J., Ebbesen, T.W., and J.M. Gibson, “Exceptionally high Young's modulus observed for individual carbon nanotubes,” Nature **381** (1996) 678-680.

59. Dillon, A.C., Jones, K.M., Bekkedahl, T.A., Kiang, C.H., Bethune, D.S., and M.J. Heben, “Storage of hydrogen in single-walled carbon nanotubes,” Nature **386** (1997) 377-379.

60. Terrones, M., Grobert, N., Olivares, J., Zhang, J.P., Terrones, H., Kordatos, K., Hsu, W.K., Hare, J.P., Townsend, P.D., Prassides, K., Ceetham, A.K., Kroto, H.W., and D.R.M. Walton, "Controlled production of aligned-nanotube bundles," Nature **388** (1997) 52-55.

61. Tans, S.J., Devoret, M.H., Dai, H., Thess, A., Smalley, R.E., Geerligs, L.J., and C. Dekker, "Individual single-wall carbon nanotubes as quantum wires," Nature **386** (1997) 474-477.

62. Ren, Z.F., Huang, Z.P., Xu, J.W., Wang, j.H., Bush, P., Seigal, M.P., and P.N. Provencio, "Synthesis of large arrays of well-aligned carbon nanotubes on glass," Science **282** (1998) 1105-1107.

63. Smith, B.W., Monthioux, M., and D.E. Luzzi, "Encapsulated C_{60} in carbon nanotubes," Nature **396** (1998) 323-324.

64. Liu, C., Fan, Y.Y., Liu, M., Cong, H.T., Cheng, H.M., and M.S. Dresselhaus, "Hydrogen Storage in Single-Walled Carbon Nanotubes at Room Temperature," Science **286** (1999) 1127-1129.

65. Berber, S., Kwon, Y.K., and D. Tomanek, "Unusually High Thermal Conductivity of Carbon Nanotubes," Physical Review Letters **84** (2000) 4613-4616.

66. Vigolo, B., Pénicaud, A., Coulon, C., Sauder, C., Pailler, R., Journet, C., Bernier, P., and P. Poulin, "Macroscopic Fibers and Ribbons of Oriented Carbon Nanotubes," Science **290** (2000) 1331-1334.

67. Kociak, M., Kasumov, A.Yu., Gueron, S., Reulet, B., Khodos, I.I., Gorbatov, Yu.B., Volkov, V.T., Vaccarini, L., and H. Bouchiat, "Superconductivity in ropes

of single-walled carbon nanotubes," Physical Review Letters **86** (2001) 2416-2419.

68. Collins, P.C., Arnold, M.S., and P. Avouris, "Engineering Carbon Nanotubes and Nanotube Circuits Using Electrical Breakdown," Science **292** (2001) 706-709.

69. Schonenberger, C., and L. Forro, "Multiwall carbon nanotubes," Physics World, June (2000), http://physicsweb.org/articles/world/13/6/8.

70. http://www.pa.msu.edu/cmp/csc/ntproperties/

71. Salvetat, J.P., Briggs, G.A.D., Bonard, J.M., Bacsa, R.R., and A.J. Kulik, "Elastic and shear moduli of single-walled carbon nanotube ropes," Physical Review Letters **82** (1999) 944-947.

72. http://www.applied-nanotech.com/cntproperties.htm#Mechanical%20Properties

73. Yu, M.F., Yakobson, B.I., and R.S. Ruoff, "Controlled sliding and pullout of nested shells in individual multiwalled carbon nanotubes," Journal of Physical Chemistry B **104** (2000) 8764-8767.

74. Cumings, J., and A. Zettl, "Low-friction nanoscale linear bearing realized from multi-wall carbon nanotubes," Science **289** (2000) 602-604.

75. Yu, M.F., Files, B.S., Arepalli, S., and R.S. Ruoff, "Tensile loading of ropes of single wall carbon nanotubes and their mechanical properties," Physical Review Letters **84** (2000) 5552-5555.

76. Reich, S., Thomsen, C., and J. Maultzsch, "Carbon nanotubes – Basic Concepts and Physical Properties," Wiley-VCH (2004).

77. Frank, S., Poncharal, P., Wang, Z.L., and W.A. de Heer, "Carbon nanotube quantum resistors," Science **280** (1998) 1744-1746.

78. Sanvito, S., Kwon, Y.K., Tomanek, D., and C.J. Lambert, "Fractional quantum conductance in Carbon Nanotubes," Physical Review Letters **84** (2000) 1974-1977.

79. Hone, J., Whitney, M., and A. Zettl, "Thermal conductivity of single-walled carbon nanotubes," Synthetic Metals **103** (1999) 2498-2499.

80. Che, J., Cagin. T., and W.A. Goddard III, "Thermal conductivity of carbon nanotubes," Seventh foresight conference on Molecular Nanotechnology (1999).

81. Ramirez, A.P., Haddon, R.C., Zhou, O., Fleming, R.M., Zhang, J., Mcclure, S.M., and R.E. Smalley, "Magnetic susceptibility of molecular carbon: nanotubes and fullerite," Science **265** (1994) 84-86.

82. Wang, X.K., Chang, R.P.H., Patashinski, A., and J.B., Ketterson, "Magnetic-susceptibility of buckytubes," Journal of Materials Research **9** (1994) 1578-1582.

83. Chauvet, O., Forro, L., Bacsa, W., Ugarte, D., Doudin, B., and W.A. de Heer, "Magnetic anisotropies of aligned carbon nanotubes," Physical Review B **52** (1995) R6963-R6966.

84. http://www.applied-nanotech.com/cntproperties.htm#Field%20Emission%20Properties%20of%20Carbon%20Nanotubes

85. de Heer, W.A., Chatelain, A., and D. Ugarte, "A carbon nanotube field-emission electron source," Science **270** (1995) 1179-1180.

86. Bonard, J.M., Salvetat, J.P., Stockli, T., Forro, L., and A. Chatelain, "Field emission from carbon nanotubes: perspectives for applications and clues to the emission mechanism," Applied Physics A **69** (1999) 245-254.

87. Baughman, R.H., Zakhidov, A.A., and W.A. de Heer, "Carbon nanotubes – the route toward applications," Science **297** (2002) 787-792.

88. Dai, H., Hafner, J.H., Rinzler, A.G., Colbert, D.T., and R.E. Smalley, "Nanotubes as nanoprobes in scanning probe microscopy," Nature **384** (1996) 147-150.

89. Wong, S.S., Harper, J.D., Lansbury, P.T., and C.M. Leiber, "Carbon nanotube tips: high-resolution probes for imaging biological systems," Journal of American Chemical Society **120** (1998) 603-604.

90. Wong, S.S., Woolley, A.T., Joselevich, E., Cheung, C.L., and C.M. Leiber, "Covalently-functionalized single-walled carbon nanotube probe tips for chemical force microscopy," Journal of American Chemical Society **120** (1998) 8557-8558.

91. Dai, H.J., Franklin, N., and J. Han, "Exploiting the properties of carbon nanotubes for nanolithography," Applied Physics Letters **73** (1998) 1508-1510.

92. Delzeit, L., Nguyen, C.V., Stevens, R.M., Han, J., and M. Meyyappan, "Growth of carbon nanotubes by thermal and plasma CVD and application in microscopy," Nanotechnology **13** (2002) 280-284.

93. Robertson, J., "Realistic applications of CNTs," Materials Today (2004) 46-52.

94. Biercuk, M.J., Llaguno, M.C., Radosavljevic, M., Hyun, J.K., Johnson, A.T., and J.E. Fischer, "Carbon nanotube composite for thermal management," Applied Physics Letters **80** (2002) 2767-2769.

95. Rao, A.M., Andrews, R, and F. Derbyshire, "Nanotube composite carbon fibers," Energia **9** (1998) 1-6.

96. Collins, P.G., and P. Avouris, "Nanotubes for electronics," Scientific American (December 2000), 62-69.

97. Graham, A.P., Duesberg, G.S., Seidel, R., Liebau, M., Unger, E., Kreupl, F., and W. Honlein, "Towards the integration of carbon nanotubes in microelectronics," Diamond and Related Materials **13** (2004) 1296-1300.

98. Ando, Y., Zhao, X., Sugai, T., and M. Kumar, "Growing carbon nanotubes," Materials Today (October 2004) 22-29.

99. Huang, Z.P., Wang, D.C., Wen, J,G., Sennett, M., Gibson, H., and Z.F. Ren, "Effect of nickel, iron and cobalt on the growth of aligned carbon nanotubes," Applied Physics A **74** (2002) 387-391.

100. Shin, Y.M., Jeong, S.Y., Jeong, H.J., Eum, S.J., Yang, C.W., Park, C.Y., and Y.H. Lee, "Influence of morphology of catalyst thin film on vertically aligned carbon nanotube growth," Journal of Crystal Growth **271** (2004) 81-89.

101. Vinciguerra, V., Buonocore, F., Panzara, G., and L. Ochipinti, "Growth mechanisms in chemical vapor deposited carbon nanotubes," Nanotechnology **14** (2003) 655-660.

102. Chen, M., Chen, C.M., Koo, H.S., and C.F. Chen, "Catalyzed growth model of carbon nanotubes by microwave plasma chemical vapor deposition using CH_4 and CO_2 gas mixtures," Diamond and Related Materials **12** (2003) 1829-1835.

103. Hsu, C.M., Lin, C.H., Lai, H.J., and C.T. Kuo, "Root growth of multi-wall carbon nanotubes by MPCVD," Thin Solid Films **471** (2005) 140-144.

104. Lee, C.J., Lee, T.J., Lyu, S.C., Huh, Y., and J.Y. Lee, "Growth of vertically aligned bamboo shaped carbon nanotubes," Journal of Korean Physical Society **39** (2001) S59-S62.

105. Baker, R.T.K., "Catalytic growth of carbon filaments," Carbon **27** (1989) 315-323.

106. Saito, Y., "Nanoparticles and filled nanocapsules," Carbon **33** (1995) 979-988.

107. Jung, M., Eun, K.Y., Lee, J.K., Baik, Y.J., Lee, K.R., and J.W. Park, "Growth of carbon nanotubes by chemical vapor deposition," Diamond and Related Materials **10** (2001) 1235-1240.

108. Lee, T.Y., Han, J.H., Choi, S.H., Yoo, J.B., Park, C.Y., Jung, T., Yu, S.G., Yi, W.K., Han, I.T., and J.M. Kim, "Effect of source gases on the growth of carbon nanotubes," Diamond and Related Materials **12** (2003) 851-855.

109. Kuttel, O.M., Groening, O., Emmennegger, C., and L. Schlapbach, "Electron field emission from phase pure nanotube films grown in methane/hydrogen plasma," Applied Physics Letters **73** (1998) 2113-2115.

110. Qin, L.C., Zhou, D., and D.M. Gruen, "Growing carbon nanotubes by microwave plasma-enhanced chemical vapor deposition," Applied Physics Letters **72** (1998) 3437-3439.

111. Lin, C.H., Chang, H.L., Hsu, C.M., Lo, A.Y., and C.T. Kuo, "The role of nitrogen in carbon nanotube formation," Diamond and Related Materials **12** (2003) 1851-1857.

112. Kim, T.Y., Lee, K.R., Eun, K.Y., and K.H. Oh, "Carbon nanotube growth enhanced by nitrogen incorporation," Chemical Physics Letters **372** (2003) 603-607.

113. Lee, J.Y., and B.S. Lee, "Nitrogen induced structure control of vertically aligned carbon nanotubes synthesized by microwave plasma enhanced chemical vapor deposition," Thin Solid Films **418** (2002) 85-88.

114. Valentini, L., Kenny, J.M., Lozzi, L., and S. Santucci, "Formation of carbon nanotubes by plasma enhanced chemical vapor deposition: Role of nitrogen and catalyst layer thickness," Journal of Applied Physics **92** (2002) 6188-6194.

115. Lin, C.H., Lee, S.H., Hsu, C.M., and C.T. Kuo, "Comparison of properties and growth mechanisms of carbon nanotubes fabricated by high pressure and low pressure plasma-enhanced chemical vapor deposition," Diamond and Related Materials **13** (2004) 2147-2151.

116. Jung, M., Eun, K.Y., Baik, Y.J., Lee, K.R., Shin, J.K., and S.T. Kim, "Effect of NH_3 environmental gas on the growth of aligned carbon nanotube in catalystically pyrolising C_2H_2," Thin Solid Films **398-399** (2001) 150-155.

117. Makris, T.D., Giorgi, R., Lisi, N., Pilloni, L., Salernitano, E., Sarto, F., and M. Alvisi, "Carbon nanotubes growth by HFCVD: effect of process parameters and catalyst preparation," Diamond and Related Materials **13** (2004) 305-310.

118. Han, J.H., Choi, S.H., Lee, T.Y., Yoo, J.B., Park, C.Y., Kim, H.J., Han, I.T., Yu, S.G., Yi, W., Park, G.S., Yang, M., Lee, N.S., and J.M. Kim, Effect of growth parameters on selective area of carbon nanotubes," Thin Solid Films **409** (2002) 126-132.

119. Li, W.C., Wen, J.G., Tu, Y., and Z.F. Ren, "Effect of gas pressure on the growth and structure of carbon nanotubes by chemical vapor deposition," Applied Physics A **73** (2001) 259-264.

120. Wang, B.B., Lee, S., Xu, X.Z., Choi, S., Yan, H., Zhang, B., and W. Hao, "Effect of pressure on growth of carbon nanotubes by plasma-enhanced hot filament CVD at low substrate temperature," Applied Surface Science **236** (2004) 6-12.

121. Munoz, E., Maser, W.K., Benito, A.M., Martinez, M.T., de la Fuente, G.F., Maniette, Y., Righi, A., Anglaret, E., and J.L. Sauvajol, "Gas and pressure effects on the production of single-walled carbon nanotubes by laser ablation," Carbon **38** (2000) 1445-1451.

122. Lee, C.J., Park, J., Huh, Yoon, and J.Y. Lee, "Temperature effect on the growth of carbon nanotubes using thermal chemical vapor deposition," Chemical Physics Letters **343** (2001) 33-38.

123. Takizawa, M., Bandow, S., Torii, T., and S. Iijima, "Effect of environment temperature for synthesizing single-wall carbon nanotubes by arc vaporization method," Chemical Physics Letters **302** (1999) 146-150.

124. Lee, H., Kang, Y.S., Lee, P.S., and J.Y. Lee, "Hydrogen plasma treatment on catalytic layer and effect of oxygen addition on plasma enhanced chemical vapor deposition of carbon nanotube," Journal of Alloys and Compounds **330-332** (2002) 569-573.

125. Yen, J.H., Leu, I.C., Lin, C.C., and M.H. Hon, "Effect of catalyst pretreatment on the growth of carbon nanotubes," Diamond and Related Materials **13** (2004) 1237-1241.

126. Gao, J.S., Umeda, k., Uchino, K., Nakashima, H., and K. Muraoka, "Plasma breaking of thin films into nano-sized catalysts for carbon nanotubes synthesis," Materials Science and Engineering A **352** (2003) 308-313.

127. Yan, H., Li, Q., Zhang, J., and Z. Liu, "Possible tactics to improve the growth of single-walled carbon nanotubes by chemical vapor deposition," Carbon **40** (2002) 2693-2698.

128. Huang, J.H., Chuang, C.C., and C.H. Tsai, "Effect of nickel thickness and microwave power on growth of carbon nanotubes by microwave-heated chemical vapor deposition," Microelectronic Engineering **66** (2003) 10-16.

129. Zhang, H., Ding, Y., Wu, C., Chen, Y., Zhu, Y., He, Y., and S. Zhong, "The effect of laser power on the formation of carbon nanotubes prepared in CO_2 continuous wave laser ablation at room temperature," Physica B **325** (2003) 224-229.

130. Ebbesen, T.W., "Carbon Nanotubes – Preparation and properties," CRC Press (1997), Boca Raton, Florida.

131. "AX 5000 and AX5400, Plasma Deposition Source, Operation Manual", Applied Science and Technology Inc., Woburn, MA.

132. MKS Instruction manual, Type 250C Pressure/Flow controller, Andover, MA.

133. MKS Instruments, MKS Baratron Type 127 Absolute Pressure Transducer manual, Andover, MA.

134. MKS Instruction manual, Type 247C - 4 Channel Readout mass flow meter, Andover, MA.

135. MKS Instruction manual, MKS flow controllers 100 Series models, 1159B/1160B/1161B/2159B/2160B/2161B, Andover, MA.

136. Fleming, Jr., Marshall, J.S., William, A.W., and J. Eric, "Reduction of foreign matter on semiconductor wafers," US Patent No 5,294,570 dated March 15, 1994.

137. Jung, K.H., Boo, J.H., and B. Hong, "Synthesis of carbon nanotubes grown by hot filament plasma-enhanced chemical vapor deposition method," Diamond and Related Materials **13** (2004) 299-304.

138. Arepalli, S., Nikalaev, P., Gorelik, O., Hadjiev, V.G., Holmes, W., Files, B., and L. Yowell, "Protocol for characterization of single-wall carbon nanotube material quality," Carbon **42** (2004) 1783-1791.

139. Wright, A.C., Xiong, Y., Maung, N., Eichhorn, S.J., and R.J. Young, "The influence of the substrate on the growth of carbon nanotubes from nickel clusters – an investigation using STM, FE-SEM, TEM and Raman Spectroscopy," Materials Science and Engineering C **23** (2003) 279-283.

140. Jang, J.W., Lee, C.E., Lee, T.J., Lee, C.J., and S.J. Noh, "Atomic force microscopy of bamboo-shaped multiwalled carbon nanotube structures," Solid State Communications **127** (2003) 29-32.

141. Ives, L.K., "Electron Microscopy," National Institute of Standards and Technology.

142. JEOL JSM-6400 manual, JEOL, Peabody, Massachusetts.

143. JEOL 100 CX II STEM manual, JEOL, Peabody, Massachusetts.

144. http://www.pacificnanotech.com/afm-tutorial.html

145. Dimension™ 3100 series scanning probe microscope instruction manual, Digital Instruments, Santa Barbara, California.

146. Mallika, K., "Analytical and Experimental studies on microwave assisted CVD diamond coatings on Si_3N_4 and cemented WC tools an growth of polycrystalline

diamond in several transition metals," Ph.D Dissertation, Mechanical and Aerospace Engineering, Oklahoma State University, May 1998.

147. Iyengar, S.K., "Diamond coatings on cutting tools by hot filament CVD," M.S. Thesis, Mechanical and Aerospace Engineering, Oklahoma State University, December 1995.

148. Ramakrishnan, M.P., "Experimental study on microwave assisted CVD growth of carbon nanotubes on silicon wafer using cobalt as a catalyst," M.S. Thesis, Mechanical and Aerospace Engineering, Oklahoma State University, May 2005.

149. Nidadavolu, A.G.R., "Synthesis of carbon nanotubes by microwave plasma enhanced CVD on silicon using iron as catalyst," M.S. Thesis, Mechanical and Aerospace Engineering, Oklahoma State University, May 2005.

APPENDIX

INSTRUMENT SPECIFICATIONS

1. Microwave Power Generator

Model: AX S-1500i power supply and control unit with HS-1500 power head

Power output: 0.125 to 1.5 kW CW

Regulation: 0.5% of output power

Ripple: <1% of output power

Frequency: 2455 MHz, ± 15 MHz

Frequency stability: < 1 MHz long term drift after initial warm up. Less than 2 MHz pulling from 300W to 150W output

2. Mass Flow Meters

Model: MKS type 247C with 4 channel read out

Input signal range: 0 to +5 V DC (5.5 V maximum)

Output range: 0 to +5 V DC

Zero correction: ± 3 % of full scale

Set point adjust: 0.1 % to 100 % of full scale (flow)

: 0.1 % to 100 % of input level (ratio)

Display accuracy: ± 0.1 % to ±1 digit

3. Mass Flow Controller

Model: MKS type 1159B with closed loop PID controller

Maximum inlet pressure: 150 psig

Full scale ranges: 500 sccm (H_2), 100 sccm (N_2) and 100 sccm (CH_4)

Control range: 1 to 100 % of full scale

Accuracy: ± 1 % of full scale

Repeatability: ± 0.2 % of full scale

Resolution: 0.1% of full scale

Setting time: <2seconds to within 2% of the set point

4. Pressure Controller

Model: MKS type 250C with closed loop PID controller

Input signal: 0 to 10 V DC, or 0 to 1 V DC, or 0 to 0.1 V DC

Valve outputs: Current: 0 to 120 mA

Valve outputs: Voltage: 0 to 110 V DC

Voltage outputs: Input signal – 0 to 10 volts (5K minimum resistance)

: Controller output – 0 to 10 volts (5K minimum resistance)

Accuracy: ± 0.25 % of full scale

5. Pressure Transducer

Model: MKS type 127A

Lowest recommended pressure reading: 2 X 10^{-3} Torr

Lowest pressure control: 5 X 10^{-2} Torr

Full scale range: 100 torr

Accuracy: 0.15% of reading (± of temperature coefficients)

Temperature coefficients: Zero: 0.005 % of full scale /°C

: Span: 0.02 % of full scale/°C

Operating temperature range: 15 °C to 40 °C; temperature controlled at 45 °C

Time constant: <16 msec

Input: ± 15 V DC @ 250 mA, regulated ± 5%

Output: 0 to + 10 V DC into ≥ 10 kW load

6. Dual Wavelength Infrared Pyrometer

Model: Williamson Tempmatic 8000 Series with automatic emissivity compensation

Field of view: Minimum 0.64 cm of diameter at working distance of 46 cm

Temperature range: 500 – 1200 °C

Working distance: 15 to 91 cm

Accuracy: ± 1 % of span

Repeatability: 0.25 % of full scale

Response time: (adjustable) 0.2 to 5 seconds

VITA

Devanathan Raghavan

Candidate for the Degree of

Master of Science

Thesis: SYNTHESIS OF MULTI-WALLED CARBON NANOTUBES BY PLASMA ENHANCED MICROWAVE CVD USING COLLOIDAL FORM OF IRON OXIDE AS A CATALYST

Major Field: Mechanical Engineering

Biographical:

Education: Received Bachelor of Engineering degree in Mechanical Engineering from Karunya Institute of Technology, Bharathiar University, Coimbatore, Tamilnadu, India in May 2000.

Completed the requirements for the Master of Science degree with a major in Mechanical and Aerospace Engineering at Oklahoma State University in May 2005.

Experience: CADD Engineer, CADD Center India Private Limited, Chennai, India, December 2000 – June 2001.

Student intern in Design and Engineering department, Macon Engineers, Chennai, India, Summer 1998.

Graduate Research Assistant in Mechanical and Aerospace Engineering Department, Oklahoma State University, Stillwater, Oklahoma, January 2002 - present.

Professional Membership: AIChE, ASME.